University of Stavanger

FACULTY OF SCIENCE AND TECHNOLOGY

MASTER'S THESIS

Study programme/specialisation: Marine and Offshore Technology	Spring/ Autumn semester, 2020 Open / Confidential
Author: Vladislav Mikhalkin	
Programme coordinator: Muk Chen Ong Supervisor(s): Ove Tobias Gudmestad (UiS), Anatoly Borisovich Zolotukhin (Gubkin University)	
Title of master's thesis: DEVELOPMENT CONCEPT OF OIL FIELD-A IN THE PECHORA SEA UNDER CONDITIONS OF INITIAL DATA UNCERTAINTY	
Credits: 30 ECTS	
Keywords: Pechora sea, Field layout, Development concept, EOR screening, Gravity-based structures	Number of pages: …99…… + supplemental material/other: …… Stavanger, …….. date/year

ABSTRACT

The development strategy of equipping an oil field of the Pechora Sea is discussed in this thesis. Because of the confidential data on the field received from PJSC Rosneft, the field is conventionally called Field-A in this work.

The philosophy of the thesis is the analysis of four groups of factors that determine the efficiency of using one or another development strategy. These groups are:

1. Group of the situational factors;
2. Geological group;
3. Technological group;
4. Economic group.

Each group is a core of the corresponding chapter. An analysis of each group of factors allows in the first chapter to decide on suitable concepts and further determine their technical and technological features and economic efficiency at the end.

CONTENT

Introduction

In recent years, the interest of major oil and gas producing companies in the development of Arctic resources has increased significantly, primarily due to the high hydrocarbon potential of the Arctic shelf. Despite the harsh climatic conditions of this region, a number of projects have already been implemented at the moment, while oil and gas companies are planning to commission new deposits of the Arctic shelf in the near future. For some of these projects, accepted development concepts already exist; for other projects, development concepts continue to be actively developed. The latter include field A.

In the near future, Rosneft, the largest Russian oil and gas company that owns the license area of the field, plans to put this field into operation. In the process of developing offshore oil and gas fields, the issue of their equipment is important. The purpose of this work is to develop a concept for the development of field a based on data obtained on the basis of confidentiality rights [1] from Rosneft. The data provided by the company includes a description of the field design conditions, as well as a hydrodynamic model of the reservoir.

1. Field-A engineering design conditions

1.1. Oil and gas fields development in the Arctic conditions

The Arctic is a unified physical-and-geographical area of the Earth. It includes vast territories: the outskirts of the continents of Eurasia and North America, almost the entire Arctic Ocean with islands, as well as parts of the Pacific and Atlantic oceans [1,2]. There are several approaches to determining the southern border of the Arctic. So, the border of the Arctic Circle can be the southern border; isotherm of average monthly temperatures, corresponding to +10 C° throughout the year; forest line and others [3]. Various ways of determining the southern border are shown in Figure 1.1.

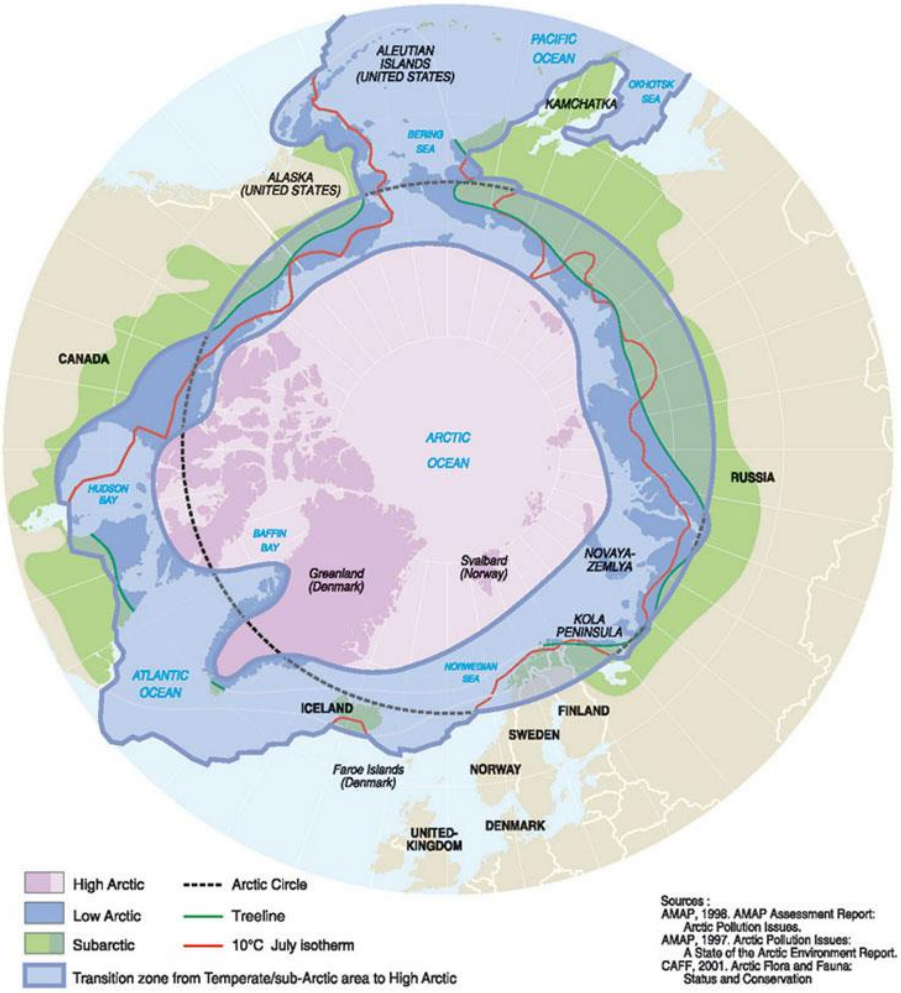

Figure 1.1 Ways of the Arctic borders determination [3]

Even if the Arctic Circle is adopted as the southern border (in this case, the Arctic area is approximately 21 million km^2 – 4.1% of the globe), the region is characterized by high hydrocarbon reserves. Thus, according to [1], the Arctic region contains 18.56 BTO of oil and 39.70 TCM of gas or 61.14 BTOE of oil and gas, which is ~ 15% of all

world hydrocarbon reserves. The Arctic is one of the least studied regions of the world, and, according to [4], has an even more significant hydrocarbon potential. Moreover, most of the undiscovered resources are located on the Russian continental shelf [1].

The Arctic region, however, is characterized by harsh climatic conditions. Low temperatures, the presence of first-year and multi-year ice, a short summer period, the presence of icebergs, hummocks, stamukhas and other features of many Arctic waters are significant obstacles to the development of offshore oil and gas fields on the Arctic shelf. These features in the conditions of the region remoteness from the markets for products and the lack of developed infrastructure in the region require not only a specific approach to the development of projects in the Arctic (including using new technologies) but also significant capital investments in their implementation [5]. Under such conditions, the environment is at higher risk than in other regions where hydrocarbons are produced, and the consequences of any accidents are more harmful to the environment.

Despite this, many projects have already been implemented in the conditions of the Arctic shelf, while oil and gas companies are planning to place under production new Arctic deposits soon [6]. For some of these projects, accepted development concepts already exist; for other projects, development concepts continue to be actively developed. The latter include field A.

As noted above, the Arctic region covers a significant territory of the globe. Therefore, each water area of the region has some deviations from the general regional characteristics, which were given above. Thus, each project is fraught with specific difficulties for its implementation, which largely determine the concept of development (therefore, the concept of arrangement). Therefore, the description and consideration of design conditions in a single region or a separate area remain extremely important. The design conditions for field A are given in Section 1.2 of this chapter.

Nevertheless, the analysis of the experience gained in the implementation of other projects and the consideration of this experience also remains an essential component in the field concept development for each project. In this regard, to systematize the accumulated knowledge, an analysis was carried out of projects of the Arctic and water areas with similar natural and climatic conditions that were

implemented and planned to be placed under production soon. The analysis was carried out based on [6–12]. The list of projects with their brief characteristics is presented in Table A1.1. It includes almost all existing projects in the Arctic, except for most projects in the Norwegian Sea. The experience of projects and other water areas with similar natural and climatic conditions (the Okhotsk Sea, the Baltic Sea, the Zhili Gulf, the Caspian Sea, etc.) was also taken into account. Further, under the Arctic conditions and Arctic projects will be understood, including environmental conditions of these water areas and the projects implemented in them.

The diagram in Figure 1.2 shows the number of completed and planned projects for the next decade. Among them are the projects of Russia, the USA, Norway, Canada, as well as China and Kazakhstan.

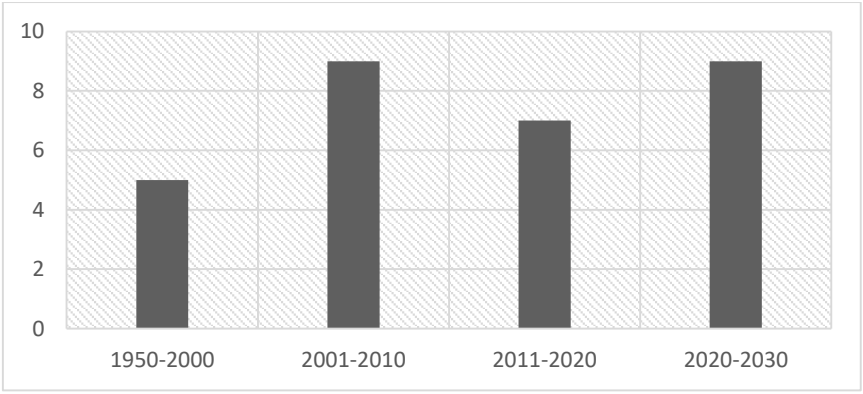

Figure 1.2 The number of projects implemented in the Arctic and subarctic conditions

Offshore oil and gas fields development is associated with such processes as exploration and production drilling, production (sometimes storage) of hydrocarbons, primary processing and transportation of hydrocarbons.

Drilling of wells, including exploration ones, in the Arctic, is carried out using such Offshore Oil and Gas Structures (OSGS) and Mobile Offshore Drilling Units (MODU) as drilling barges, drilling vessels, SPAR platforms, semi-submersible platforms, Jack-Up platforms, as well as stationary, gravity platforms and artificial islands [6,7,13]. The latter (gravity platforms and artificial islands) are also used mainly in hydrocarbon production. So, in Figure 1.3, a represented diagram is showing how many Arctic projects a particular type of OSGS is involved in hydrocarbon production (based on table A1.1). From now on, Norwegian projects are not included in the analysis due to reasonably mild climatic conditions compared with the ones of

the Pechora Sea. Nevertheless, the projects implemented in the Norwegian Sea are one of the most significant and diverse. Some of them are also given in A1.1.

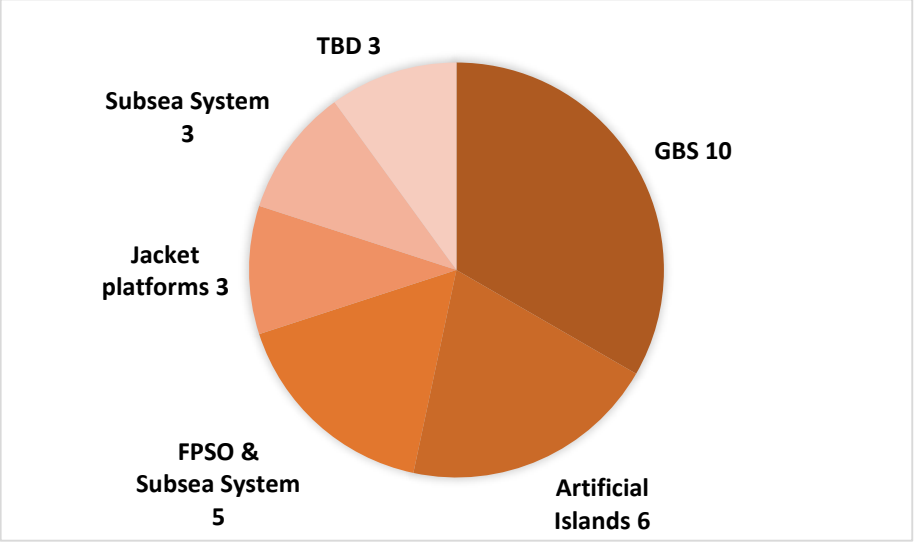

Figure 1.3 Types of OSGS that are utilized for the hydrocarbons production in the Arctic and subarctic conditions

According to [7], it could be distinguished four main types of the offshore field arrangement. Among them: *above-ground*, to which, according to Table A1.1, 6 projects relate to where artificial islands are used; *surface*, which includes 13 projects that use steel and gravity platforms; *subsea* – 3 projects using Subsea Production Systems (SPS); *combined* – 5 projects using SPS and FPSO.

Hydrocarbons are transported in the Arctic conditions by offloading of raw materials to tankers (including ice-class tankers) or using a multiphase or single-phase pipeline system (see Figure 1.4, Table A1.1) [7].

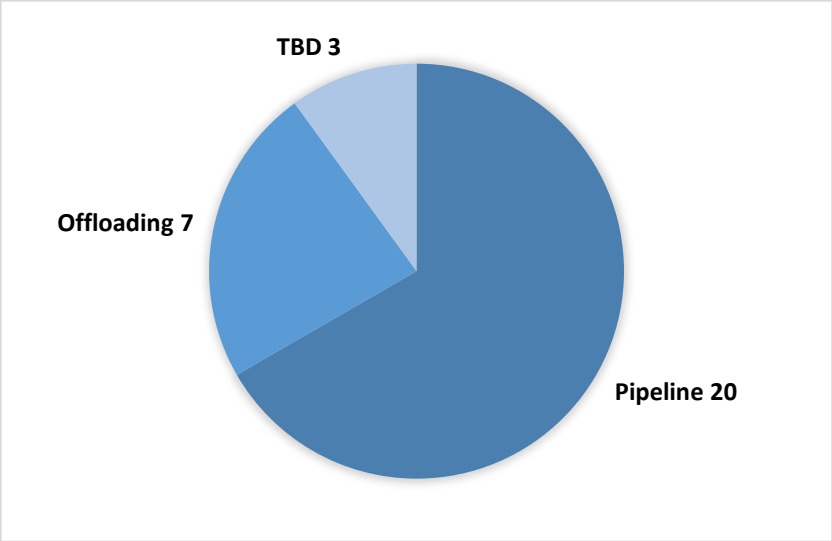

Figure 1.4 Ways of hydrocarbons transportation implemented in the Arctic and subarctic conditions

Despite the small number of projects existing in the Arctic environment, six basic layout schemes can be distinguished (see Table 1.1). It should be noted that the experience of using dedicated schemes in Arctic conditions does not limit the use of any of the schemes in the same way that the existence of dedicated schemes does not limit the development and implementation of new or already used in non-Arctic conditions. However, this experience should be taken into account along with the features of the design conditions when developing concepts for the offshore oil and gas fields.

Table 1.1

Arrangement field layouts typical for Arctic conditions and experience of their application

Field layout	Features		Application experience
Artificial island + pipeline (above-ground arrangement) – Six projects	High reliability; Technologies and equipment can be used without restrictions associated with a limited area; An artificial island does not require liquidation upon	Long build period	In the coastal zone; At depths of up to 12 meters; In the presence of first-year and multi-year ice.

	completion of operation; Technology tested in practice.		
Gravity-based platform + pipeline (surface arrangement) - 6 projects	Wellheads are on the surface; High reliability and resistance to severe weather conditions; The ability to store oil.	Low mobility	At depths from 15 up to 48 m; In the presence of first-year and multi-year ice, and icebergs.
Gravity-based platform + offloading to the tanker (surface arrangement) - 3 projects		Low mobility	At depths from 20 up to 95 m; In the presence of first-year ice and icebergs.
Stationary platform + pipeline (surface arrangement) - 3 projects	Wellheads are on the surface; Low cost.	Reduced resistance to severe weather conditions.	At depths of up to 85 m; In the presence of first-year ice.
FPSO + SPS + pipeline (combined arrangement) - 4 projects	High mobility; The ability to store oil.	Reduced resistance to severe weather conditions.	At depths from 120 up to 420 m; In the presence of first-year ice and icebergs.
SPS + pipeline (subsea arrangement) - 3 projects	Autonomy		At depths from 55 up to 340 m; In the presence of first-year and multi-year ice.

1.2. Field-A engineering design conditions

Field A is located in the Pechora Sea waters at a distance of 6 km from the coast, more than 1000 km from the Murmansk city. The Pechora Sea is part of the Barents Sea. Its boundaries are shown in Figure 1.5.

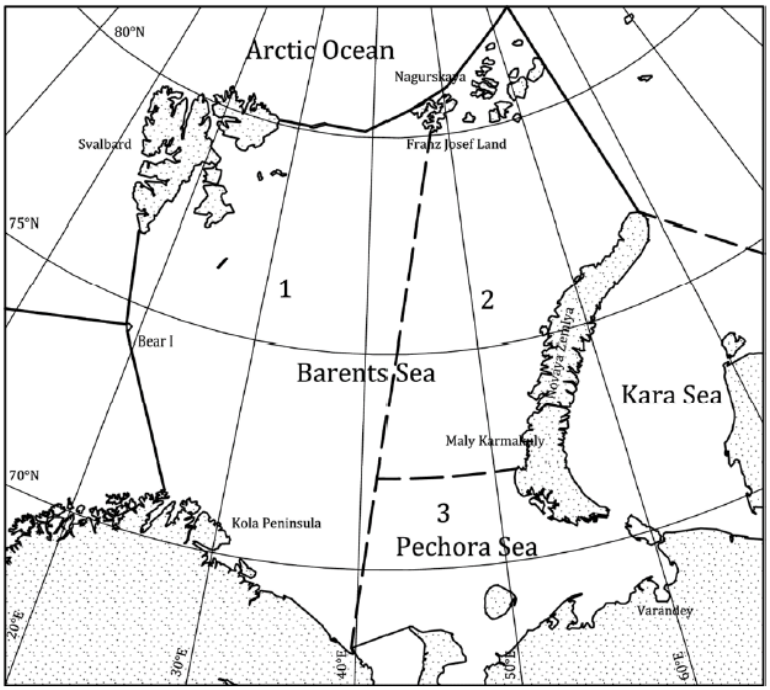

Figure 1.5 Borders and regions of the Barents Sea [10]

Field A has a significant oil-bearing area and extends ~ 30 km to its north-west from the southern border along the license area, while the northern border is ~ 28 km offshore. Most of the water zone of the license area is a vast underwater plain slightly sloping in the northeast, north directions. The southern boundary of the site is located close to the peninsula M and island P. The island T is located at the eastern border of the site.

1.2.1. Meteorological and oceanographic conditions

The climate of the Pechora Sea is determined by its high latitude position, features of atmospheric circulation and radiation balance, as well as the nature of the underlying surface – warm waters of the Barents Sea in winter and relatively cold waters of the Arctic basin in summer.

Unlike the southwestern part of the Barents Sea, the climate here is more severe, which is associated with a decrease in the influence of warm Atlantic currents and the presence of ice cover for 7-8 months a year. The impact of planetary processes of interaction between the Icelandic minimum and the Siberian maximum, which has a seasonal orientation, leads to the monsoon nature of the climate. The duration and boundaries of the climatic seasons are shown in Table 1.2.

Table 1.2

Duration and boundaries of climatic seasons [14,15]

Season	Period	Duration
Winter	November – April	6
Spring	May – June	2
Summer	July – August	2
Autumn	September – October	2

Among the geographical features, it is worth noting: the formation of arctic water masses in the north of the sea and marine polar in the south. The alternation of cold and warm currents, the presence of numerous islands, sea ice and frontal zones on the surface of the water affect the intensity of synaptic processes. The presence of polar day and night leads to an uneven supply of solar radiation to the sea during the year.

In the cold season, when the influx of solar radiation is absent or very small due to the low height of the Sun above the horizon, the primary climate-forming role is played by the circulation of the atmosphere and sea waters.

In winter, the heterogeneity of climatic conditions is more pronounced. In summer, the central role in climate formation is played by radiation conditions and ice melting; atmospheric circulation is weakened. The duration and boundaries of the climatic seasons do not coincide with the calendar dates.

The average monthly air temperature within the licensed area ranges from –18C° (February) to +8 C° (August). The absolute summer minimum (June) was –13 C°, winter minimum (February) –48 C°. Absolute maximums were observed in June and December and amounted to +29 C° and +2 C° respectively. Dates of the stable transition of air temperature through 0 C° are June 3 and October 10, the average number of days with negative air temperature is 236.

The frequency of strong winds at a speed of 15 m/s and higher in the winter months is about 10%. In the summer months, winds at a rate of 5–6 m/s are most likely. A continuous duration of winds of more than 20 m/s usually does not exceed 12–18 hours. The maximum possible wind speed once every 50 years (at an altitude of 10 m

above the surface, averaging is 10 minutes) is 30 m/s, a gust of wind is 42 m/s. The highest speeds and maximum gusts of wind reach the highest values in the autumn-winter period [14,16].

The main reasons affecting the range of visibility are fogs, precipitation and low cloudiness turning into a fog. Often such phenomena are observed in areas of the ice. With the increase in the fogs occurrence frequency in the summer months, a decrease in the visibility range during this period is usually associated. In winter, a reduction in visibility is often due to rainfall.

According to [14], the estimated lower limit of the velocity of the total currents in the navigation period in the surface layer of the sea in the area of work once in 100 years can reach 0.6 m/s. The maximum of the instrumentally measured velocity of the total currents was 0.4 m/s with their stability of 25%.

The prevailing directions of the total currents are oriented along the axis of developed tidal flows of the SE (high tide) – NW (low tide). Tidal currents are stable (90%). Their semidiurnal component, isolated from instrumental data, is estimated at 0.14 m/s. Quasi-constant currents are directed to the north with velocities of 0.03 m/s. Stock flows of the Pechora River are weak (0.01 m/s in June).

A great danger for all floating objects is icing [17]. The icing of ships in the area of work is possible in the autumn, winter and spring months, from October to March in the absence of ice cover.

1.2.2. Relief and soil

The bottom surface in the deposit area has a weak overall slope (0.0002), but in the centre, there is an oval uplift with an excess of 2 m. The relief consists of gentle elongated elevations and degradations of 1-2 m, in which currents with velocities of 9.8–15.9 cm/s act to a maximum of 0.44 m/s [14]. The soil is represented by sand, loam and clay of a dark grey colour. Table 1.3 presents the engineering-geological section of the soil.

Table 1.3

Engineering-geological section of the soil [14]

Depth (m)	Soil description	Properties
0.0-1.1	Fine-grained soil with properties of sand	c=4 kPA The angle of internal friction = 35 E=33 MPa
1.1-19.1	Intercalation of loam of dark grey colour and fine grey sand.	c=25 kPA, The angle of internal friction = 21 E= 16MPa
19.1-36.2	Dark gray clay	c= 50 kPA, Angle of internal friction = 18.5 E=19.5 MPa

As can be seen from Table 1.3, the soil conditions can be characterized as very mild. This fact is also noted in [18]. However, the soil in [18] has a significantly higher bearing capacity than in [14]. The permafrost layer begins at a depth of 10 m and spreads down.

1.2.3. Water depth

The sea depth at the southern boundary of the field is 14 m and increases to 22 meters up to the latitude of the northern border of the field. Therefore, in this work it is assumed that the depth increases by 0.36 m when moving from the southern border to the north by 1 km.

According to [14], in the licensed area, the estimated maximum value (range) of the total sea-level fluctuations can be 4.5 m once every 50 years and 4.7 m once every 100 years, which corresponds to the data presented in [19]. Such effect occurs due to the combined action of the circulation tides and non-periodic storm surge.

1.2.4. Waves

The maximum height for 100 years in the vicinity of the licensed area in [14] is set equal to 12.7 m, the period between wave peaks is given as 11.3 s, these values are somewhat consistent with the data provided in [19]. Values are averaged and assumed constant regardless of depth.

1.2.5. Ice conditions

According to long-term observations, ice formation in the licensed area begins in November – December and less often in mid-October. Cleansing from ice occurs in June – early July, sometimes in early August. The ice period averages 200 days, under extreme conditions – 250 days [14], which is typical for the Pechora Sea [11,19].

The Pechora Sea as a whole is characterized by the presence of annual ice of local origin, which form three main ice zones: the fast ice zone, the intermediate zone (interaction zone) and the drift ice zone [19].

Figure 1.6 shows the long-term mean positions of the fast ice edge in the southeastern part of the Pechora Sea from mid-November to March and from April to June. The approximate location of the license area is indicated by the shaded area.

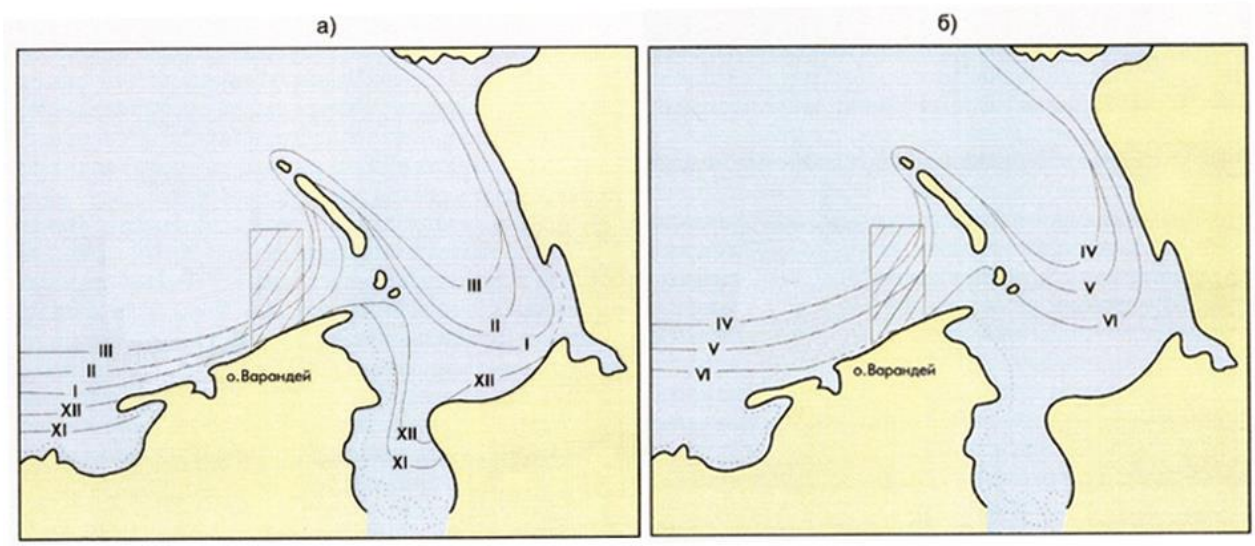

Figure 1.6 Average long-term positions of the fast ice edge in the southeastern part of the Pechora Sea a) from mid-November to March b) from April to June [14]

Considering the features of the field location (see Section 1.2) and the fact that the transition zone can extend from several hundred meters to several kilometres from the fast ice edge [19], it can be concluded that field A can be in any of the three zones. So, in the period from January to May (I - V) inclusive, the field is located in the fast ice zone, in June, November and December (VI, XI-XII) in the transition zone, or the drift ice zone.

In the fast ice zone, the thickness of the average maximum thickness of flat ice is from 0.9 to 1.1 m [10,19] and can reach 1.6 m [14]. Fast ice, however, is unstable

and its breaking often occurs during winter as well. As a result, the formation of ice ridges is possible, and up to 80% (3-4 points) of the entire sea surface in this zone can be occupied by hummocks [14,19].

In the interaction zone, the most intense interaction of ice fields (fast ice and drifting ice) occurs. Here a large number of hummocks, ice ridges and stamukhas are formed. According to [11,19], stamukhas are located at depths of 7–15 m and do not occur at depths higher than 20 m. When the stamukhas are formed, seabed gouging is possible with the formation of gouges. The hummocking in this zone is the most significant and can reach 5 points.

In the drifting zone, the maximum ice thickness averages 1.1 m and reaches a value of 1.6 m [19]. Lamination of ice up to 2.5-3 m thick is possible [11]. According to [14], in the southern part of the Pechora Sea, the speed of movement of ice floes under the influence of wind and currents reached 60–80 cm/s. According to calculated data, extreme drift here can occur at a speed of up to 140 cm/s. The general direction of such a drift is northeast.

According to [10,14], in the Pechora Sea water area there is no multi-year ice; in [11], however, the possibility of its migration from the Kara Sea is noted, and the probability is considered extremely low. In the licensed area, according to[10,20] the likelihood of an iceberg appearing is extremely low.

The hummocking in each of the zones, as already noted, is significant. Table 1.4 shows the hummock data in the area where the field is located.

Table 1.4

The hummocking data in the area of the deposit location (points) [14]

Month	Nov	Dec	Jan	Feb	March	Apr	May	June	July
Average	1	1.5	2	2.5	3	3.5	2.5	2	1
Maximum	1.5	2	3	3.5	4	4.5	4	3	2
Hummocking once in 50 years	2	3	3.5	4	4.5	5	4.5	4	2.5

Hummocking once in 100 years	2.5	3.5	4.5	4.5	5	5	5	4.5	3

The sizes and shapes of hummocks are diverse. However, for engineering calculations, the assumption is made that hummocks are symmetrical. The ideal hummock layout is shown in Figure 1.7.

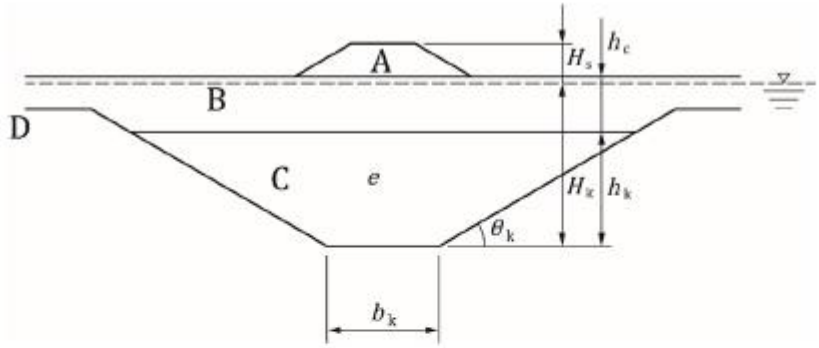

Key

A	ridge sail	h_c	consolidated layer thickness
B	ridge consolidated layer	h_k	vertical distance between the base of the consolidated layer and the base of the keel
C	ridge keel		
D	level ice	b_k	width of the base of the keel
H_s	sail height	e	keel porosity
H_k	keel depth	θ_k	keel angle from horizontal

Figure 1.7 The ideal hummock layout [10]

The thickness of the ridge consolidated layer (B) can exceed the thickness of the surrounding ice by 1.2–2.1 times [21]. In the case of deterministic calculations, the thickness of the consolidated layer should be taken equal to the double thickness of the surrounding ice [10]. Thus, for the ice conditions of the license area, the maximum possible value of the consolidated layer can be considered $h_c = 1.6 \cdot 2 = 3.6$ m. Also, following [14], the keel depth in the zone of the license area should be taken equal to the water depth minus the thickness of the consolidated layer (for the depths of the license area), angle internal friction equal to 30 degrees, keel cohesion – 10 kPa, porosity – 0.3.

1.2.6. Transport infrastructure in the Pechora Sea

Currently, in the north-west of Russia, oil is transported by railways or by pipeline to the ports of the White and Barents Seas (Arkhangelsk, Vitino, Murmansk).

Hydrocarbons are delivered to these ports by sea by tankers, including from the Pechora Sea from the Varandey stationary marine ice-resistant unloading terminal (MIUT) and Prirazlomnaya platform

MIUT «Varandey» is installed at a depth of 17 m more than 22 km from the coast and approximately 40 km from field A. The MIUT has a height of more than 50 m and weighs more than 11,000 tons. The design consists of a support base with accommodation for 12 people with technological systems and a rotary device for mooring and loading with a crane and helipad. The octagonal support base can withstand high ice loads. MIUT is installed at the bottom with 24 piles and connected to the shore by two subsea pipelines. The terminal operates with zero discharge, all industrial and human waste is collected in specific containers and transported ashore for subsequent disposal, which ensures environmental safety [22].

The infrastructure of the terminal, in addition to the MIUT itself, includes [23]:

- Onshore oil depot with a capacity of 325 000 m^3;
- Pump station;
- Power-generating facility;
- Tanker fleet (3 tankers);
- Auxiliary fleet (icebreaker and tugboat);
- Floating storage and offloading unit with a lifting capacity of 260 000 t;
- Shift camp for 180 people.

The characteristics of the tanker fleet are given in Table 1.5.

Table 1.5

Characteristics of the MIUT «Varandey» tanker fleet [23]

Name	Deadweight	Class	Type
Vasily Dinkov	71250 t	Arc6	PANAMAX
Kapitan Gotskiy	71230 t	Arc6	PANAMAX
Timofey Guzhenko	71290 t	Arc6	PANAMAX

Oil is delivered to the Varandey terminal via oil pipelines from the fields of PJSC Lukoil in the Nenets Autonomous Okrug. Since the beginning of 2018, PJSC Lukoil has been offloading oil in the Kola Bay via the Kola storage tanker, which is capable of processing 12 million tons per year. The tanker is able to unload 100–140 thousand tons of oil from the terminal simultaneously. Another storage tanker located in the Kola Bay is the Umba tanker owned by Gazprom Neft PJSC. Umba is equipped with separate storage systems for raw materials from the Novoportovskoye and Prirazlomnoye fields. The Umba tanker is equipped with oil intake, storage and shipment systems and is capable of receiving vessels standing simultaneously on both sides of it. Oil transhipment is carried out around the clock. The volume of cargo transhipment from Umba in 2017 amounted to 8.24 million tons.

According to [24], the application of storage tankers in the transport scheme for the handling of bulky cargo provides significantly higher efficiency of export deliveries compared to direct deliveries, due to the reduced duration of round trips for ice-class tankers. The use of such a logistic scheme is possible since the Kola Bay does not freeze.

The Prirazlomnoye field, which is currently the only hydrocarbon field on the Arctic continental shelf, can be considered a unique feature of the Pechora Sea. The field is located on the shelf of the Pechora Sea, 55 km north of the village of Varandey. Oil from the Prirazlomnaya OIFP is offloaded throughout the year to the Umba tanker on Arc 6 ice-class oil tankers equipped with an ice-breaking bow and stern [7,23,25]. The characteristics of the oil tankers of the Prirazlomnaya OIFP are shown in Table 1.6. Tankers provide reliable shipment of up to 6 million tons of crude oil, supplied to the world market with year-round navigation in harsh conditions. Tankers can move without the help of icebreakers in ice up to 1.2 m thick in winter.

Table 1.6

Characteristics of the Prirazlomnaya OIFP oil tankers [25]

Name	Deadweight	Class	Type
Kirill Lavrov	71053 t	Arc6	PANAMAX
Mikhail Ulyanov	69830 t	Arc6	PANAMAX

From the ports of the White and Barents Seas, oil is then transferred to tankers for subsequent transportation by sea to the west either directly or through oil transhipment complexes in the Kola Bay. The main sea transport routes run along the coast of Norway in the provinces of Vestlandet, Trøndelag, Nordland, Tromsø and Finnmark [23]. Most of the oil is transported to Rotterdam. A part is transported to the UK, Germany, Belgium, the Netherlands, France and the USA [26].

1.3. Analysis of the situational factors

As already noted, when choosing a system for arranging an offshore oil and gas field, several factors (criteria) should be taken into account. They can be divided into the following groups [1]:

1. Group of the situational factors;
2. Geological group;
3. Technological group;
4. Economic group.

The design conditions for field A, described in Section 1.2 of this chapter, belong to the group of situational factors (criterion). Using the criteria of only this group is not enough to fully justify the choice of the offshore oil and gas field arrangement system. However, it is enough to narrow down the range of potential options significantly.

The most significant situational factors include the depth of the sea, the ice conditions, the distance to the shore, the presence or absence of infrastructure on the coast, the location of consumers, soil properties and environmental conditions [1].

1.3.1. Sea depth and ice conditions

Based on the first two criteria (sea depth and ice conditions), we can conclude which OSGS, MODU and vessels can be operated in these conditions. To do this, based on the data presented in [1,7,9,13,28,29], the analysis of the possibility of using various OSGS, MODU and vessels at depths from 14 to 22 m (not only in the Arctic conditions), as well as in the presence of first-year ice, was carried out. The results are presented in Table 1.7.

Table 1.7

OSGS, MODU and vessels that can be applied for hydrocarbons production (or production and storage)

Vessel/structure	Production	Production Storage	Water depth = 14..22 m	Ice environment	
				First year ice	Ridges 4-5 b.
Rock/Gravel/Sand Island	FP	FP	FP	FP	FP
GBS	FP	FP	FP	FP	FP
Jack-Up	Q	NO	FP	FP	TBD
Jacket	FP	NO	FP	FP	TBD
FPSO	FP	FP	Q	FP	TBD
Drilling Ship	C	C	FP	FP	TBD
Round Shaped FPSO	Q	Q	NO	FP	TBD
Semi-submersible	FP	C	NO	FP	TBD
TLP	C	C	NO	FP	TBD
SPAR	C	Q	NO	C	TBD
Subsea Glory Hole	FP	NA	Q	FP	TBD
	Transportation of product				
Tankers	FP		FP	FP	FP
Pipeline	FP		FP	FP	FP
FP - field proven; Q - qualidied; C - Concept; NO - does not meet requiments ; NA - not applicable					

As can be seen from Table 1.7, according to the selected criteria for an operation to equip field A, gravity platforms can be used as oil and gas production or oil production and storage facilities. For transportation of products, both Arc 6 ice-class tankers and pipelines with the need for burial can be used, which was already mentioned in section 1.2.6.

The application of stationary platforms is also possible, according to the studied criteria for hydrocarbon production. However, there is no data on the use of this type of platform in the high hummock conditions specific to the licensed area of field A (see Section 1.2.5).

As can be seen from Table 1.7, SPS Glory Hole designs are used in first-year ice conditions, however, according to [6], at the moment there are no completed projects where this design would be used at depths of up to 76 m. In existing projects (see Table P. 1.1) the Glory Hole design is mainly used to protect against the effects of icebergs. Even though in [6] noted the technical feasibility of applying this design at depths of 15 m and more, the article does not contain information on the permissible degree of

hummocking and the allowable characteristics of hummocks and stamukhas in the area of SPS installation. In [7], in general, the inexpediency of using subsea and combined methods of arrangement (see 1.1) at depths less than 50 m in conditions of freezing seas is noted. Thus, the SPS of the Glory Hole design is not considered further in the concept development for field A.

Artificial islands, according to [9], it is advisable to use at depths of 10-12 m (see Table. 1.1). However, the possibility of application even at depths up to 20 m is considered in some works [6,27]. Nevertheless, there is no reliable evidence that such projects can be cost-effective. At the same time, the construction of an artificial island at depths of up to 12 m is only profitable if there is a sufficient amount of building material near the field [9,28]. There are no data on the availability of adequate volumes of stone, gravel, etc. in the vicinity of deposit A. Thus, it cannot be concluded that it is advisable to use artificial islands for concept development of the field A.

1.3.2. Location of the end-consumers

The location of the end-consumers largely determines the way oil transportation from the field. In the conditions of the transport infrastructure of the Pechora Sea (see 1.2.6) and the lack of developed support on the shore, it is advisable to export the produces hydrocarbons to Europe through the port in the Murmansk city. Murmansk is located at a distance of more than 1000 km west of field A. The construction of a pipeline at such a distance in the ice conditions of the Pechora Sea is unprofitable.

Pipeline transportation of oil to the Varandey terminal (see 1.2.6) (over a distance of more than 40 km east of the field), followed by transportation of Arc 6 class tankers (see 1.2.6) to the Murmansk city is also not economically viable. Such a method could significantly reduce capital costs due to the absence of the need for the temporary storage of hydrocarbons at the producing OSGS. However, the investments necessary to build a pipeline, pump hydrocarbons over long distances, rent the terminal, increase the number of elements of the logistics chain and the total length of the route in comparison with the direct offloading to tankers from producing OSGS, will significantly increase the capital costs of the project.

Thus, the hydrocarbons offloading directly from OSGS with their further transportation by Arc 6 class tankers to the port of Murmansk is the only rational transportation option for oil export to Europe. Moreover, the OSGS used for production should be able to store hydrocarbons for a particular time. In this case, the application of stationary platforms for hydrocarbon production becomes impossible (see Table 1.7), and the only suitable OSGS for the development of field A is a gravity-type platform.

1.3.3. Gravity-based platform

Gravity-based platforms can be used not only for oil production and storage but also for drilling wells. They are used in a large number of Arctic projects (see Fig. 1.3; A 1.1).

According to [18], if it is necessary to store hydrocarbons, at depths up to 30 m, gravity-based platforms of the caisson type should be used.

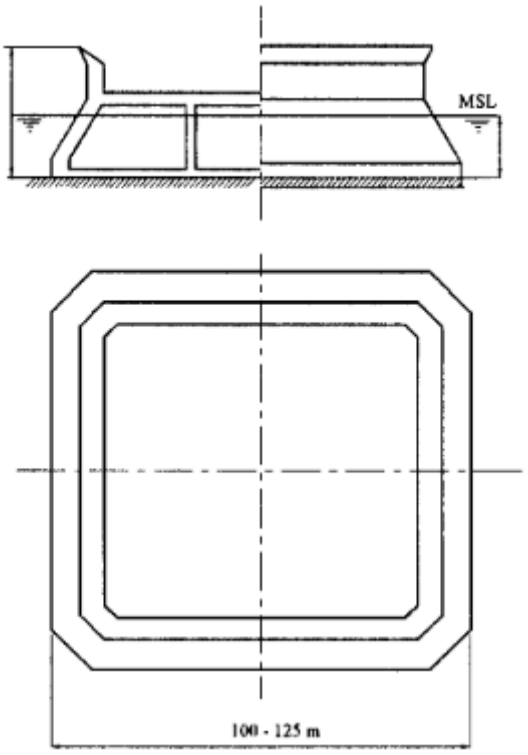

Figure 1.8 Gravity-based platform of the caisson type

Gravity-based platforms have a significant mass, which ensures their overall stability when exposed to external loads from ice, wind and waves. So, gravity platforms of the caisson type can weigh more than 30 000 tons significantly.

1.3.4. Soil

Due to the massiveness of the platforms, their installation is possible only in water areas, with the soil of sufficient bearing capacity [7,9,18].

As noted in Section 1.2.2, the soil conditions on the license area are characterized as mild. Thus, if it is necessary to install a caisson-type gravity platform on the license area, it is required to carry out work to replace part of the soil at the installation site to a depth of 10 m (the beginning of the permafrost layer) (see 1.2.2) with more durable material. It is worth noting that, in contrast to the construction of an artificial island, in this case, significantly smaller amounts of soil material are required.

1.3.5. Principal layouts of the field

As noted in Section 1.1, the application of the gravity-based platform for oil production and storage with its subsequent offloading to the tanker determines one of the basic layouts for the development of offshore oil and gas fields in the Arctic (see Table 1.1). This field layout refers to the surface type of offshore field development and is represented by three Arctic projects: Hebron, Hibernia, Prirazlomnoye (see A1.1). The platforms of the first two projects are located in the waters of the Big Newfoundland Bank at depths of 95 and 80 m, respectively, and do not belong to the caisson type.

The Prirazlomnaya platform, as noted in 1.2.6, is located in the Pechora Sea at a depth of 20 m. The platform consists of three sections: the upper structure, the intermediate deck and the gravity-type caisson. The dimensions of the caisson are 126x126 m at the base and 102x102 m in the upper part, the height is 24.3 m. The internal volume of the caisson is used both for oil storage (124 000 m^3) and for storage of diesel fuel, water and drilling fluids. Oil is offloaded to tankers (see Table. 1.6) with the help of automated remote devices. The logistic scheme of transportation is considered in 1.2.6.

The platform weighs 247 000 tons with solid ballast and 117 000 tons without it. Forty wells were drilled from the platform, the production volume is 21 000 m^3 per day. The staff is 200 people. The autonomy of the platform is 60 days [7].

The Prirazlomnoye project is a confirmation of the possibility of successful implementation of the considered arrangement layout in the conditions of the Pechora Sea. Technical and technological solutions of this project can also be used in concept development for field A.

1.3.6. Distance to the shore and coastal infrastructure

The implementation of the considered arrangement layout (see 1.3.4) requires the presence of a specific infrastructure both for the platform's construction and for its maintenance.

In [18], the possibility of using such enterprises of the Sverdlovsk and Arkhangelsk regions as the Northern Machine-Building Enterprise, Zvyozdochka, and others for the construction of platforms is noted. A supply base is needed to service the platforms. The supply base can be built by the company. However, this involves not only substantial capital costs for the construction of the base itself, but also the development of the necessary additional infrastructure. Therefore, a more rational solution is to rent coastal supply bases in the area of the Varandey shift camp. Distances from various points of the licensed area to the village can be considered moderate (see 1.2, 1.2.6).

1.3.7. Conclusions

Analysis of situational factors allows to draw the following conclusions.

The development of field A should be carried out using one of the basic layouts for the development of offshore oil and gas fields used in Arctic conditions. This layout involves the use of a gravity-based platform for drilling, production, primary processing and storage of hydrocarbons, followed by their offloading to ice-class tankers. This scheme (field layout) should be taken for the further development considerations of field A, taking into account its following features.

1) The gravity-based platform should belong to the caisson type of gravitational platforms;
2) It is presumably necessary to replace the soil at the platform installation site;
3) Supply bases should be rented;

4) Oil offloading should be carried out to the Arc 6 ice-class tankers with characteristics similar to those given in Table 1.5, 1.6;
5) Transportation should be carried out to the transhipment base in the Murmansk and then transported to Europe.

The further process of concept development of field A involves an analysis of the remaining groups of factors (see 1.3). So, the next chapter is devoted to the study of a group of geological factors.

2. Characteristics of the field-A

This chapter analyses the geological factors that influence the selection of the field-A development concept.

The features of the field reservoir system are examined, and conclusions are drawn about possible development methods along with the feasibility of using enhanced oil recovery methods.

2.1. Characteristics of the field-A

Field-A includes 9 productive formations of various ages (A1-A9). Table 2.1 presents the averaged characteristics of reservoir properties and the properties of their saturating fluids. The table is based on the results of well logging, dynamic well testing, seismic surveys conducted by Rosneft. Three objects of development can be distinguished according to the proximity of reservoir properties of the formations, and the similarity of physicochemical properties and compositions of the formation fluids at the field [14].

The first object (from now on referred to as object A) includes layers A1, A2, A3, A4. They are characterised by significantly lower initial pressures and temperatures compared with the layers of the second (A5) and third objects (A6, A7, A8, A9), and also higher density, viscosity and lower solution gas-oil ratio in these reservoirs (see Table. 2.1). The layers of the second and third objects, however, occur at much greater depths, which implies higher capital costs during well construction if they are used. Besides, they have more significant rock fracturing and contain less than 10% of the initial geological reserves, that is why they are not considered as operational objects in this work.

All reservoir beds belong to the carbonous Lower Permian oil-and-gas-bearing complex, composed mainly of carbonate rocks. Within the framework of the first development object, two deposits can be distinguished – northern and southern [14]. The conventional border of the deposits is shown in Figure 2.1 (see 2.1.2).

Table 2.1

Reservoir properties and properties of saturating fluids of the field-A formation system

Parameters	A1	A2	A3	A4	A5	A6	A7	A8	A9
The average depth of the layer cap (absolute depth mark), m	1353	1398	1420	1440	2412	3214	3241	3272	3353
Type of deposit	Bedded, massive, tectonically and lithologically screened deposit			Bedded, massive, tectonically screened deposit		Layer-uplifted, tectonically screened deposit			
Type of reservoir	Cavernous-fractured, mixed, carbonated					Cavernous-fractured			
Oil productive area, thousands m^2	52 276	45 904	60 488	54 845	24 084	14 150	12 871	5 844	1 257
Averrage net pay zone, m	29.6	20.9	15.5	42.8	25.1	14.4	18.9	10.7	6.7
Porosity	0.103	0.129	0.108	0.103	0.060	0.032	0.035	0.032	0.033
Oil saturation factor, fraction unit	0.861	0.796	0.825	0.887	0.880	0.900	0.900	0.900	0.900
Core permeability, 10^{-3} μm^2	4.1	5.1	3.1	0.5	1.6	-	-	-	-
Permeability (faults), 10^{-3} μm^2	-	-	-	-	60.0	211.0	211.0	-	0.7
Permeabilitydynamic testining, 10^{-3} μm^2	65.6	168.7	125.8	4.5	60.0	-	394.5	-	0.7
Net-to-gross ratio, fraction unit	0.40	0.67	0.33	0.36	0.24	0.72	0.59	0.36	0.90
Initial formation temperature, °C	30.3	31	33.5	35	56	71	72	79	86
Initial formation pressure, MPa	13.9	14.4	15	15.4	25.4	45.7	45.9	46.2	57.2
In-situ oil viscosity, mPa s	45	45	45	45	5	0.62	0.62	0.62	0.62
Oil density at surface, kg/m^3	932	932	932	932	851	805	805	805	805
Oil Water Contact True Vertical Depth, m	-1564.4	-1564.4	-1564.4	-1564.4	-2499.3	-3582.6	-3582.6	-4193	-3757.4
Formation volume factor, fraction unit	1.032	1.032	1.032	1.032	1.136	1.468	1.468	1.468	1.468
Bubble-point pressure, MPa	5.65	5.65	5.65	5.65	7	21.05	21.05	21.05	21.05
Gas-oil ratio, m^3/m^3	18.8	18.8	18.8	18.8	80	182.5	182.5	182.5	182.5
Reservoir water viscosity, t/m^3	0.738	0.738	0.738	0.738	0.738	0.738	0.738	0.738	0.738
Water density at surface, t/m^3	1.041	1.041	1.041	1.041	1.041	1.041	1.041	1.041	1.041
oil	6.58	6.58	6.58	6.58	-	26.68	26.68	26.68	26.68
water	4.3	4.3	4.3	4.3	4.3	4.3	4.3	4.3	4.3
rock	6.6	6.4	8	6.8	11.8	5	5	5	5

Rosneft PJSC provided the hydrodynamic model (HDM) of the first development object in three probabilistic implementations as initial data: P10, P50, P90. A probabilistic assessment allows anticipating risks when making technological and technical decisions on the method of development and operation of the field. So,

the implementation of P50-case can be used for a fundamental economic assessment of various development methods, and P10-case and P90-case allow to assess the impact of uncertainty in this evaluation [29].

2.1.1. Initial geological reserves

A probabilistic approach is also used to estimate resources of a field, where P90-case correspond to proven, P50-case to probable, P10-case to possible [30]. Table 2.2 shows the initial geological reserves of field A for the first development object, corresponding to each case of the HDM. The proximity of the geological reserves for the P50 and P90 is primarily due to the same level of oil-water contact in both cases (see 2.1.3), as well as a similar distribution of other reservoir properties (see 2.1.4).

Table 2.2

Initial geological reserves of the object A

Case of HDM	P10	P50	P90
Initial geological reserves, million tons	760	495	478

2.1.2. Oil-bearing contour

In Section 1.2, it was already noted that field A has a significant oil productive area, which is mainly determined by the layers of object A and varies in the range from 4590 to 6049 (ha) (see Table 2.1). The oil productive area has an elongated shape.

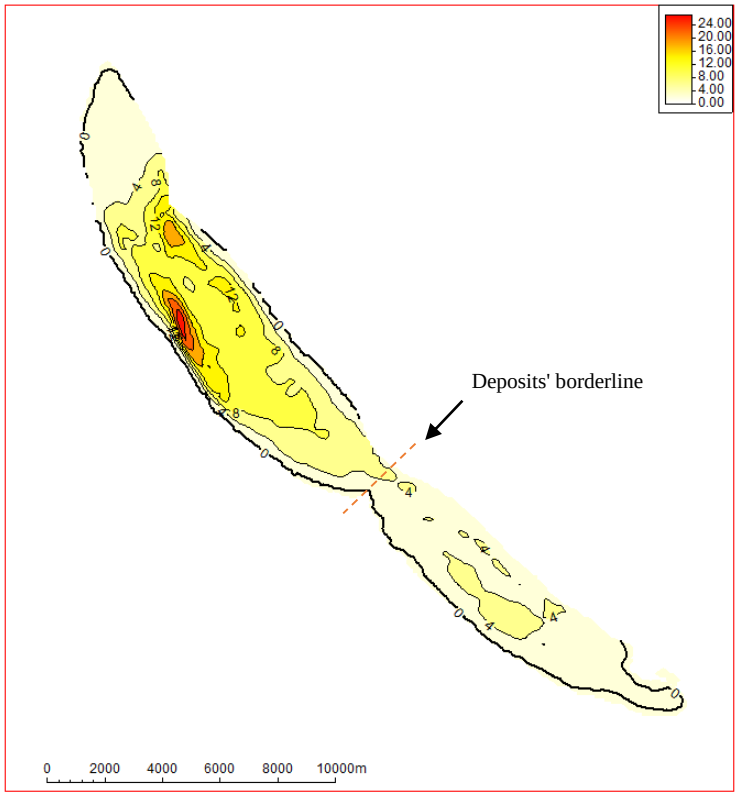

Figure 2.1 Map of the density distribution of the initial geological reserves of object A, t/ha (P50)

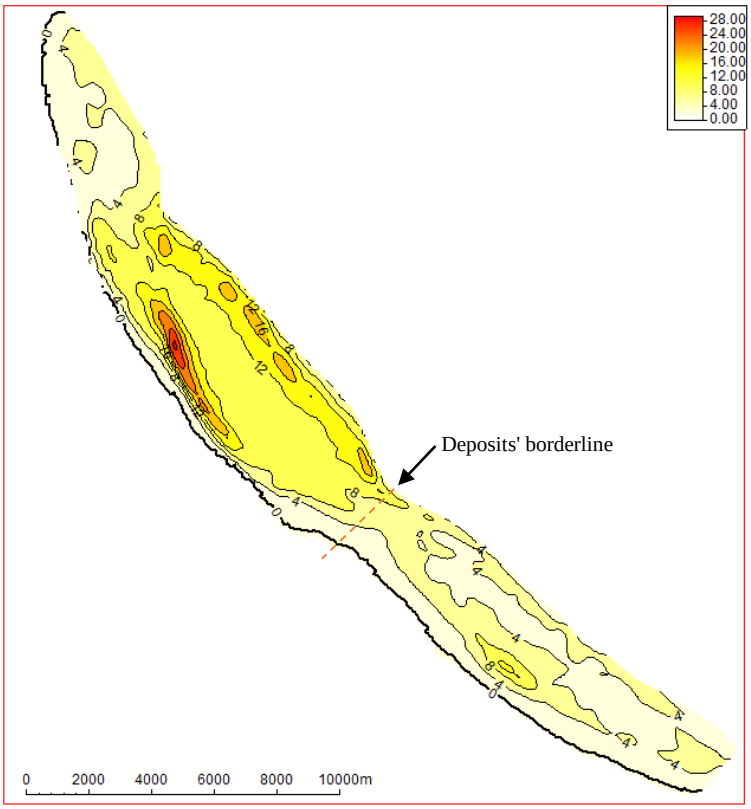

Figure 2.2 Map of the density distribution of the initial geological reserves of object A, t/ha (P10, P90)

Figure 2.1 shows a map of the density distribution of the initial geological reserves of the object A development for the implementation of P50-case. This pattern of the density distribution of geological reserves is also characteristic of the cases P10, P90 (Fig. 2.2). As can be seen from Figure 2.1, the southern deposit has significantly lower oil reserves (less than 20% of the initial geological reserves of the entire object).

The utilisation of the maps shown in Fig. 2.1, 2.2, the absolute distances from one point inside the contour to another could be determined.

2.1.3. Initial conditions of the hydrodynamic model

hydrodynamic reservoir models, equilibrium initialization is implemented [31], . at the initial moment of time, in each cell of the region, the value of reservoir pressure is calculated according to the hydrostatic distribution of the pressure specified at a certain depth. The reservoir temperature is set by the corresponding constant (see table. 2.1). At the water-oil contact (WOC), oil saturation corresponds to residual oil saturation, which is achieved by setting the corresponding capillary pressure at the contact (see 2.1.6).

The level of WOC for the P50-case and P90-case is selected following Table 2.1 as the most reliable (determined by the lower perforation hole). The value 1771.5 is chosen as the WOC for the implementation of P10-case as the last closed hypsographic curve. Figures 2.3 and 2.4 show a 3D model of Object A with the oil saturation distribution for the realisation of HDM. Table 2.3 shows the WOC levels of the layers of object A.

Figure 2.3 Oil saturation distribution for object A (P10)

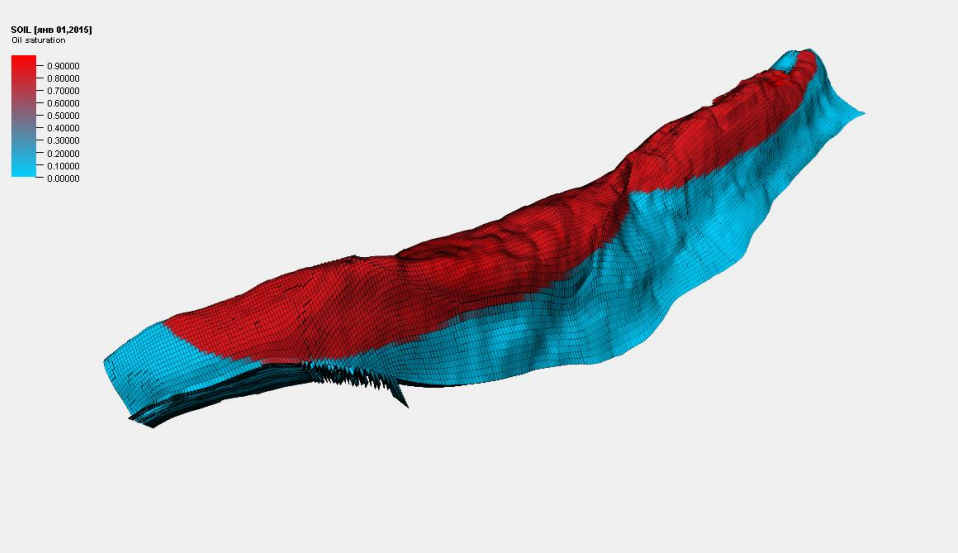

Figure 2.4 Oil saturation distribution for object A (P50, P90)

Table 2.3

WOC levels of layers of object A

Layer	Formation pressure, MPa	WOC level, m		
		P10	P50	P90
A1	13.6	1771.5	1564.4	1564.4
A2	13.8	1771.5	1564.4	1564.4
A3	15.0	1771.5	1564.4	1564.4
A4	15.2	1771.5	1564.4	1564.4

2.1.4. The main reservoir properties of object A

The ranges of changes in the reservoir properties of object A are shown in Table 2.4. As can be seen from the table, the range variations are insignificant depending on the implementation of the HDM. The exception is permeability ranges for cases P10 and P50. Horizontal histograms of permeability distribution for implementations for these two cases are shown in Figure 2.5. The average values of permeability differ from those presented in table 2.1 due to the presence of fractures.

Table 2.4

The main reservoir properties of the layers of object A

Parameter	P10			P50			P90		
	min	aver	max	min	aver	max	min	aver	max
Net pay zone, m	0.4	100	301	0.4	103	270	0.8	99	291
Oil net pay, m	0.3	89	252	0.1	75.6	244	0.2	73	229
Porosity, fraction unit	0.04	0.11	0.23	0.04	0.11	0.24	0.01	0.11	0.24
Permeability coefficient, mD	4.8	98.7	1182	2.4	48.6	591	2.4	47	591
Oil saturation factor, fraction unit	0.27	0.87	0.98	0.24	0.86	0.97	0.28	0.81	0.98

Fracturing in the hydrodynamic model was taken into account by the use of a certain theoretical model of fractures in the form of a permeability factor adjusted according to the testing results. Fracture sizes below the level of resolving power of methods which could evaluate their properties. In this case, the application of dual-porosity models is impractical.

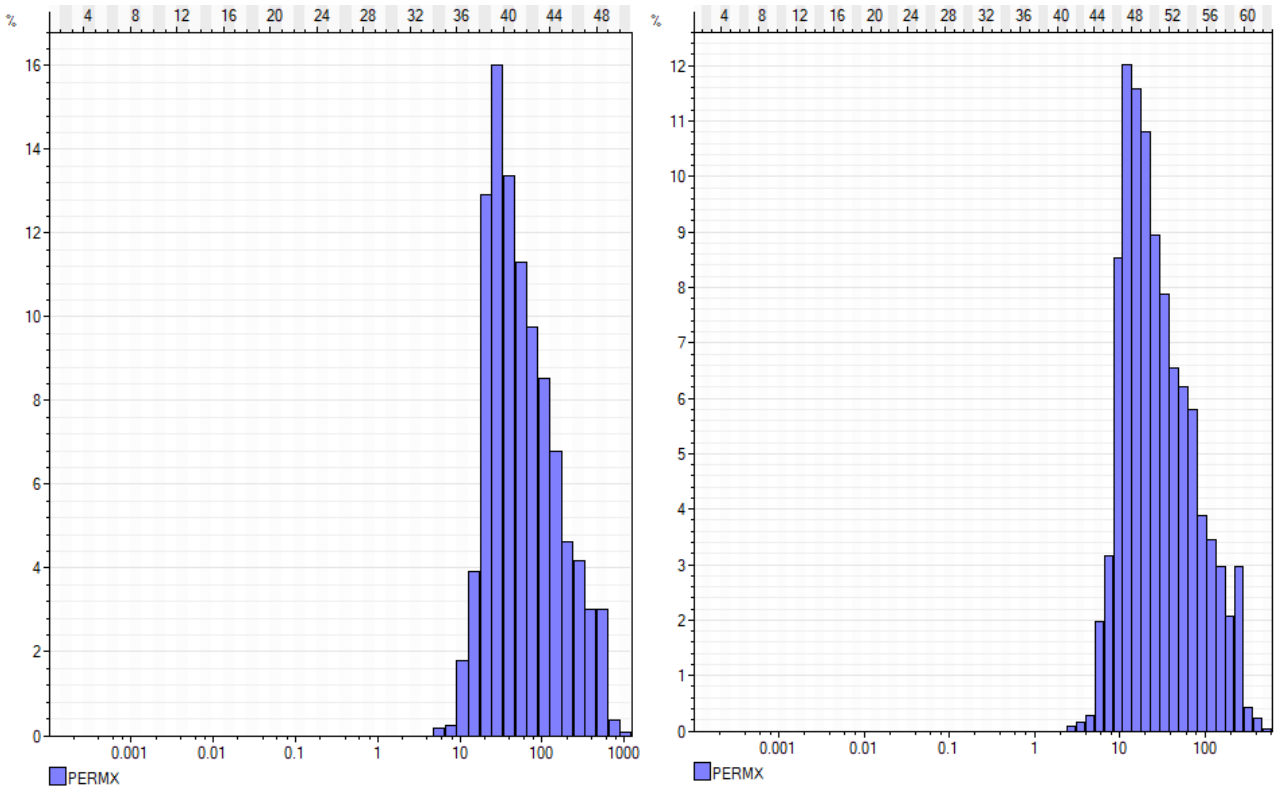

a) b)

Figure 2.5 Permeability distribution histograms a) P10 b) P50

2.1.5. Properties of the formation fluids

The oil properties of object A vary significantly depending on the chosen implementation case of HDM. So, the oil corresponding to the P10-case (see Table 2.5), according to the classification given in [32] can be classified as low-viscosity. P50-case oil refers to high viscosity oils, while oil of P90-case can be attributed to highly viscous. Other oil characteristics of object A for each case are shown in Table 2.5. It is worth noting that for all the layers of object A, the oil properties are determined to be the same in the framework of one case of HDM.

Table 2.5

Oil properties of object A

Parameters	P10	P50	P90
In-situ oil viscosity, mPa*s	28.7	45	61.3
Oil density:	-	0.92	-

in-situ, t/m^3			
at surface, t/m^3	0.923	0.932	0.962
Formation volume factor, fraction unit	1.051	1.032	1.03
Bubble-point pressure of the oil, MPa	-	5.65	-
Gas-oil ratio, m^3/m^3	20.5	18.8	14.25
Compressibility factor, 10^{-5} 1/MPa	76	65.8	32

The properties of brine water are assumed to be constant in all layers of object A, regardless of the selected case of the HDM. The features are presented in Table 2.6. In [14], compatibility of brine water with seawater was noted.

Table 2.6

Properties of brine water from object A

Brine water density at the surface, kg/m^3	1041
Brine water density in-situ, kg/m^3	1033
Brine water viscosity, mPs*s	0.738
Brine water compressibility, $1/bar*10^{-5}$	4.33

2.1.6. Relative phase permeability curves and capillary pressure

Relative phase permeability (RPP) in the water-oil system of formations rocks of object A, which describes the ability of a porous medium to pass through a phase that is not inert concerning the formation matrix, is shown in Figure 2.6. The shape of these curves, to a large extent, determines the efficiency of reserves recovery.

It is impossible to draw a firm conclusion about the type of wettable rocks in the form of the shown RPP curves. Nevertheless, rocks of layers A1 and A2 can be more likely to be classified as hydrophilic, and layers A3 and A4 to hydrophobic. For reservoirs A3 and A4, it is also worth noting a significant amount of residual oil saturation. The type of RPP curve does not depend on the case of HDM.

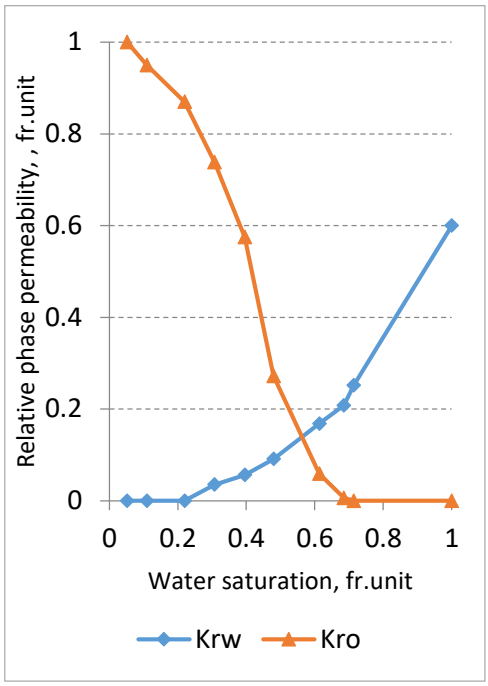

a)

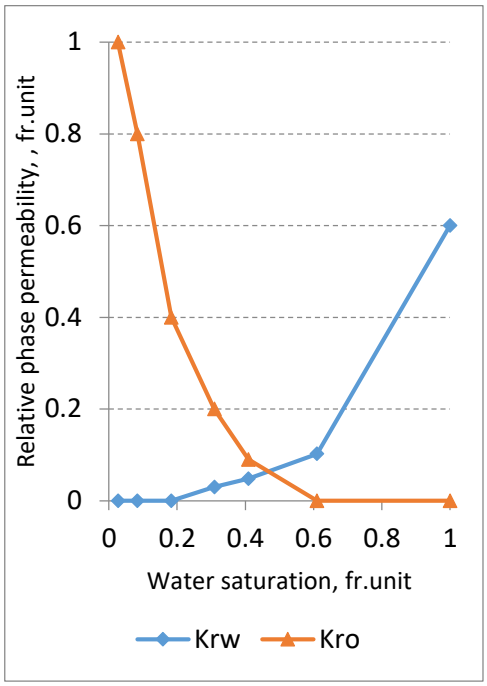

b)

Figure 2.6 RPP curves in the water-oil system for layers a) A1, A2 b) A3, A4

Figure 2.7 shows the capillary pressure curves, which also do not depend on the cases of the HDM. Based on these curves, the equilibrium initialization is implemented in the HDM (see 2.1.3).

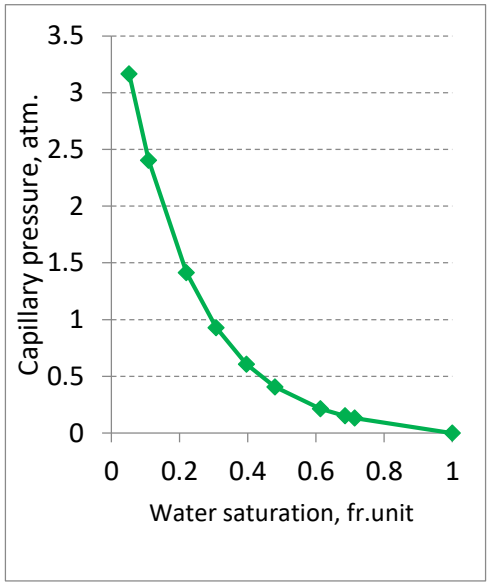

a)

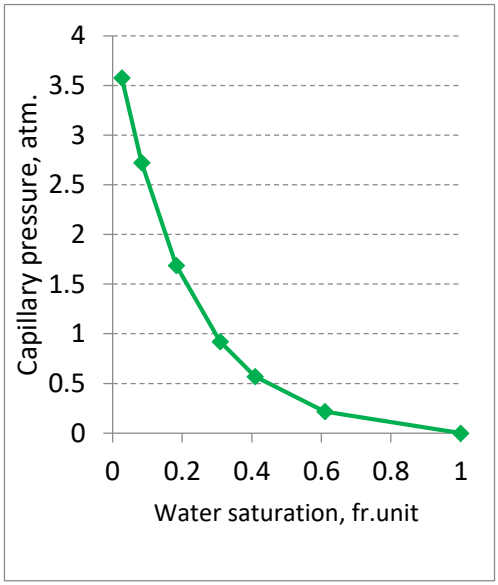

b)

Figure 2.7 Capillary pressure for layers a) A1, A2 b) A3, A4

2.2. Screening for enhanced oil recovery methods

The selection of the concept development of offshore oil fields largely depends on the choice of the influence method on the oil reservoir.

Although many fields are developed under natural recovery drive, for profitable development, it is necessary to influence the reservoir in one way or another. Thus, more than 80% of all oil deposits are developed using the method of maintaining reservoir pressure by injecting water into reservoirs. However, in this case, the oil recovery factor (ORF) remains quite low [33]. In addition to water flooding, there are other methods of influencing the oil reservoir, which can increase the oil recovery factor, for example, enhanced oil recovery (EOR) methods.

According to [34], EOR includes “reservoir stimulation methods that provide an increase in the final oil recovery coefficient compared to some basic method”. At the same time, the primary method can be both a method of maintaining reservoir pressure (water flooding) and a natural recovery drive.

According to the type of injected medium, EOR can be divided into [33]:

1. Hydrodynamic;
2. Chemical;
3. Thermal;
4. Gaseous;
5. Microbiological.

Today, there are a large number of methods for selection of EOR method. Moreover, only three main approaches are used in their construction [34,35]:

- Boolean logic;
- Fuzzy-set theory;
- Systems of artificial intelligence.

Regardless of the construction approach, any of the methods is based on a generalisation of the results of EOR industrial application. Generalisation revealed that different EOR could give a positive technological effect only in specific ranges of the geological and physical parameters of the formation and the physicochemical

properties of the formation fluids and gases. These ranges of values determine the applicability criteria for the EOR method.

Thus, the effectiveness of each EOR methods can be evaluated by comparing the values of the geological and physical parameters of the formation and the physicochemical properties of the formation fluids and gases of the field with the application criteria for EOR (EOR screening).

In this thesis, to construct a system for selection of EOR method for field A, we use a technique based on the theory of fuzzy sets [33].

Initially, based on the available data on the field, a list of the main parameters necessary for screening the EOR method is compiled (2.2.1). Then, the applicability criteria for each EOR (2.2.2) are determined from the list of selected parameters. For the subsequent determination of the compliance degree of the selected geological and physical parameters of the formation with the applicability criteria, the concept of the membership function is used [33] (2.2.3). After that, the value of the applicability function of each EOR (2.2.4) is determined.

The next step evaluates the factors that complicate the application of suitable EOR methods. Complicating factors include geological and physical parameters that may affect the final assessment of the applicability of EOR methods or even make their use impossible, however, not included in the initial list of basic parameters due to the low reliability of numerical values [35] (2.2.6).

The step-by-step screening process of EOR method for field A is considered below.

2.2.1. Selection of the reservoir system parameters necessary for the methodology and determination of the ranges of their values

For field A, among the parameters describing the formation properties and the properties of reservoir fluids, the parameters listed in Table 2.7 were selected. The parameters were selected based on the experience of [35] as the main ones. For most parameters, based on an analysis of Tables 2.1-2.6, ranges of their possible changes were identified due to uncertainties (variation based on a variety of absolute values). For some parameters that remain constant for each case of HDM, the range of the

parameter variation is defined as the difference between its maximum and minimum values for the object (change based on the range of absolute values) (Table 2.1).

Table 2.7

Parameters used for the EOR method screening

Parameter	Range of variation		Variation basis
The average depth of formation, m	1353	1500	range of absolute values
Average oil net pay, m	73	89	probabilistic assessment
Porosity	0.11	0.12	probabilistic assessment
Permeability, mD	47	98.7	probabilistic assessment
Average oil saturation	0.86	0.88	probabilistic assessment
Formation temperature, C°	30	35	range of absolute values
In-situ oil viscosity, cPs	28.7	61.3	probabilistic assessment
Initial formation pressure, MPa	13.9	15.4	range of absolute values

2.2.2. Determination of the applicability criteria for EOR method

Each EOR corresponds to a set of membership functions (MF) for each of the parameters of Table 2.7. Membership functions $\mu(x)$ and determine the degree of belonging to a variable x to the applicability criterion for EOR method. The MF of each criterion is characterised by certain values $x_{1\min}$, x_1, $x_{1\max}$, $x_{2\max}$, x_2, $x_{2\max}$. In this case, $x_{1\min}$, $x_{2\max}$ determine the zeros of the membership function; when x, equal to x_1 or x_2, the function takes a value equal to 0.5; $x_{1\max}$, $x_{2\max}$ determine the interval at which the degree of membership is 1. Thus, these values determine the shape of the curve of the membership function - determine the applicability criterion. $x_{1\min}$, x_1, $x_{1\max}$, $x_{2\max}$, x_2, $x_{2\max}$ for each applicability criterion of each EOR method is selected based on the generalised results of Russian and foreign EOR implementation projects [33–35].

$$\begin{cases} \mu(x) = 0,\ x \in (0, x_{1\min}] \cup [x_{2\max}, \infty) \\ \mu(x) = 1,\ x \in [x_{1\max}, x_{2\min}] \\ \begin{cases} \mu(x) = (1 + Y(x))^{-1} \\ Y(x) = \left[\left(\dfrac{x_{i\max} - x_i}{x_i - x_{i\min}} \right) \left(\dfrac{x - x_{i\min}}{x_{i\max} - x} \right) \right]^{2\cdot(-1)^i} \\ \begin{cases} i = 1, x \in (x_{1\min}, x_{1\max}) \\ i = 2, x \in (x_{2\max}, x_{1\min}) \end{cases} \end{cases} \end{cases} \quad (2.1)$$

2.2.3. Determination of the degree of belonging of the selected parameters to the relevant applicability criterion of the EOR method

To perform this task, along with a subsequent comparison of the screening results of EOR methods, was written an algorithm in Python. Its code is presented in Appendix 2.

As noted above, in Table 2.7, each parameter is specified by a range of values. In this case, the algorithm calculates the values of the membership function according to equations (2.1) for values belonging to ranges with a specific elementary interval and then determines their average value.

This thesis examines the screening of the following EOR methods.:

Thermal: steam treatment (ST), well steam treatment (WST), hot water injection (HW), steam-assisted gravity drainage (SAGD);

Gaseous: dry gas injection (DG), rich gas injection (RG), NGL injection (NGL), CO^2 injection (CO^2), nitrogen injection (N^2), water-alternated-gas injection (WAG), water-alternated-gas injection with foam (WAG-f).

Chemical: polymer flooding (PF), surfactant flooding (SF).

For each parameter of Table 2.7, the degree of its belonging to each of the listed EOR methods according to the relevant applicability criteria is determined. The results are presented in Table 2.8.

2.2.4. Determination of the applicability function of each EOR

The applicability function can be determined by several types of estimates [34]. Among them are optimistic, weighted average and pessimistic. In this thesis, a pessimistic assessment is used. In this case, the applicability function is determined by equation (2.2).

$$c_i = \min \mu_{ji}, \tag{2.2}$$

where i - EOR method, j - applicability criteria.

Depending on the values of the applicability function, four groups of applicability degree can be distinguished: $c_i = 0.8 - 1$ - ideal conditions, $c_i = 0.5 - 0.8$ - good conditions, $c_i = 0.2 - 0.5$ - adverse conditions, $c_i = 0 - 0.2$ - method is not applicable.

From Table 2.8 it can be seen that the parameters of Table 2.7 give poor conditions for surfactant flooding, as a result of which the possibility of using this method is not considered further, and excellent conditions for polymer flooding. The remaining methods for conditions for field A are not applicable.

Figure 2.8 shows the values of the membership functions of the selected ranges of parameter values (see Table 2.7) to the applicability criteria of polymer flooding. The figure is a screenshot of the code execution results piece presented in Appendix 2. The figure also shows the applicability functions for parameters not considered. These parameters are not taken into account due to lack of information.

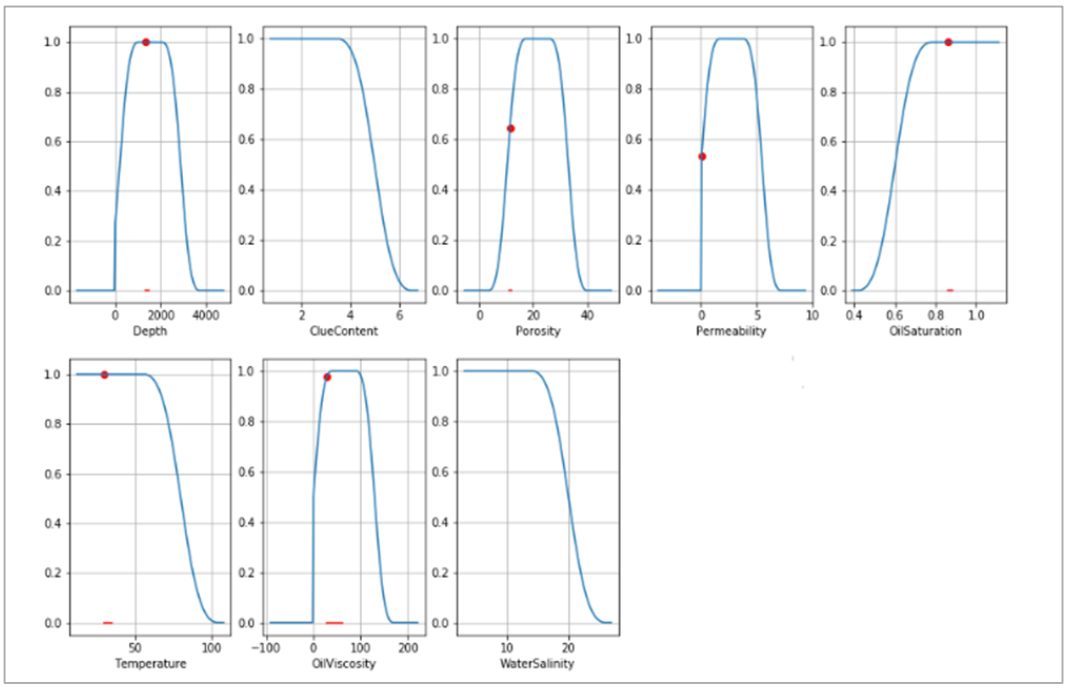

Figure 2.8 The belonging of the selected ranges of parameter values (see table. 2.7) to the applicability criteria for polymer flooding. The blue lines – the MF, the red lines – the ranges of values, the red dots – the values of the MF

Table 2.8

Values of membership functions of the ranges of selected parameters and applicability functions of the considered EOR methods for field A

Applicability criteria	ST	WST	HW	SAGD	DG	RG	NGL	CO^2	N^2	WAG	WAG-f	PF	SF
Average depth of formation	0.55	0.55	0.55	0.02	1.00	1.00	0.34	1.00	1.00	0.04	0.04	1.00	1.00
Average oil net pay	1.00	1.00	1.00	1.00	0.00	0.00	0.00	0.00	1.00	0.00	0.00	1.00	1.00
Porosity	0.00	0.00	1.00	1.00	1.00	1.00	1.00	0.69	0.99	0.69	0.69	0.66	0.69
Permeability	0.00	1.00	0.00	0.00	0.91	1.00	0.88	1.00	1.00	0.71	0.76	0.54	0.45
Average oil saturation	1.00	1.00	1.00	1.00	1.00	1.00	1.00	1.00	1.00	1.00	1.00	1.00	0.99
Formation temperature, C°	1.00	1.00	1.00	1.00	1.00	1.00	1.00	0.96	1.00	1.00	1.00	1.00	1.00
In-situ oil viscosity	0.35	1.00	0.93	0.00	0.00	0.00	0.00	0.89	0.00	0.00	1.00	1.00	0.90
Initial formation pressure	1.00	1.00	1.00	1.00	0.00	1.00	1.00	1.00	1.00	0.28	0.28	1.00	1.00
Applicability function value (min)	**0**	**0**	**0**	**0**	**0**	**0**	**0**	**0**	**0**	**0**	**0**	**0.54**	**0.45**

2.2.5. Features of polymer flooding

The primary mechanism for enhanced oil recovery during polymer flooding is to increase the sweep efficiency [36] of the layer in height and area. This effect is achieved by changing the properties of water when a polymer is added to it. Thus, an increase in its viscosity contributes to the alignment of the displacement front due to a change in the ratio of the non-wetting and wetting phases mobilities. Also, when applying polymer flooding, an improvement in the displacement ratio is noted [34].

The effectiveness of polymer flooding is characterised by a flow resistance factor determined by the ratio of water mobility to the mobility of the polymer solution. Figure 2.9 shows the dependence of the resistance factor on the filtration rate. From this dependence, it is seen that with the filtration rate increase, the mobility of the polymer solution gradually decreases due to an increase in viscosity. Such effect ensures alignment of the displacement front. This feature allows the use of polymer flooding, including in fractured reservoirs [37,38].

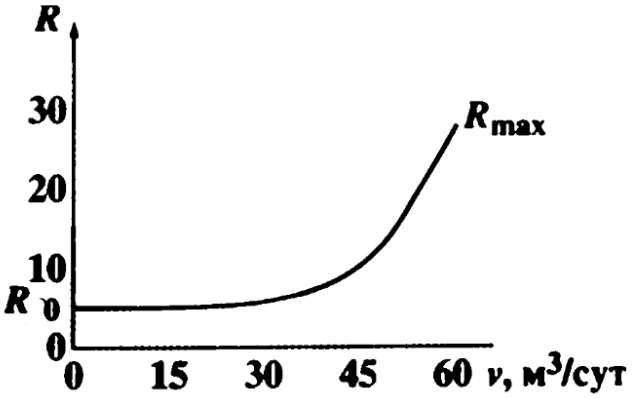

Figure 2.9 The dependence of the resistance factor R on the filtration rate v [34]

2.2.6. Complicating factors

The main criteria for the applicability of polymer flooding are presented as membership functions in Fig. 2.8. Further, complicating factors are considered, based on the analysis of which we can conclude that it is possible to use EOR methods in developing field A, in this case, polymer flooding.

One of the complicating factors in the application of polymer flooding is the predominance of carbonate rocks in the reservoirs of field A. This is because most

polymers are adsorbed in carbonates with a high degree. Nevertheless, this fact is not critical and, although, in smaller quantities, there are projects where polymer flooding is effectively used in carbonate rocks (see. [37]). In this case, it is necessary to use polymer solutions of a slightly higher concentration than in the case of terrigenous rocks.

Another complicating factor is the lack of accurate data on the salinity of brine water. So, in the case of differences in the salinity of the water used to create the polymer solution, and brine water, their mixing can significantly affect the efficiency of polymer flooding. In the case of polymer flooding at the last stages of field development, the salinity of brine water approximately corresponds to the salinity of the injected. In the case of polymer flooding, it is necessary to pre-pump the water rim from the beginning of development. In this case, according to [37], the effect of the difference in water salinity will have a smaller impact on the efficiency of polymer flooding.

2.2.7. EOR Screening Conclusions

Thus, according to the results of EOR methods screening, it can be concluded that of all the EOR considered (see 2.2.3), only polymer flooding can be used in the development of field A (according to the selected methodology for calculating the applicability function). In the case of applying the method from the beginning of development, it is necessary to pump the rim of water before the start of the polymer rim injection.

2.3. Analysis of geological factors

The most significant geological factors (criteria) include the area of the field, oil-bearing contour, the physical properties of the rocks and their saturating fluids, and the features reservoir system bedding

2.3.1. Field area and oil-bearing contour

The vast oil productive area (see 2.1.2) and significant geological reserves (see 2.1.1) of field A involve the drilling of a large number of wells. Nevertheless, the number of wells when drilling offshore is limited due to both technical features and their cost. Thus, the need for drilling a field with a rather rare grid of wells on large

areas is growing. In such cases, as well as in cases of an extended oil-bearing contour, according to [36], development layouts with centre-to-edge waterflooding and high intensity should be used, which include single-row well placement systems. Moreover, in the case of using horizontal wells, a staggered pattern should be applied. A single-row system involves drilling the same number of production and injection wells. Figure 2.10 shows an element of a single-row development system.

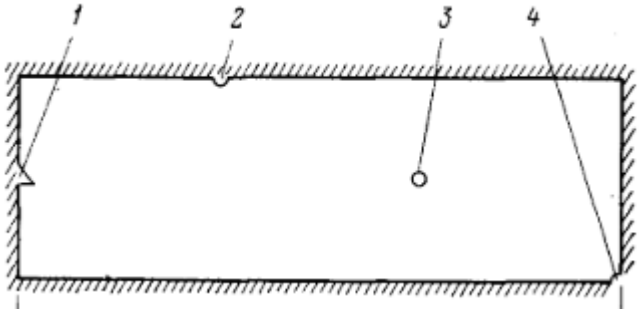

Figure 2.10 An element of a single-row development system [36]: 1 – “quarter” of an injection well; 2 – “half” of an injection well with a linear arrangement of wells; 3, 4 – respectively, “quarter” and “half” of the injection well

In the case of the implementation of the basic arrangement, the drilling of wells is carried out from one gravity platform. Therefore, a significant area of the field also indicates that the lengths of the unproductive part of the wellbore will be quite extensive.

So, in the case of the platform installation near the border of the Southern and northern deposits (see Fig. 2.11) and drilling the entire oil productive area of object A, the well deviation from the platform is on average 9 km. It means that the average length of the unproductive part of the wellbore is at least 9 km. The maximum magnitude of deviation is about 13 km.

Even in the case of significantly shorter well lengths (non-productive part of the wellbore) the costs of their construction, especially when developing an offshore oil and gas field, make up a significant, and in some cases, the most substantial part of the project investment. Therefore, bringing into the development of object A using the accepted (basic) arrangement scheme can be considered inappropriate.

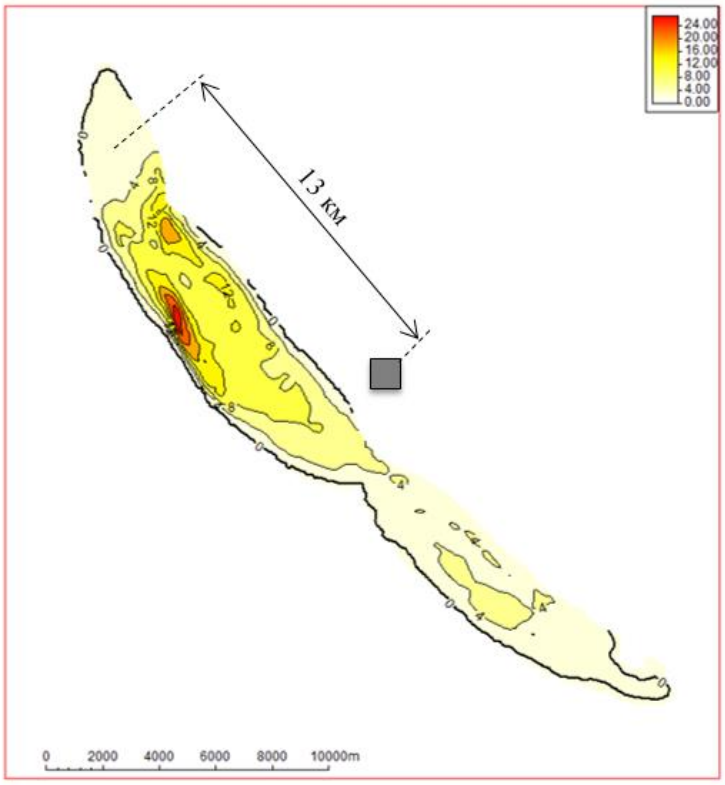

Figure 2.11 A possible installation site for the platform if it is necessary to drill the entire oil productive area of object A (shown in a gray square)

2.3.2. Initial geological reserves

As noted in 2.1.2, most of the reserves of field A are concentrated within the northern deposit (see 2.1). At the same time, the southern deposit simultaneously has both a lower density of geological reserves and a smaller oil content area (see Fig. 2.9). In this regard, we can conclude that for the development of the southern deposit will require fewer wells. At the same time, the expected value of the density of the well grid should be higher (less dense grid of the well placement system).

Thus, we can conclude that it is necessary to disaggregate the designated development object (object A) into two independent objects: the Northern and Southern deposits. The disaggregation of object A allows considering the possibility of using the basic field layout for introducing only the Northern deposit into development or finding an alternative field layout.

2.3.3. Field A development layouts

1. **Basic field layout**

In the case of applying the basic field layout for developing only the Northern deposit (see Fig. 2.10) and installing the platform in the area shown in Figure 2.12, the average distance between wells and the platform is 2.8 km. This, obviously, will significantly reduce the investment of the project. Nevertheless, in this case, the Southern deposit remains not involved in the development.

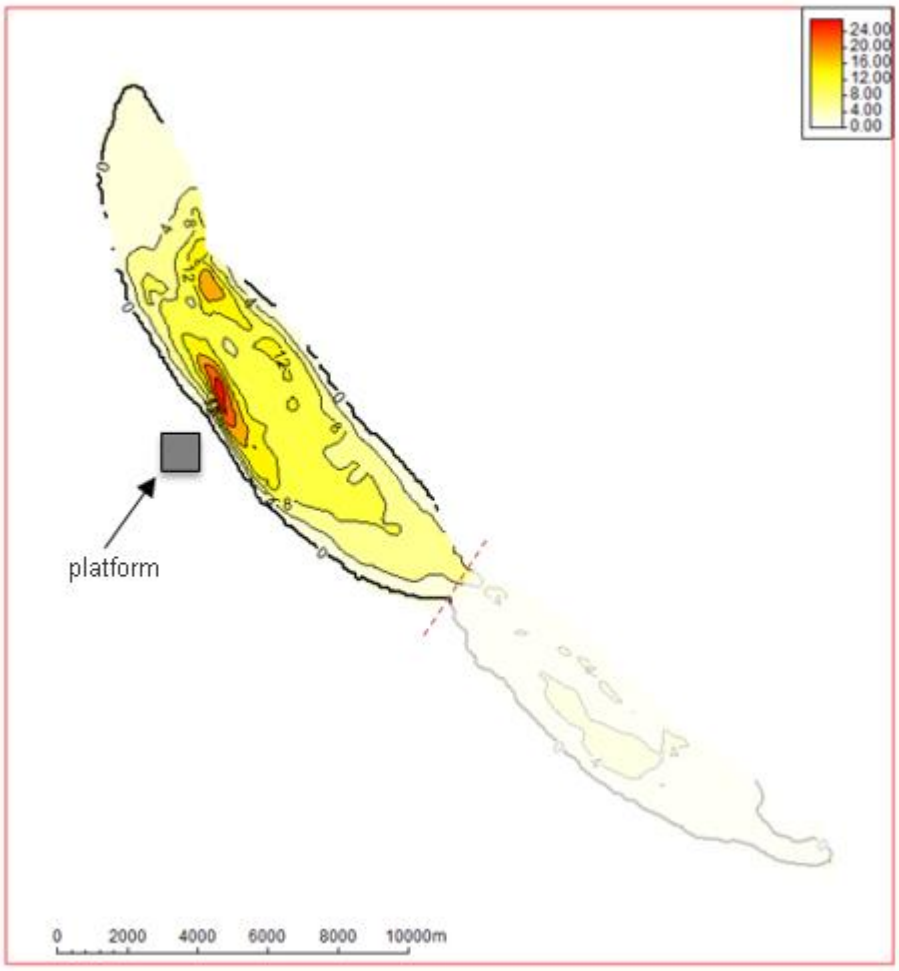

Figure 2.12 Schematic representation of the basic field layout application for the development of the Northern deposit on the map of the density of its reserves, tons/ha

2. Alternative field layout

An alternative field layout implies the application of an additional wellhead platform. Wellhead platform, in this case, is used for drilling a small number of wells (10-20) and hydrocarbon production. In this case, the primary processing of hydrocarbons before offloading to the tanker is carried out on the central platform.

The central platform, in this case, is a technological unit, it is used for the production, storage, processing and offloading of oil to a tanker. Hydrocarbons produced from the wellhead platform are transported to the central platform via a

pipeline system. The pipeline system also includes a line for transferring water (or polymer solution) from the technological platform, where it is prepared, to the wellhead platform, as well as pump modules necessary for pumping liquids. At the same time, trenching is necessary for pipelines (see 1.3.1).

This layout can be utilised both in the development of two deposits (first implementation) (see Fig. 2.13) and only the Northern (second implementation) (see Fig. 2.14). Moreover, in both cases, the use of this field layout can reduce capital costs relative to the use of the basic field layout for the development of both deposits. It is also achieved by significantly reducing the required well deviation from the platform. So, in the case of developing two deposits, the average well deviation is 4 km for the central platform and 2.7 km for wellhead platform. In the case of development of the Northern deposit – 3.1 km and 2.7 km, respectively. At the same time, the cost of construction and maintenance of the wellhead platform and the pipeline should be less than the difference in investment received by reducing the total penetration when drilling wells.

The costs required to implement the first option are more considerable since it involves the construction of a longer pipeline (12–15 km) than the construction of the second (5-8 km), as well as the drilling of wells of slightly higher length (in this case, the difference is not so significant). Nevertheless, the first option allows setting into operation two development objects, which can increase the final recovery factor.

In the case of using any of field layouts, the central platform is installed at a depth of 18 m. The wellhead platform is installed at a depth of 15 m in the first implementation and 20 m in the second.

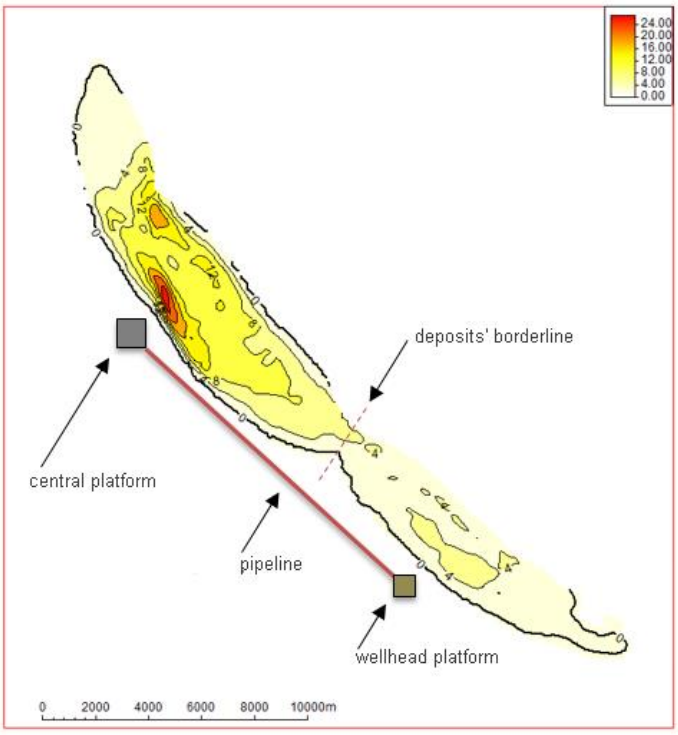

Figure 2.13 Schematic representation of the application of an alternative field layout for the development of the North and South deposits (first implementation) on the map of the reserves density of object A, tons/ha

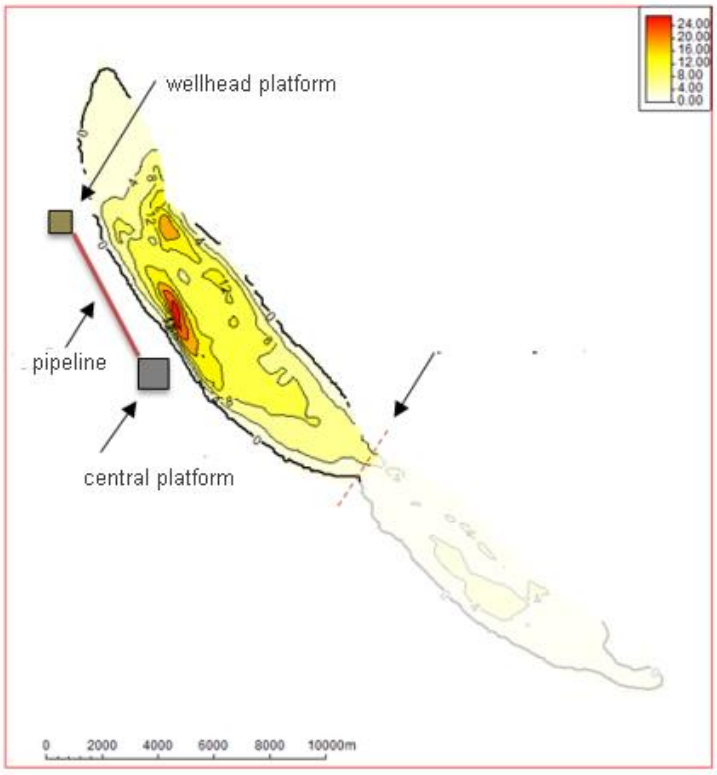

Figure 2.14 Schematic representation of the application of an alternative field layout for the development of the North and South deposits (second implementation) on the map of the reserves density of object A, tons/ha

2.3.4. Physical properties of rocks and liquids saturating them, features of the bedding system

Given factors largely determine the degree of applicability of specific EOR methods. So, according to the results of EOR screening, it was revealed that the water flooding and polymer flooding could be used as methods of influencing the formation system of object A.

Polymer flooding is by far the most common method among chemical EORs [37] and can increase the recovery factor by 5-8% [34]. When, as shown in [39], the cost of producing a unit of oil in polymer flooding may be lower than in traditional flooding.

The low prices and small dimensions of the equipment necessary to create a polymer solution make it possible to efficiently use this EOR method in the development of an offshore oil and gas field [40,41].

Among the features of the bedding system of object A, it can be noted that all four reservoirs lie one above other and have comparable oil productive area and net-oil thicknesses that range from 15.5 to 42.8 m. With such thicknesses, it is possible to consider the use of multilateral wells. The use of a multilateral well in the revelation of producing horizon, in this case, will allow us to drill one productive wellbore in each of the layers. Such approach should significantly increase the production capacity of the well, as well as increase the sweep efficiency by waterflooding compared to the case of horizontal wells when one well will have to open productive layers at some angle.

2.3.5. Conclusions

An analysis of geological factors has led to some conclusions.

Firstly, the development of the field should be carried out using a single-row well placement system with the staggered pattern.

Secondly, in the future, it is worth considering the use of two types of wells: directional wells and multilateral directional wells.

Thirdly, the development of the object A should be carried out using one of the following EOR methods: water flooding or polymer flooding.

Fourth, to develop a field, it is necessary to disaggregate field A into two separate objects: the Northern deposit and the Southern deposit.

Fifth, the development of the field can be carried out using one of two field layouts, which are referred to as the basic field layout and alternative field layout in the framework of this work. In this case, the basic layout is designed to use only the Northern deposits, while the alternative can be used to develop only the Northern deposits, and both deposits. Thus, further, we consider three types of implementation of field layouts.

The basic field layout is the arrangement scheme adopted in Chapter 1 (1.3.1). An alternative field layout is a variation of the arrangement scheme adopted in the first chapter, which implies the use of two platforms: technological (central) and wellhead connected by a pipeline system (see 2.3.3). Further, for convenience, the base version platform will be called technological, central or primary.

The further process of the concept development of field A involves an analysis of the remaining groups of factors (see 1.3). So, the next chapter is devoted to the study of a group of technological factors.

3. Analysis of technical and technological factors

3.1. Choosing the optimal development strategy

In this section, the optimal well spacing, well types, and stimulation methods are discussed.

The considered well spacing values are as follows:

- 64 he/w;
- 81 he/w;
- 100 he/w;
- 121 he/w;
- 144 he/w.

The following types of well completing are considered:

- Directional well (DW);
- Multi-lateral directional well (MLDW).

Considered stimulation methods are as follows:

- Waterflooding;
- Polymer flooding

Preliminary calculations were carried out for the North Deposit P50-case using the Petrel software package. Group constrains for injection wells included injection ratio equal to one. For producers bottom hole pressure was set not less than 6 MPa, because of the bubble point pressure limitation. The single-row with a staggered line pattern was considered. A typical gravity-based structure comprises around 40-50 wells [7]. So 50 wells were considered in consultation.

The efficiency of applied technology or method evaluated by the analysis of $\Delta NPV_j - ORF_j$, где ΔNPV_j - the difference between the net present value in the calculation $j\ (j \geq 2)$ and the net present value in the calculation $j = 1$ (base-calculation); ORF_j is the oil recovery factor in j calculation.

To calculate ΔNPV_j the following formula is applied:

$$\Delta NPV_j = \sum_{i=1}^{n} \left(\Delta R_{ji} - \Delta w_{ji} - \Delta p_{ji} - \Delta tx_{ji} - \Delta tr_{ji} \right) / \left(1 + dr\right)^i \quad (3.1)$$

где $\Delta R_{ji} = R_{ji} - R_{(j=1)i}$, $\Delta p_{ji} = p_{ji} - p_{(j=1)i}$, $\Delta R_{ji} = tx_{ji} - tx_{(j=1)i}$, $\Delta R_{ji} = tr_{ji} - tr_{(j=1)i}$

и $R_{ji}, w_{ji}, p_{ji}, tx_{ji}, tr_{ji}$ - respectively, revenue from sales of products, amortization of wells, costs of polymer flooding, costs of transportation, taxes and other payments for a year i of a j calculation; dr - discount rate, n - the life-time of the project.

This approach is used due to the lack of data on the part of the capital and operating costs. The same filed layout is considered for all calculations.

3.1.1. Well spacing

The well spacing is defined by the equation (3.2) [36].

$$S_c = \frac{S}{n_{скв}}, \quad (3.2)$$

where S - oil productive area, $n_{скв}$ - the total number of wells.

To determine the optimal well density with the selected well grid arrangement, several calculations were performed. The calculations were carried out for well grids with the following well densities: 64, 81, 100, 121, 144 ha/well. For each value, the calculation was carried out twice: with different rates of putting well in production: 10 wells/year and 5 wells/year, which may correspond to the use of two or one drilling complex on the platform. First, the calculation was carried out for the HW. The results of an economic performance evaluation conducted by formula (3.1) are presented in Figure 3.1. The optimal well density is 121 ha / well. Therefore, in all subsequent calculations well density is considered equal 121 ha/well. The well cost per meter is assumed to be equal to 11000 dollars / m in accordance with [14].

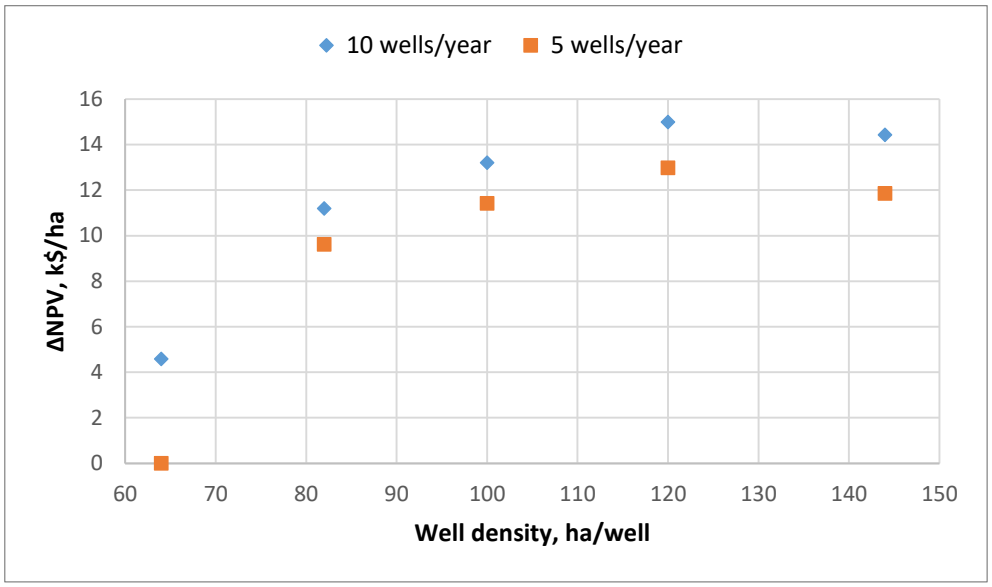

FIgure 3.1 Efficiency of using a single-row well arrangement system with different densities of well grids

3.1.2. Well types and the stimulation method

To determine the effectiveness of polymer flooding and determine the appropriate type of well, a joint series of calculations was carried out:

The cases are:

1. Waterflooding with 50 DW (base-calculation);
2. Polymer flooding with 50 DW;
3. Waterflooding with 25 DW for injection and 25 MLDW for production;
4. Polymer waterflooding with 25 DW for injection и 25 MLDW for production.

The sketches of wells are shown in Figures 3.2 and 3.3.

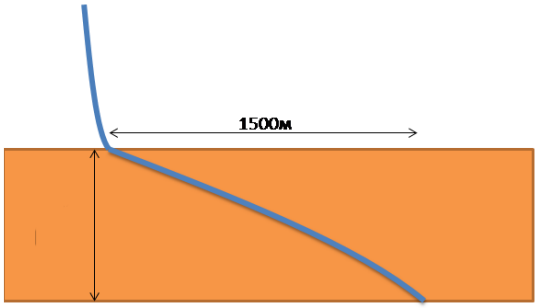

FIgure 3.2 Sketch of DW

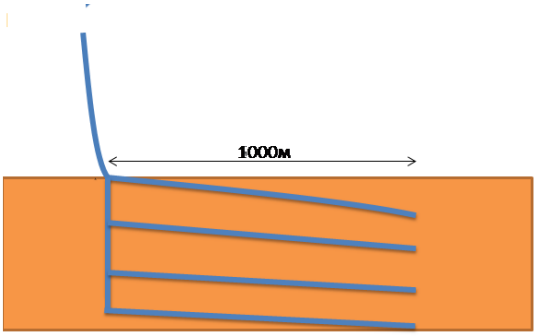

FIgure 3.3 Sketch of MLDW

It is proposed to use PAA as the polymer for creating the polymer solution. Modeling of polymer flooding consists of calculating in each cell of the model the concentration of the polymer solution, the corresponding viscosity and recalculation of the viscosity value. The viscosity was recalculated by the values given in table 3.1. A polymer was injected with a concentration of 0.4 kg / m3 as the most rational in the case of field A in accordance [14,37]. The cost of the polymer is taken equal to 4 dollars/kg in accordance with [42].

Table 3.1

The dependence of the viscosity of the polymer solution on the concentration of the polymer [14]

Концентрация ПАА, кг/м^3	0	0.4	0.75	1.5	2	2.5
Множитель на вязкость	1	2.9	7.5	28.2	64.5	138

The effectiveness of each case is determined by expression (3.1). At the same time, the NPV differences are calculated for three cases of oil prices: $ 30, 45 and 60 per barrel. The results are presented in figures 3.4-3.5. Table 3.1 presents the calculation results for the case of an oil cost of $ 45 per barrel. Figures 3.7 and 3.8 show the profiles of accumulated oil production and annual oil production, respectively. A comparative analysis of diagrams 3.4–3.5 and graphs 3.7–3.8 shows that the effectiveness of the use of MLDW is significantly dependent on changes in oil prices. Nonetheless, the drilling of the oil refineries significantly increases oil production. It can be seen from the diagram (Fig. 3.6) that the most effective is the combined use of polymer waterflooding and oil-gas condensate treatment.

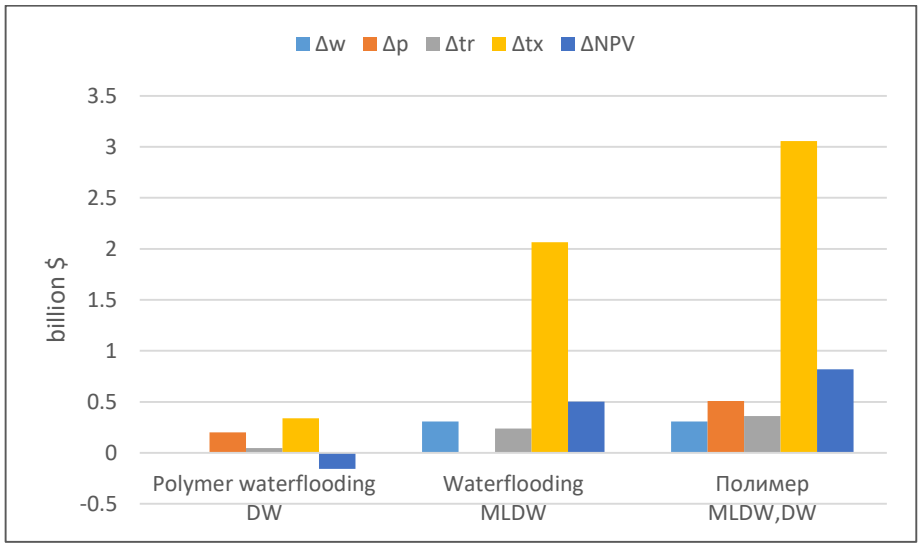

FIgure 3.4 Change of ΔNPV

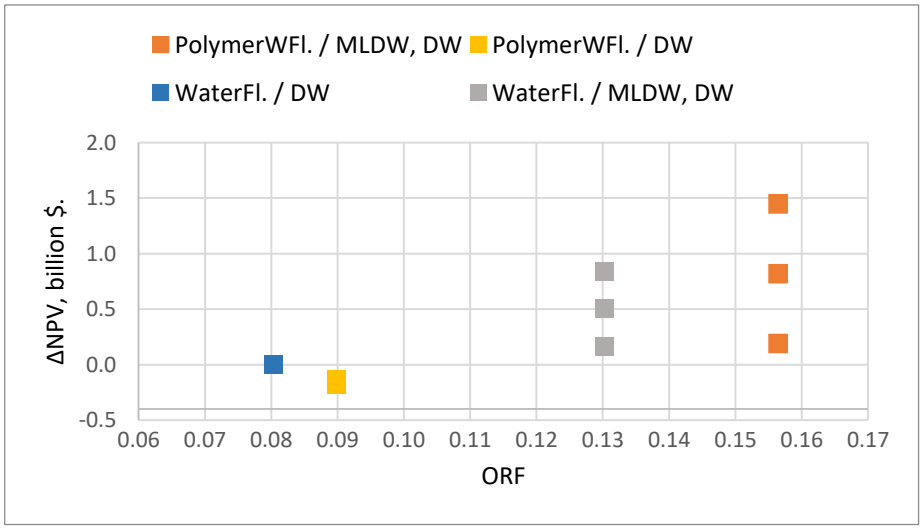

FIgure 3.5 Change of ΔNPV depending on oil price

t is also worth noting that the maximum oil production in the case of polymer flooding using MLDW is 2.7 million tons / year (see Fig. 3.7), 7592 tons / day, or 8145 m^3. This value can be used for a preliminary assessment of the design capacity of the technological platform, nevertheless, it is worth considering the condition of uncertainty. Thus, additional calculations showed for P10-case model, the maximum production is 5.6 million tons / year, 15449 tons / day or 16738 m3.

Table 3.2

the effectiveness of the use of polymer flooding and oil refineries at an oil price of $ 45 per barrel

Calculation		Well type		Δw, mln. $.	Δp, mln, $	Δtr, mln, $.	Δtx, mln, $	Volume of water injected, mln.m^2	Cumulated oil (50 years), mln, tonnes	ORF	ΔNPV, mln. $.	ΔORF
		Prod.	Inj.									
1	WaterFl. / DW	DW	DW	0	0	0	0	124.7	39.7	0.08	0.0	0.00
2	Polymer / DW	DW	DW	0	202	46	339	126.0	44.5	0.09	-159.0	0.01
3	Water / MLDW, DW	MLDW	DW	308	0	238	2065	386.7	64.5	0.13	502.6	0.05
4	Полимер / MLDW, DW	MLDW	DW	308	509	362	3056	317.9	77.4	0.16	817.4	0.08

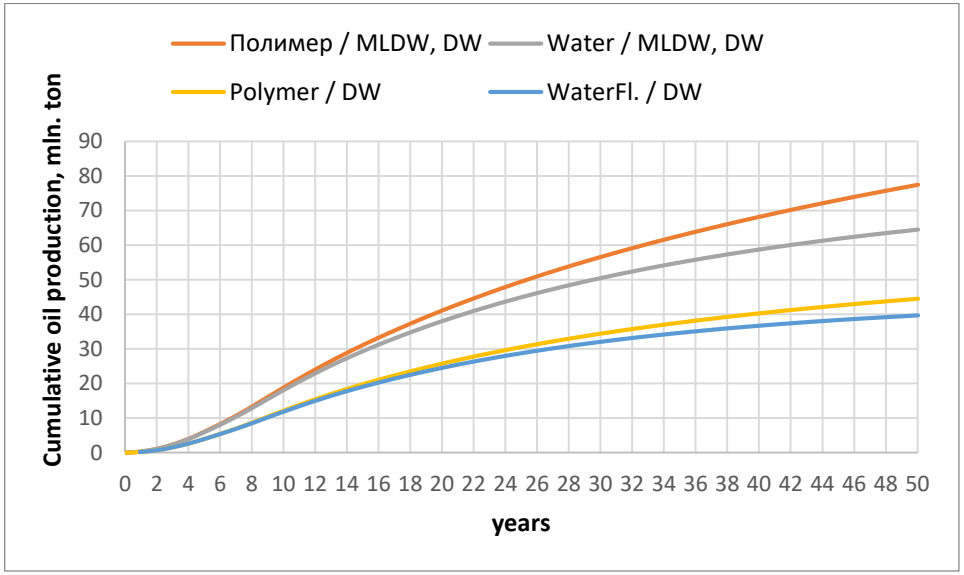

FIgure 3.6 Cumulative oil production

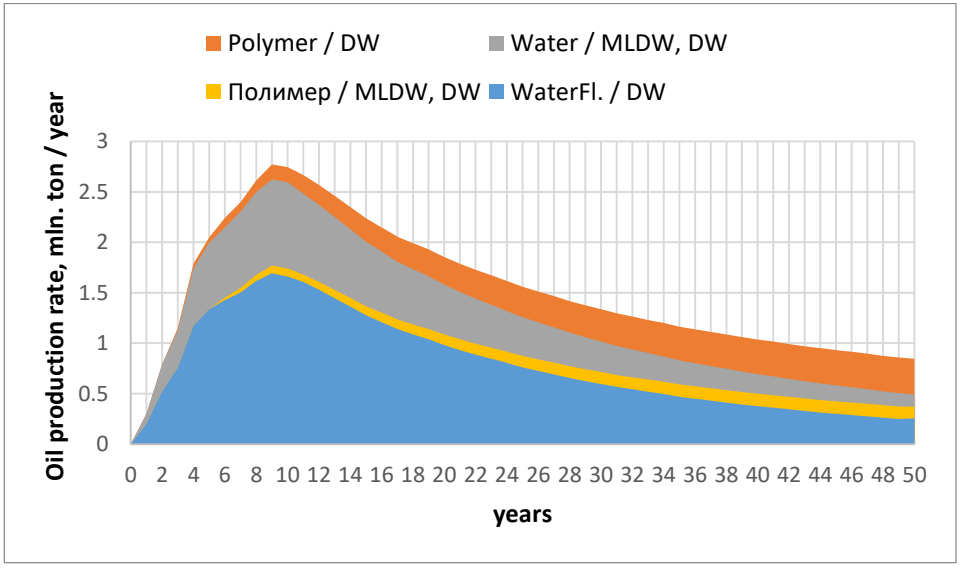

FIgure 3.7 Oil production rate

3.2. Gravity-based platforms

The basic field layout involves the use of a single gravity-based platform of caisson type (see 1.3.3). An alternative layout involves the use of two platforms, with the central platform-plate belonging to the caisson type platform as well, while the wellhead platform can belong to any of the types of gravity platforms (see 1.3.3) due to the absence of the need to store hydrocarbons (see 1.3. 1).

In the case of basic field layout only one caisson type gravity base platform is used.

Regardless of the field layout the dimensions of gravity-base structure and other characteristics are determined based on the characteristics of the upper structures of the platforms.

3.2.1. Upper structures of gravity-based platforms

The upper structures of the platforms consist of a complex of block modules. The sizes and the number of modules are determined based on the requirements for the functionality of the platform and the characteristics of the technological systems necessary to implement the required functionality.

In the case of both basic and alternative field layout, the main functions of the central platform are:

• Drilling of production and injection wells

• Preparation of formation and seawater for injection into the reservoir to maintain reservoir pressure.

• Preparation of polymer solution.

• Stabilization of downhole products

• Disposal of solution gas.

• Storage of crude oil.

• Shipment of products to shuttle tankers.

• Organization of residential modules, as well as the engineering equipment of the platform for the safe operation of facilities in the Arctic with zero emissions of hydrocarbons into the environment.

The wellhead platform has less functionality, which is limited by the following functions:

• Drilling of production and injection wells with one drilling rig.

• Disposal of solution gas.

• Storage of crude oil.

• Organization of residential modules, as well as the engineering equipment of the platform for the safe operation of facilities in the Arctic with zero emissions of hydrocarbons into the environment.

With such requirements for functionality, forecasted levels of fluid production, the upper structures of the technological platform should have an area of at least 9,000 m^2 and can have an aspect ratio of 100 mx 90 m, wellhead platform of at least 4,000 m^2 with an aspect ratio of 70 m x 60 m [1,2]. platforms include many deck levels inside the modules, which allows you to minimize the required area. With the agreed aspect ratios, the height of the upper structures should be 36 m and 40 m for the technological and wellhead platforms, respectively. The dry weight of the upper structures of the central platform is estimated to be at least 35000 tons, wellhead - at least 16000 tons. These dimensions and masses are accepted for platforms in this work.

3.2.2. Gravity-base

For the technological platform, the gravity base in two versions is considered: steel and concrete. For any performance, the aspect ratio in accordance with the dimensions of the upper buildings is taken to be 100 x 100 m. The necessary height of the caisson is 30 m. It is calculated taking into account the depth of the installation site, which is 18 m for any of applied field layout (see 2.3.3), as well as the height of the maximum wave (see 1.2.4) and fluctuations in water level (see 1.2.3). Thus, the freeboard height is 12 m and allows avoiding wave getting on deck in the case of a maximum wave and rised water level due to the combined action of the circulation tides and non-periodic storm surge. The height of the double bottom is assumed to be 5 m, the wall thickness is 10 m. With such dimensions, the weight of the caisson is approximately 40000 tons in steel and 80000 tons in concrete, according to [14] The sketures are shown on Figures 3.8-3.9.

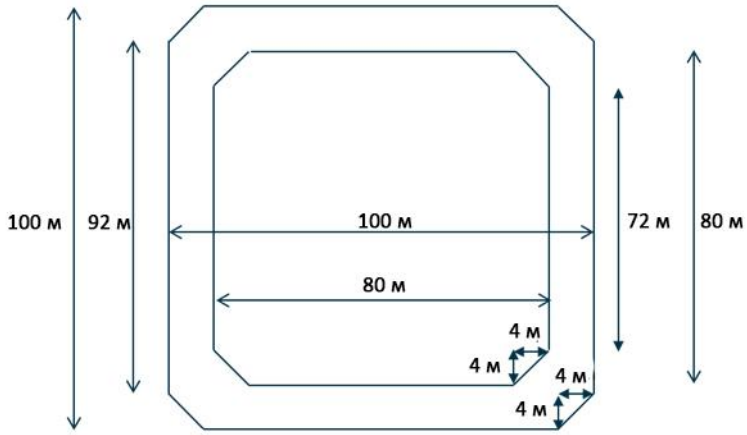

FIgure 3.8 Scheme of the the gravity base of the technological platform (top view)

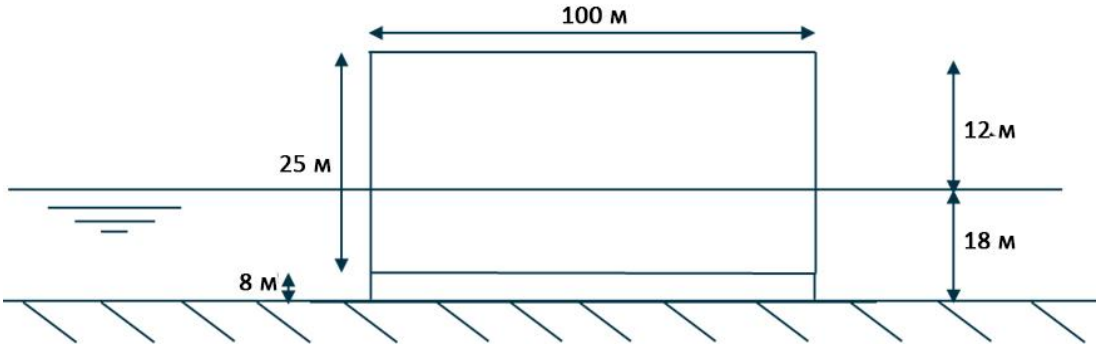

FIgure 3.9 Scheme of the the gravity base of the technological platform (side view)

3.2.3. Gravity base of the wellhead platform

The gravity base of the wellhead platform is considered in one version - a steel caisson. The use of a caisson will increase the general storage capabilities, which is necessary for applying an alternative field layout due to the supposedly higher production levels.

For the wellhead platform, the aspect ratio in accordance with the dimensions of the upper structures is taken to be 70 x 70 m. The wellhead platform, depending on the use of an alternative arrangement, is installed at depths of 15 m and 20 m and the necessary caisson heights are respectively 27 m and 32 m. The height of the double bottom is assumed to be 8 m, the wall thickness is 7 m. In the first case, the dry weight of the caisson is 24838 and 31000 tons

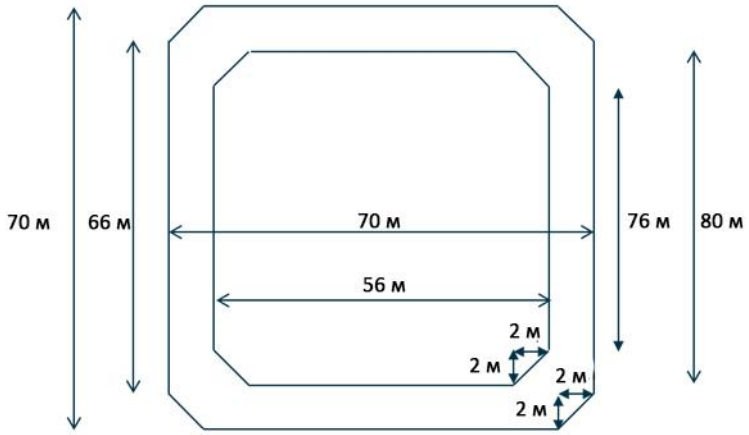

FIgure 3.10 Scheme of the the gravitational base of the wellhead platform (top view)

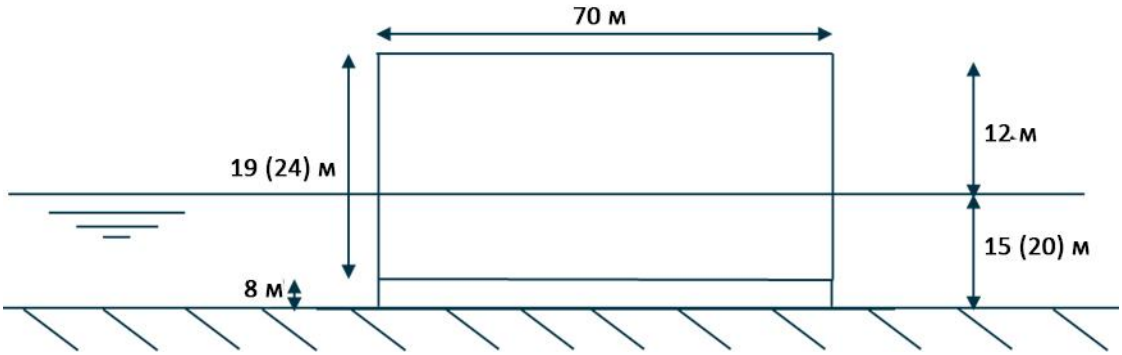

FIgure 3.11 Scheme of the gravity base of the wellhead platform (side view)

3.2.4. General platform features

For each platform, in accordance with the data [14], the main characteristics of the platforms are calculated, presented in table 3.3.

Table 3.3

General platform features

Parameter	Central platform (Steel cassion)	Central platform (Concrete caisson)	Wellhead platform installed at a depth of 15 m	Wellhead platform installed at a depth of 20 m
Number of well slots	52	52	24	24
Number of drilling rigs	2	2	1	1
Size of the upper buildings, m	100 90	100 90	70 60	70 60
The height of the upper buildings, m	36	36	40	40
Dry weight of the upper buildings, tons	35000	35000	16000	16000
The working weight of the upper buildings, tons	45000	45000	21000	21000
Type of gravity base (GB)	steel caisson	concrete caisson	steel caisson	steel caisson
The aspect ratio of GB, m	100 100	100 100	70 70	70 70
GB height, m	30	30	27	32
Installation depth of GB, m	18	18	15	20
The elevation of GB above sea level, m	12	12	12	12
The thickness of the ice barrier wall GB, m	10	10	7	7
The height of the double bottom of GB, m	5	5	8	8
Total volume (TV) of the GB, m3	300000	300000	132300	156800
The volume of GB minus the volume of the walls and the double bottom	200000	200000	95060	109760
The volume of oil storage (OS), m3	120000	120000	57036	65856
OS usage coefficient	0.92	0.92	0.92	0.92
Used OS, м3	110400	110400	52473	60588
Ration of OS to TV	0.40	0.40	0.43	0.42
The ratio of OS to TV minus the volume of the walls and the double bottom	0.60	0.60	0.60	0.60
Dry weight of GO without ballast, tons	40000	80000	24838	31000
Ballast mass in double bottom, tons	53000	53000	14000	14000
Ballast mass over a double bottom, tons	226000	226000	250000	250000
The mass of drill pipes, t	1500	1500	750	750

Total dry weight of the platform, t	355500	395500	305588	311750
Mass of OS filled with oil, t	102893	102893	48905	56468
Maximum platform weight, t	468393	508393	359493	373218

3.3. Stability of gravity platforms

Chosen dimensions and weight of gravity-based structyre, as well as interactions with the ground, should provide the initial position or initial static certainty of the structure [43]. In the case of the platforms under consideration (see 3.2) under the conditions of the licensed area of field A, a large number of horizontal forces are striving to change their initial position:

- Wind load;
- Ice load;
- Current load.

Согласно [43], conditions of shear and tilt stability is represented by the equations (3.3) и (3.4).

$$k_F = \frac{(Q - F_A) tg\varphi_g}{F_R} \tag{3.3}$$

$$k_M = \frac{QB}{2M_{on}} \tag{3.4}$$

where k_F - shear and tilt stability factors, respectively; Rollover Stability Factor Q - weight of the structure - the resultant of gravity passing through the center of the structure; F_A - the resultant force of Archimedes and the vertical component of wave pressure; φ_g angle of internal friction of the soil. F_{xR} - resultant of load forces acting on the wall of the structure; M_{on} - overturning moment; B - ширина стенки кессона.

If the coefficient values are greater than one, the platforms can be considered stable. In this paper, the forces from the influence of the current are assumed to be negligible compared to the forces from the influence of ice or waves (see 1.2.1). Therefore, the values of F_R и M_{on} will be determined by the force of ice action in winter and the force of waves action in summer. Therefore, to determine the stability of platforms, it is necessary to calculate wave and ice loads.

3.3.1. Wave load calculation

When calculating wave loads, it is first necessary to determine the theory on the basis of which the calculation will be built. This paper uses the Linear Wave Theory and the Diffraction Theory.

The task of the wave theory is to determine the relationship between the height H, period T and wave length L, as well as in the description of the characteristics of the movement of particles in the stream [44]. In all existing wave theories, assumptions are made that the bottom surface is flat, the waves exist on the plane XY, the wave is spreading in a positive direction X, and the liquid is considered incompressible and irrotational (sketch for a progressive wave train is shown in Fig. 3.7).

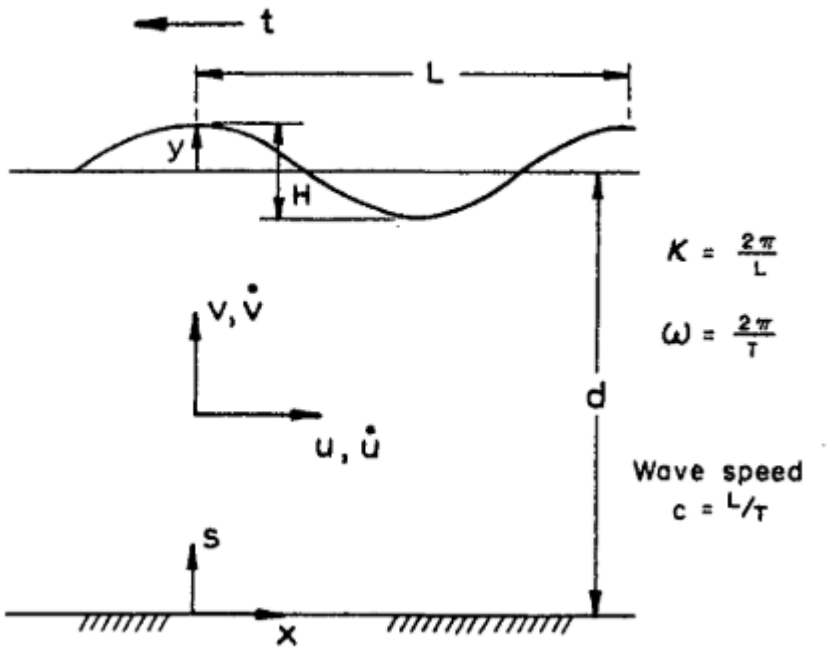

Рис. 3.12 Definition sketch for a progressive wave train [45]

The velocity potential is used to describe the characteristics of particle motion in the flow. φ. The definition of this function is the main task of the wave theory. The solution of this problem is reduced to the solution of the Laplace equation with boundary conditions at the bottom and on the free surface [45, p. 48]. This is a very complex task since the boundary conditions on the free surface are not linear and must correspond to the constantly changing boundary of the free surface. Various assumptions are used in various wave theories, which make it possible to simplify the solution of

the differential equation, however, they impose a number of theoretical restrictions on the use of a particular theory.

The simplest of theories is linear wave theory [19,44–47], in which the assumption is made that the boundary condition of the free surface can be linearized in the case of small values of wave heights relative to their length and water depth. Despite the assumptions made, the theory remains applicable beyond the limits of analytical validity over a fairly wide range, as shown in [45, p. 80]. In this work, when calculating wave loads, a linear wave theory is used, which can be considered an assumption. The basic equations of linear wave theory.

Wave profile:

$$\xi(x,t) = \xi_0 \sin(\omega t - kx) \tag{3.3}$$

where $\xi_0 = H/2$, t - time, ω - angular frequency, k - wave number (Fig. 3.7).

Velocity potential:

$$\varphi(x,z,t) = \frac{\xi_0 g}{\omega} \frac{\cosh k(z+d)}{\cosh(kd)} \cos(\omega t - kx) \tag{3.4}$$

Horizontal particle velocity:

$$u(x,z,t) = \frac{\partial \varphi}{\partial x} = \frac{\xi_0 k g}{\omega} \frac{\cosh k(z+d)}{\cosh(kd)} \sin(\omega t - kx) \tag{3.5}$$

Horizontal particle acceleration:

$$\dot{u}(x,z,t) = \frac{\partial u}{\partial t} = \xi_0 k g \frac{\cosh k(z+d)}{\cosh(kd)} \cos(\omega t - kx) \tag{3.6}$$

Dispersion relation:

$$\omega = gk \tanh(kd) \tag{3.7}$$

The dispersion equation enavles to determine the wavelength L corresponding to the period T and depth d. It is solved with iteration technique [28]. In this paper, the Newton method was used [29].

When calculating the wave, it is necessary to take into account the force regime, which can be determined with the help of dimensionless parameters H/D, $\pi D/L$ (D - characteristic body size) and the diagram Figure 3.14.

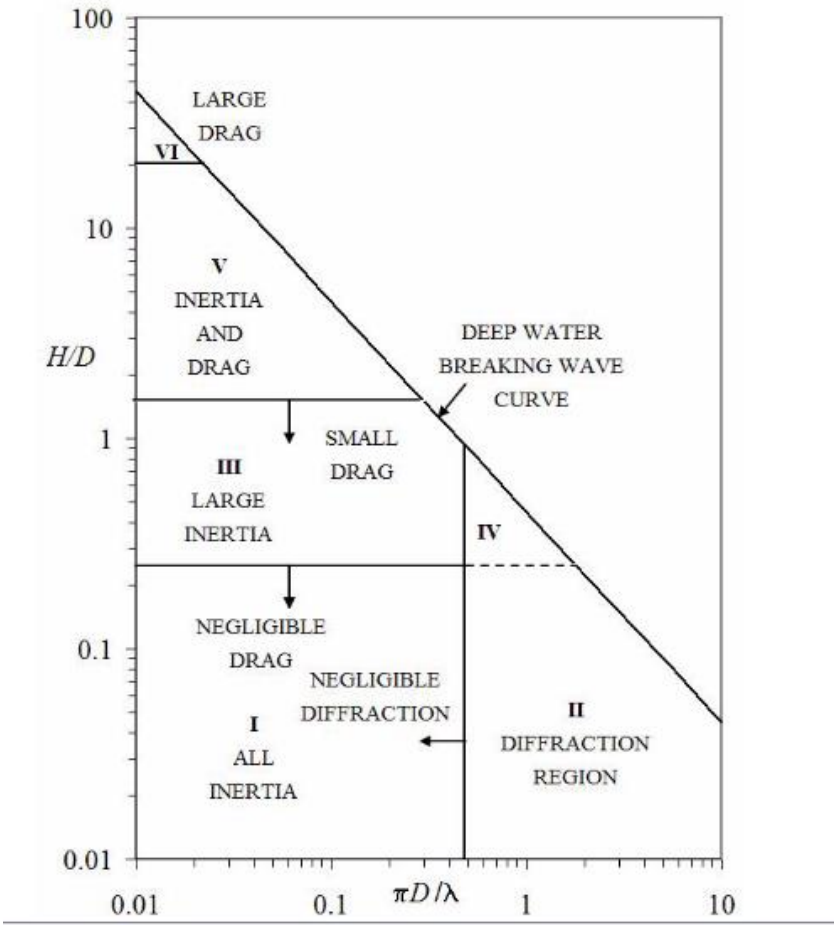

Рис. 3.13 Different force regime of the wave load [44,45]

In case of calculation of the loads on the caisson with sides $B = 100$ m и $B = 70$ m for the conditions described in 1.2.3 и 1.2.4, calculations should be carried out within the diffraction regime, the use of which is typical in calculating wave loads on large volume bodies, characteristic size of such body: $D > L/6$ [44] (the diagonal section of the caisson is taken as the characteristic size). The wave load per unit length of the cylinder in accordance with the diffraction theory (in the case of using the linear wave theory) is calculated by the equation (3.8) [45, p. 251–253].

$$f\left(x_0, z, t\right) = C_m \rho \frac{\pi D^2}{4} \dot{u}\left(x_0, z, t\right), \tag{3.8}$$

где $\dot{u}$ - particle acceleration defined by the equation (3.6); x_0 - cylinder wall coordinate; ρ - density of water; D - characteristic size of a cylinder equal to its diameter; C_m - inertia coefficient determined by the equation (3.9).

$$C_m = \frac{4}{\pi\left(kD/2\right)^2\sqrt{J_1'^2\left(kD/2\right)+Y_1'^2\left(kD/2\right)}}, \quad (3.9)$$

where J_1 и Y_1 - Bessel functions of the first kind of the first order and second kind of the first order, respectively.

M. Rahman [48] showed that equation b can be used to calculate wave loads on large volume caissons of square section if their characteristic size is determined in accordance with equation (3.10).

$$D = \frac{2B}{\pi^{0.5}}, \quad (3.10)$$

where B - width of the caisson.

Thus, the resulting force and moment acting on the caisson of square section can be determined according to the equations (3.11) and (3.12) [46].

$$F\left(x_0,t\right) = \int_{-d}^{\xi(x,t)} f\left(z,t\right)dz \quad (3.11)$$

$$M\left(x_0,t\right) = \int_{-d}^{\xi(x,t)} f\left(z,t\right)zdz \approx \cdot\frac{2}{3}dF\left(x_0,t\right) \quad (3.12)$$

Using equations (3.3) and (3.6) one can deduce:

$$F\left(x_0,t\right) = C_m\rho\frac{\pi D^2}{4}\xi_0 kg\frac{\cos\left(\omega t-kx_0\right)}{\cosh\left(kd\right)}\int_{-d}^{\xi(x_0,t)}\cosh k\left(z+d\right)dz =$$

$$= C_m\rho\frac{\pi D^2}{4}\xi_0 g\frac{\cos\left(\omega t-kx\right)}{\cosh\left(kd\right)}\sinh k\left(\xi_0\sin\left(\omega t-kx\right)+d\right)$$

To solve this equation, an algorithm was written in Python, the code of which is presented in A3. Calculations were carried out for the entire depth range of the licensed area of field A, taking into account possible fluctuations in water level (see 1.2.3). The results are presented in figure 3.9 (installation depth is given without taking into account possible fluctuations in water level).

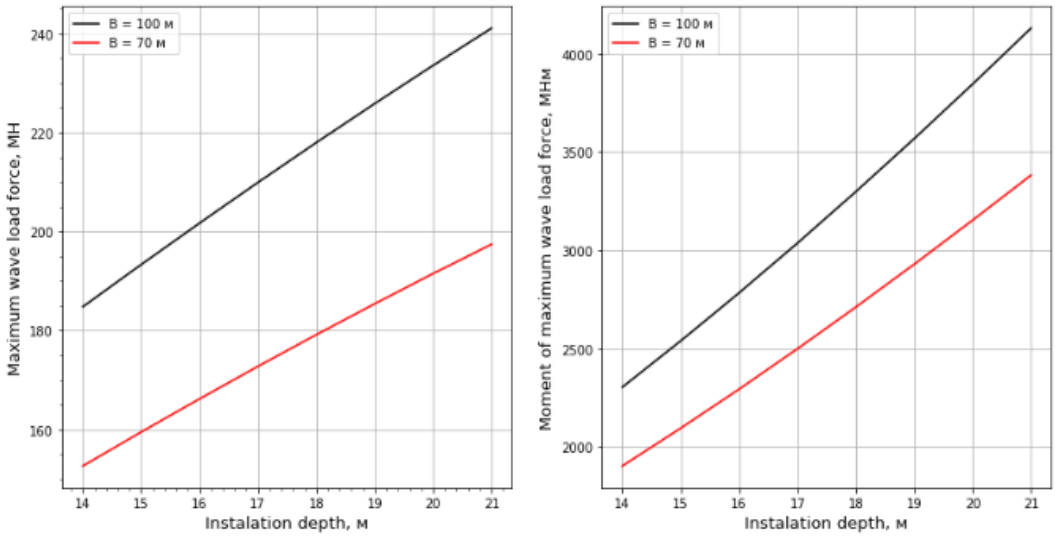

FIgure 3.14 The results of the calculation of wave loads on the platform

Examples of code (A3) execution for three cases of platforms are shown in Figures 3.10 - 3.12.

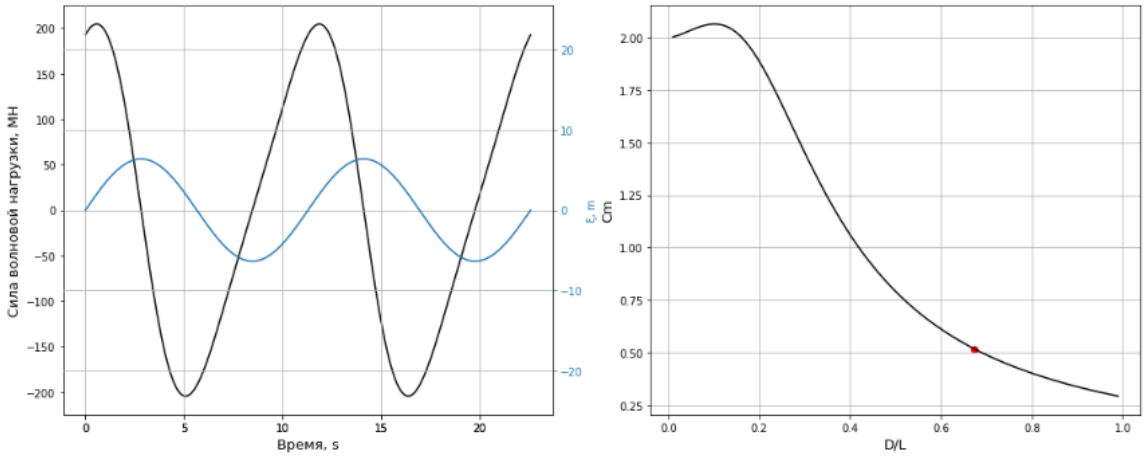

FIgure 3.15 The results of the calculation of wave loads acting on central platform installed at a depth of 18 m

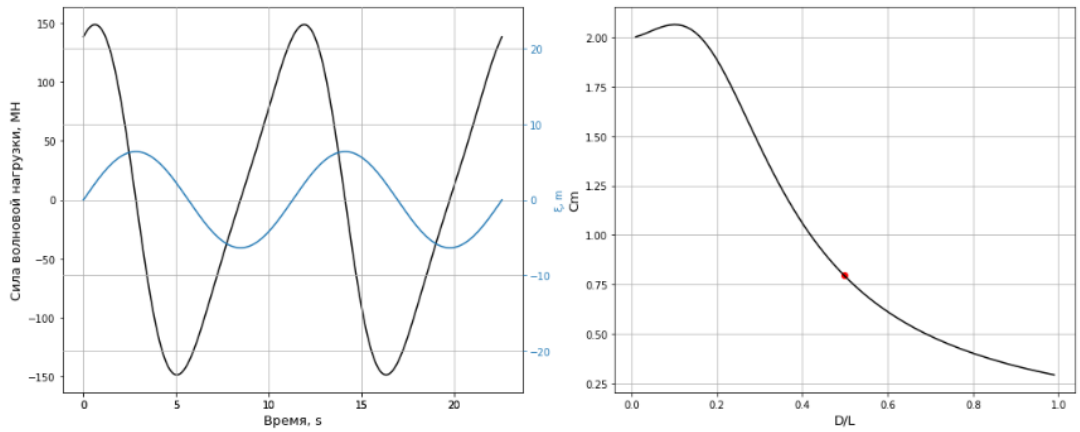

FIgure 3.16 The results of the calculation of wave loads acting on the wellhead platform installed at a depth of 15 m

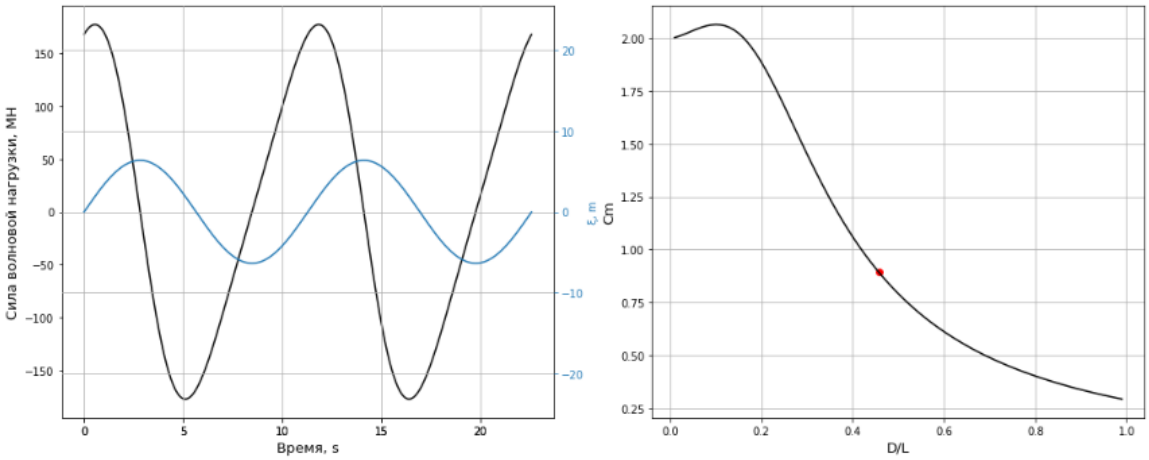

FIgure 3.17 The results of the calculation of wave loads acting on the wellhead platform installed at a depth of 20 m

The results are presented in Table 3.4.

3.3.2. Calculation of ice load

Global ice loads for the platform should be calculated, taking into account that the platforms will be in three ice zones (see 1.2.5), which means that the thickness of the fast ice, drifting ice, and ridges will affect the GBS. According to [10], global ice loads in the first two cases can be determined according to the formula.

$$F = pA, \tag{3.13}$$

где p - pressure generated by ice on the nominal contact area, A - the nominal contact area.

Nominal contact area is defined as the product of ice thickness h (consolidated layer thickness - in case of interaction with a ridge) and object width w, in this case, the side of the caisson foundation.

The pressure produced by ice on the nominal contact area is determined according to the formula (3.14).

$$p = C_R \left[\left(\frac{h}{h_1} \right)^n \left(\frac{w}{h} \right)^{-0.16} + e^{\frac{-w}{3h}} \sqrt{1 + 5\frac{h}{w}} \right], \tag{3.14}$$

where w- design width expressed in meters; h - ice thickness expressed in meters; h_1 h1 - reference thickness of one meter; n - coefficient equal to $-0.50 + h/5$ when $h < 1.0$ м and -0.30 when $h \geq 1.0$ м; C_R - ice strength coefficient expressed in MPa.

Ice strength factor C_R applicable depending on the region. For Arctic conditions, it is taken equal to 2.8 [4].

In the first two cases (impacts of fast ice and drifting ice), it is sufficient to use equations (2.1) и (2.2) to calculate ice loads. In the case of interaction with ridges equation (2.3) should be used.

$$F_t = F + F_k, \tag{3.15}$$

где F - load due to the impact on the structure of the consolidated layer of a ridge, which is determined by 2.1, 2.2; F_k -load due to the impact on the structure of the keel part of the ridge.

To determine the load due to the impact of the keel part of the ridge, there are several models. For vertical structures, passive fracture models can be used, according to which F_k can be determined by the formulas (3.16) – (3.17).

$$F_k = \mu_\phi h_k w\left(\frac{h_k \mu_\phi \gamma_e}{2} + 2c\right)\left(1 + \frac{h_k}{6w}\right), \tag{3.16}$$

$$\mu_\phi = \tan\left(45^o + \frac{\varphi}{2}\right), \tag{3.17}$$

where μ_ϕ - passive pressure coefficient; ϕ - angle of internal friction; c – the apparent keel cohesion (an average value over the keel volume should be used); w - construction width; γ_e - the effective buoyancy, in units consistent with c.

The effective buoyancy can be determined in accordance with the equation ().

$$\gamma_e = (1-e)(\rho_w - \rho_i)g, \tag{3.18}$$

where e - keel porosity, ρ_w, ρ_i - water and ice densities, respectively.

Two algorithms were written for calculating ice loads in Python: for calculating ice loads from drifting ice and fast ice (the code is presented in A4) and for calculating loads from the influence of ridges (the code is presented in A4). The initial data for the calculations are determined in accordance with 1.2.5. The calculation results are presented in Fig. 3.13 and fig. 3.14.

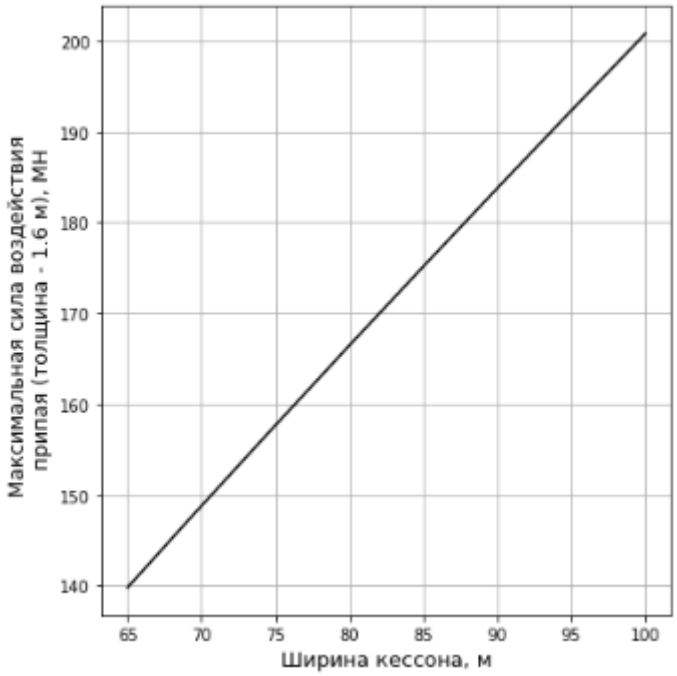

FIgure 3.18 Maximum force from fast ice action on the caisson, depending on the size

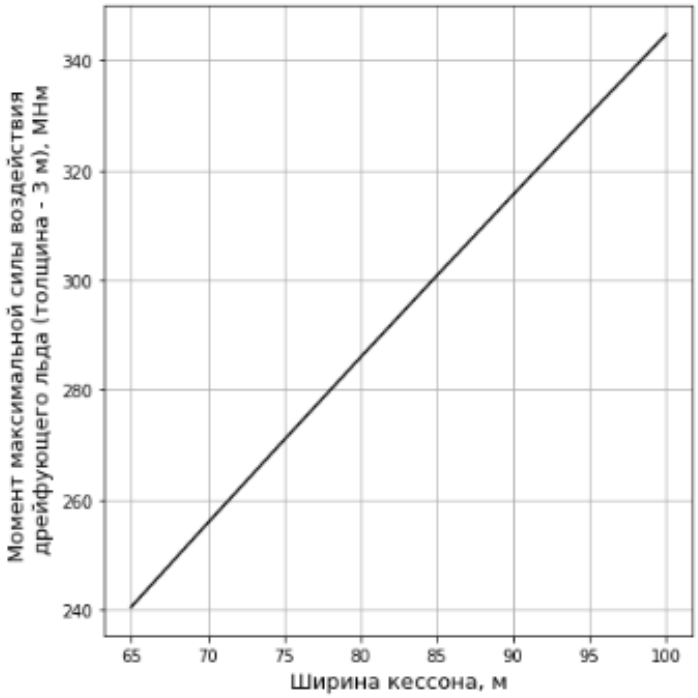

FIgure 3.19 Maximum force from drifted ice action on the caisson, depending on the size

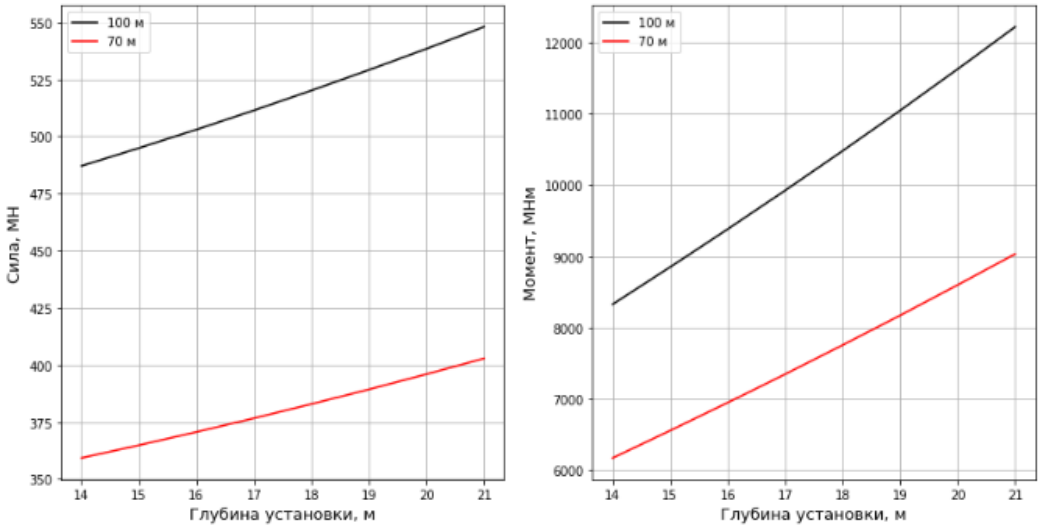

FIgure 3.20 Максимальная сила

The loads from the influence of hummocks, as can be seen from the graphs of Figures 3.13 -3.15, significantly exceed the loads from the effects of drifting ice or fast ice, therefore, in the analysis of stability from ice loads, only loads from the effects of ridges are considered, which are presented for each platform in Table 3.4.

3.3.3. Stability

Table 3.4 presents the maximum wave and ice load forces, as well as their moments relative to the base of the platform. Based on these values, as well as the characteristics of the platforms presented in Table 3.3, the shear and tipping stability factors were calculated using formulas (3.3) and (3.4). The calculations were carried out for various soil friction angles, the tables show the calculation at a soil friction angle of 35, which corresponds to the angle of internal friction of gravel, as well as the upper layers of the soil in the licensed area. The results are presented in tables 3.5 and 3.6.

The calculation was based on dry weight and total weight of platforms, including storage tanks filled with oil in the last case. Stability in the first case will provide an opportunity to fill the tank with an inert gas when oil is gone. If the platform is not stable when calculating the dry weight, then the volume of oil must be compensated by ballast water.

Table 3.4

Maximum wave and ice load forces and their moments relative to the base of the platform

Parameter / Platform	Central platform (Steel cassion)	Central platform (Concrete caission)	Wellhead platform installed at a depth of 15 m	Wellhead platform installed at a depth of 20 m
Maximum wave load force, MN	180	180	159	191
Maximum force of ice load, MN	520	520	364	395
Overturning moment of maximum wave load force, MNm	3299	3299	2094	3153
Overturning moment of maximum force of ice load, MNm	10481	10481	6550	8596

Table 3.5

Rollover Stability Factor Results

Parameter / Platform	Central platform (Steel cassion)	Central platform (Concrete caission)	Wellhead platform installed at a depth of 15 m	Wellhead platform installed at a depth of 20 m
Holding moment (on dry weight), MNm	174373	193993	104924	107039
Overturning moment, MHm	10481	10481	6550	8596
Tilt stability factor	17	19	16	12

Table 3.6

The results of calculating the shear stability coefficient

Parameter / Platform	Central platform (Steel cassion)	Central platform (Concrete caission)	Wellhead platform installed at a depth of 15 m	Wellhead platform installed at a depth of 20 m
Max. load force, MN	520	520	364	395
Safety factor	1.10	1.10	1.10	1.10
Weight (dry weight), MN	3487	3880	2998	3058
Weight (total weight), MN	4595	4987	3527	3661
Buoyancy force, MN	3017	3017	1330	1577
Tan of angle of internal friction (35)	0.70	0.70	0.70	0.70
Shear stability coefficient (dry weight)	0.58	1.06	2.92	2.39
Shear stability coefficient (total weight)	1.93	2.41	3.84	3.36

From table 3.5 it is seen that all platforms are resistant to capsizing on dry weight. The shear stability coefficient is less than unity only in the case of a central platform with a steel base. Which suggests that in case of its use it is necessary to use ballast water, which is a less preferred and expensive option [14].

3.4. Conclusions

The analysis of technical and technological factors can be resumed in the following way:

- Offshore structures involved in basic and alternative field layouts can withstand environmental loads in region of Field-A license area.
- The soil at the installation site must be replaced with soil with an internal friction angle greater than or equal to 35. The option of using the top soil layer of the license area may be considered
- Polymer waterflooding is the best option for Filed-A;
- Multi-hole completion should be used when completing production wells.

4. The field-A development concepts

Based on the conclusions from the chapters above, five development concepts can be provided. These concepts are designed based on two fields layout. Different capital and operational expenditures, as well as different development indicators, are implied for each development.

4.1. Description

The first development concept involves alternative field layout as a base for the Northern and Southern deposits development as well as drilling of 40 MLDW at the technological platform and drilling of 10 MLDW at the wellhead platform (fig. 4.1). The average horizontal displacement of the wells from the platform is 4 km and 2.7 km for the technological and wellhead platforms, respectively. It is proposed to install the wellhead platform at the water depth of 15 meters.

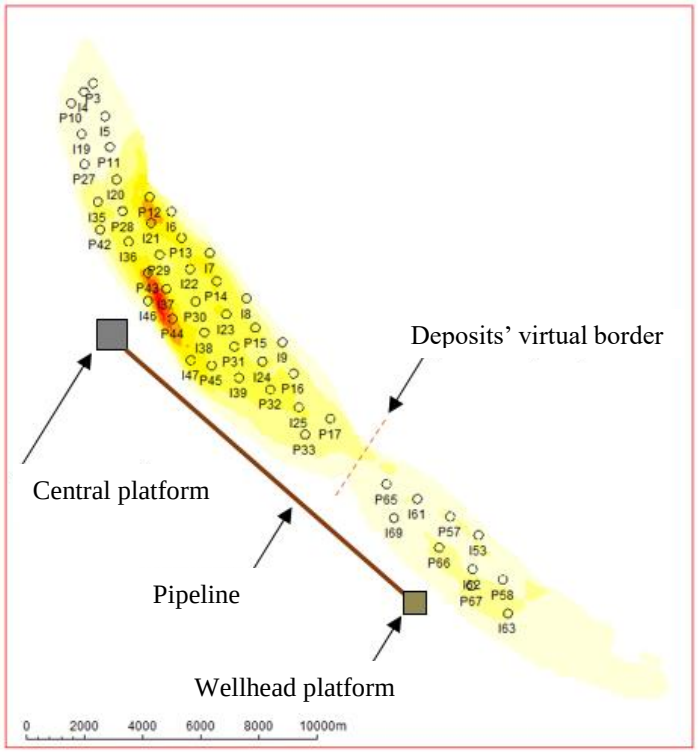

Figure 4.1 The first development concept field layout

The second development concept involves alternative field layout as a base for the Northern and Southern deposits development as well as drilling of 30 MLDW at the technological platform and drilling of 10 MLDW at the wellhead platform (fig. 4.2). The average horizontal displacement of the wells from the platform is 3.1 km and

2.7 km for the technological and wellhead platforms, respectively. It is proposed to install the wellhead platform at the water depth of 20 meters.

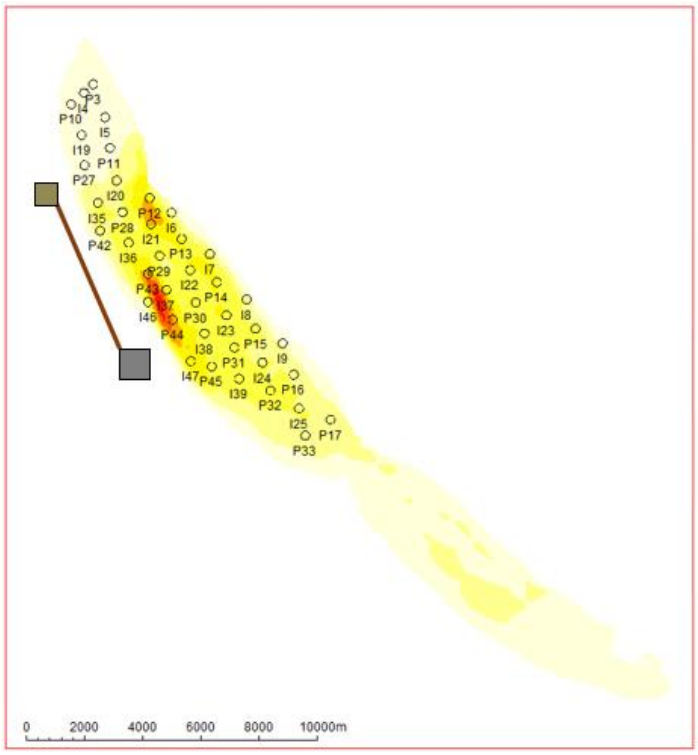

Figure 4.2 The second development concept field layout

With the basic fields layout implementation, three development concepts are proposed. For all the concepts, the water depth for the wellhead platform is 18 m.

The third development concept: drilling of 20 wells; the average horizontal displacement of the wells from the platform is 2 km.

The fourth development concept: drilling of 30 wells; the average horizontal displacement of the wells from the platform is 3.1 km.

The fifth development concept: drilling of 40 wells; the average horizontal displacement of the wells from the platform is 4 km.

The platform's installation parameters for each development concept are presented in Table 4.1.

Each concept involves using the platform in accordance with table 3.3, oil offloading from the technological platform via ice-class Arc6 tanker and the transportation of the production to the transhipment base in the Murmansk city.

In order to define the efficiency of each concept, the calculations in the Petrel soft has been done. The calculations provide P50 and P10 models. The values of the platform's working parameters are presented in table 4.2.

All development concepts involve polymer waterflooding with PAA with concentration of 0.4 kg/m^3.

Calculations allow us to draw conclusions about the capacitance characteristics of platforms. For example, table 4.2 shows the calculation of the number of days required to fully fill the tanks with oil. This number of days is compared with the number of days required for the tanker to make a flight to Murmansk and back. As can be seen from the table, practically all concepts in the case of P10 have insufficient capacity to provide this time interval. Thus, the costs included in the calculation should be increased by taking into account the additional costs for the tanker. The table also shows that using the caisson storage of the wellhead platform significantly increases the time required to fill the entire system, and therefore reduces the cost of additional tankers

As can be seen from figures 4.8 and 4.9, the optimal is the inverted concept of arrangement, which gives the highest NPV in the conditions of geological and economic uncertainty. Thus, it can be concluded that the optimal development strategy for field A is the development of the Northern Deposit with 15 producing multi-hole wells and 15 obliquely drilled injection wells using a single-row system built from one utilizing platform.

Тем не менее при реализации P50 проект остаётся убыточгым. В случае если стоимость нефти менее 65 долл. зп аррель Как видно из графика

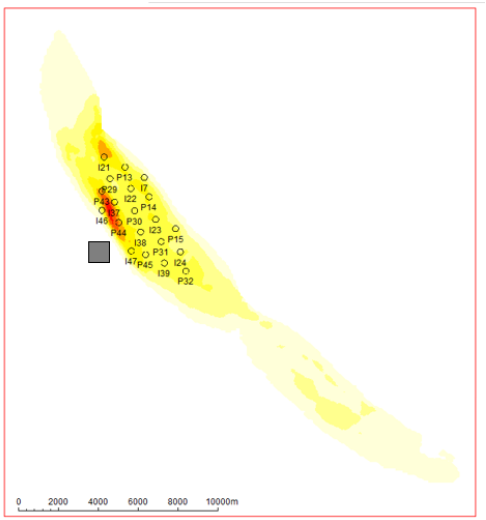

Figure 4.3 The third development concept field layout

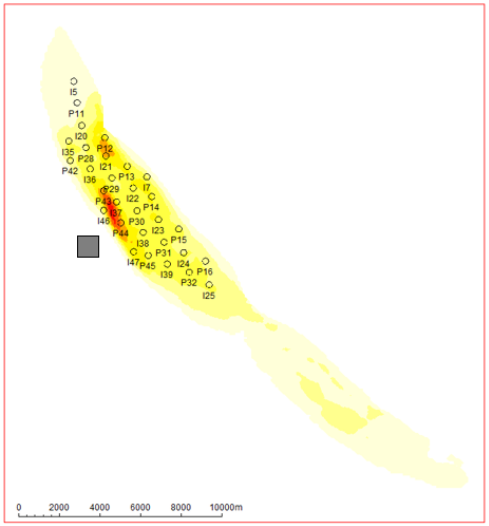

Figure 4.4 The fifth development concept field layout

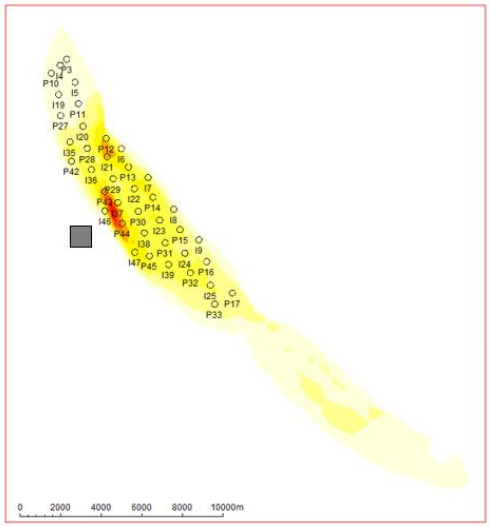

Figure 4.5 The sixth development concept field layout

Table 4.1

Platform's installation parameters

The northern displacement to the southern boundary		Installation water depth		Well's horizontal displacement from the platform, m		Number of wells		MD, m		MD, km
TP	WP	TP	WP	TP	WP	TP	WP	TP	WP	
11	3	18	15	4000	2700	40	10	282991	58309	341
11	17	18	20	3100	2700	30	10	186269	58309	245
11	-	18	-	2000	-	20	0	103755	-	103
11	-	18	-	3100	-	30	0	186269	-	186

11	-	18	-	4000	-	40	0	282991	-	283

Table 4.2

	Max oil production ths tons	Max oil production ths m^3	Technological platform's storage capacity, m^3	Wellhead platform's storage capacity , m^3	Total storage capacity	Minimal storage filling period (only technological platform)	Minimal storages filling period	Max oil production per 7.4 days in the maximum oil rate period, ths tons	Minimal tanker amount
1	7.7	8229.0	110400	52473	162873	13.4	19.8	56.8	1
2	8.5	9104.3	110400	60588	170988	12.1	18.8	56.8	1
3	5.3	5676.6	110400	0	110400	19.4	19.4	62.8	1
4	6.7	7158.9	110400	0	110400	15.4	15.4	39.2	2
5	7.6	8145.9	110400	0	110400	13.6	13.6	49.4	1
1	15.4	16554.1	110400	52473	162873	6.7	9.8	56.2	1
2	20.0	21442.6	110400	60588	170988	5.1	8.0	114.2	1
3	13.1	14079.3	110400	0	110400	7.8	7.8	120.7	1
4	16.0	17282.3	110400	0	110400	6.4	6.4	97.1	1
5	15.4	16738.2	110400	0	110400	6.6	6.6	118.0	1

The development concept field layout parameters

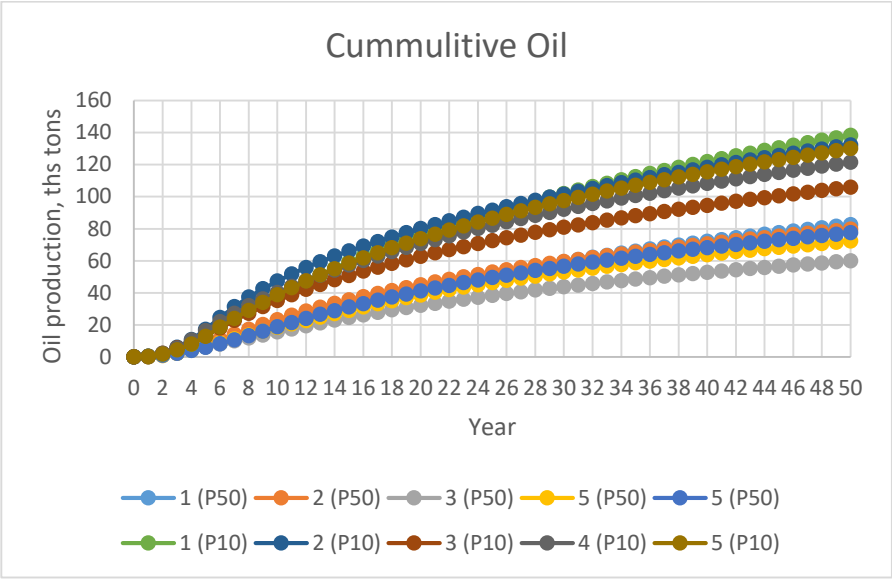
Cummulitive Oil
Oil production, ths tons
160
140
120
100
80
60
40
20
0
0 2 4 6 8 10 12 14 16 18 20 22 24 26 28 30 32 34 36 38 40 42 44 46 48 50
Year
1 (P50) 2 (P50) 3 (P50) 5 (P50) 5 (P50)
1 (P10) 2 (P10) 3 (P10) 4 (P10) 5 (P10)

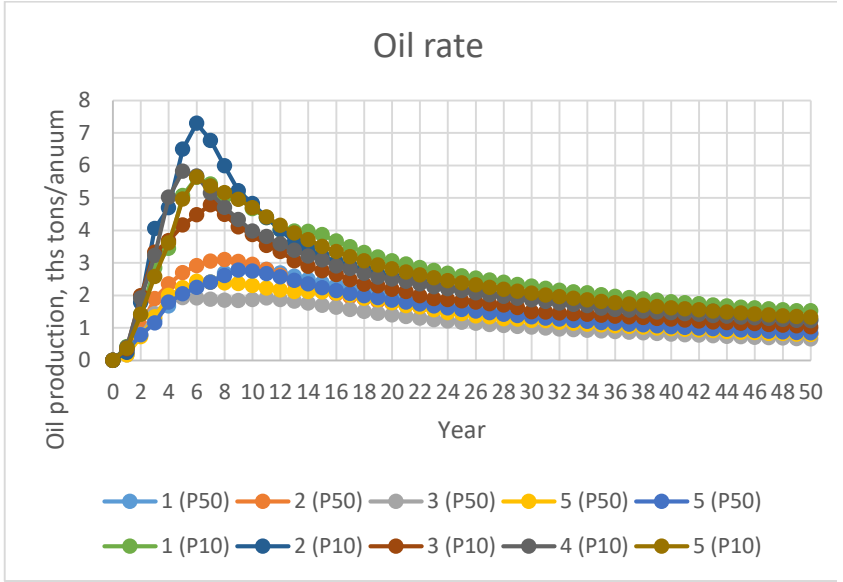
Oil rate
Oil production, ths tons/anuum
8
7
6
5
4
3
2
1
0
0 2 4 6 8 10 12 14 16 18 20 22 24 26 28 30 32 34 36 38 40 42 44 46 48 50
Year
1 (P50) 2 (P50) 3 (P50) 5 (P50) 5 (P50)
1 (P10) 2 (P10) 3 (P10) 4 (P10) 5 (P10)

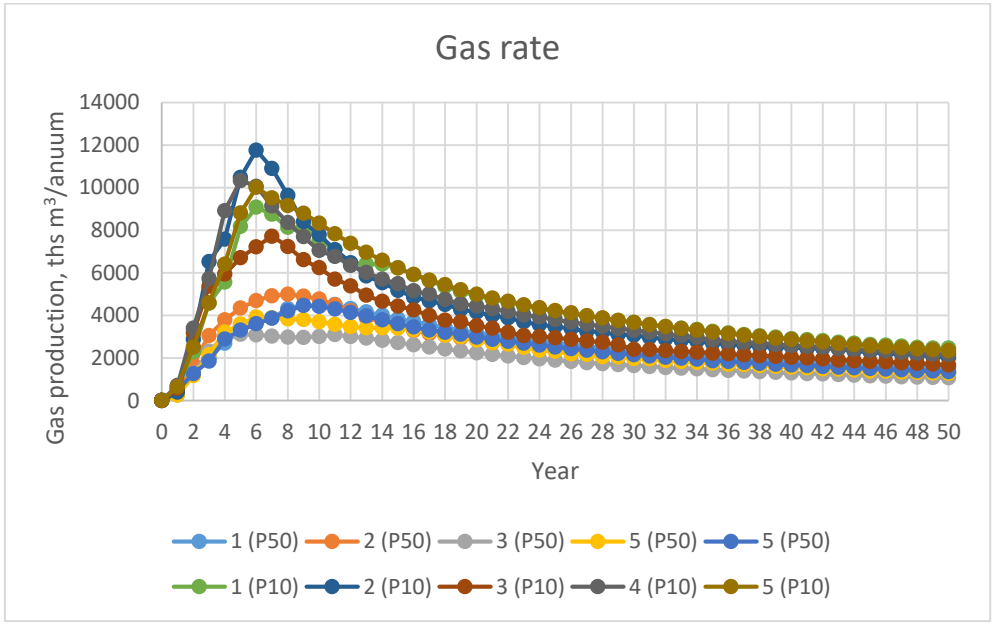
Gas rate
Gas production, ths m3/anuum
14000
12000
10000
8000
6000
4000
2000
0
0 2 4 6 8 10 12 14 16 18 20 22 24 26 28 30 32 34 36 38 40 42 44 46 48 50
Year
1 (P50)
2 (P50)
3 (P50)
5 (P50)
5 (P50)
1 (P10)
2 (P10)
3 (P10)
4 (P10)
5 (P10)

4.2. Economic parameters analysis

4.2.1. Capital investments

All the investments were estimated following the materials from [14].

1. The cost of the one headway meter is $11000.
2. The cost of ESP is $600 ths.
3. The cost of the technological platform topside is 1800 million dollars. Such estimation has been done based on the necessary functions of the platform. It was taken the same for all concepts.
4. The cost of the concrete GBS Is 400 million dollars. Such estimation has been done based on the weight and dimensions of the platform.
5. The cost of the wellhead platform is 870 million dollars. Such estimation has been done based on the necessary functions of the platform. It was taken the same for two concepts.
6. The cost of the steel GBS is 380 and 430 million dollars based on the platforms' mass.
7. The cost of pipeline

Table 4.3 Capital investments

Expenditure / Concept	1	2	3	4	5
Well drilling, bln $	3.75	2.69	1.56	2.05	3.11
ESP, bln $	0.02	0.01	0.01	0.01	0.01
Technological platform (GBS), bln $	0.40	0.40	0.40	0.40	0.40
Technological platform (topside), bln $	1.80	1.80	1.80	1.80	1.80
Wellhead platform (GBS), bln $	0.38	0.43	0.00	0.00	0.00
Wellhead platform (topside), bln $	0.87	0.87	0.00	0.00	0.00
Pipelines, bln $	0.18	0.09	0.00	0.00	0.00

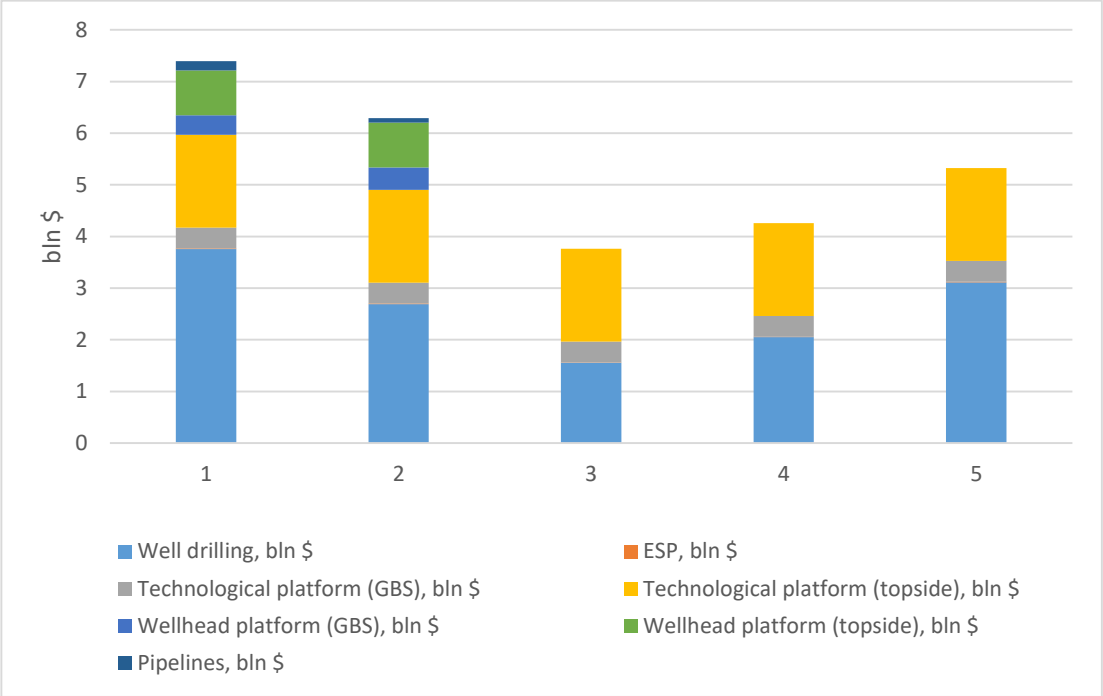

Рисунок 4.6 CAPEX for different development concepts

The table above shows that the drilling wells and the topside cost of the technological platform are the main expenditures. However, the costs for the technological platform topside do not depend on the concept of the arrangement. On the contrary, the drilling costs determin differences.

Table 4.4 Relative capital investments

Expenditure / Concept	1	2	3	4	5
Well drilling, bln $	50.8%	42.8%	41.4%	48.1%	58.5%
ESP, bln $	0.2%	0.2%	0.2%	0.2%	0.2%
Technological platform (GBS), bln $	5.4%	6.4%	10.6%	9.4%	7.5%
Technological platform (topside), bln $	24.3%	28.6%	47.8%	42.3%	33.8%
Wellhead platform (GBS), bln $	5.1%	6.9%	0.0%	0.0%	0.0%
Wellhead platform (topside), bln $	11.7%	13.8%	0.0%	0.0%	0.0%
Pipelines, bln $	2.5%	1.4%	0.0%	0.0%	0.0%

4.2.2. Operational costs (OPEX)

Operational expenditures can be divided into two groups, those which is dependent on oil production rate and those which do not change.

Independent from the oil production expenditures:

1. Platforms' service
2. Employees' salary
3. Power supply expenditures
4. Wells' workover expenditures
5. Supply vessels and ice-breakers expenditures (rent)
6. Supply vessels and ice-breakers expenditures (fuel)
7. Technical support expenditures
8. Administrative expenditures
9. Onshore supply base rent expenditures

Dependent on the oil production OPEX:

1. Polimer expenditures
2. Transportation expenditures

The comparison of CAPEX and OPEX is presented

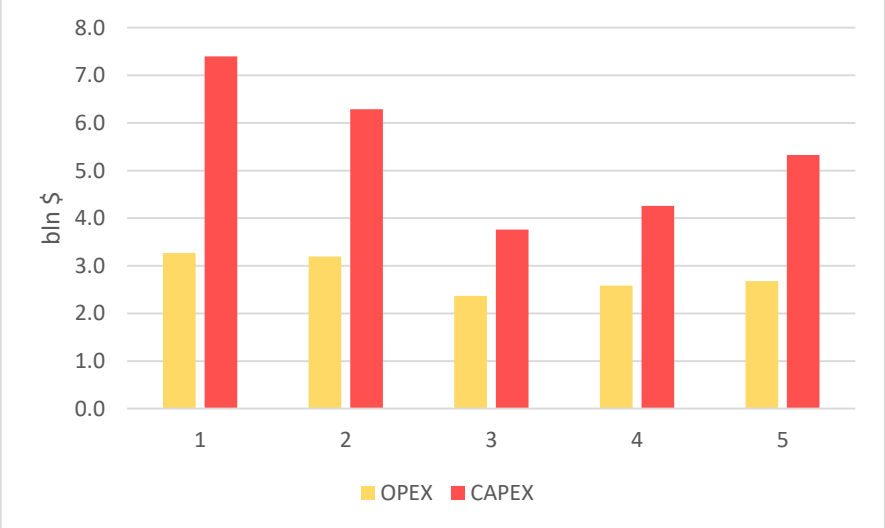

Рисунок 4.7 CAPEX – OPEX comparison diagram

4.2.3. The producing hydrocarbon cost

As can be seen from graphs 4.8 and 4.9, the fourth development option is optimal in conditions of economic and geological uncertainty.

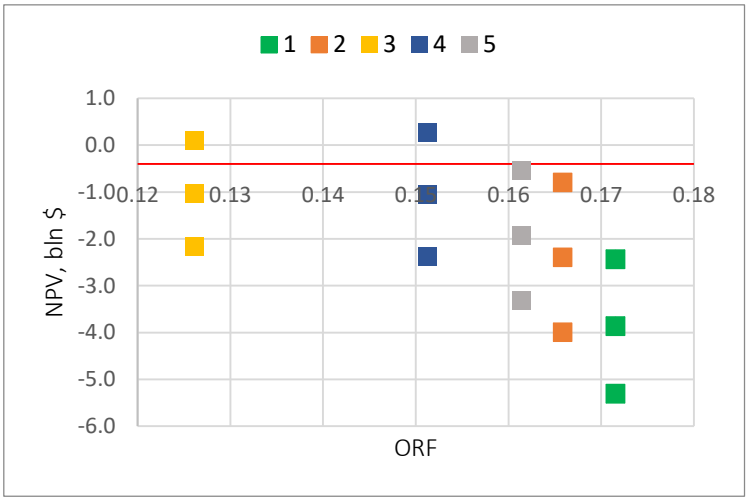

Figure 4.8 NPV – ORF depending on oil price (P50-case)

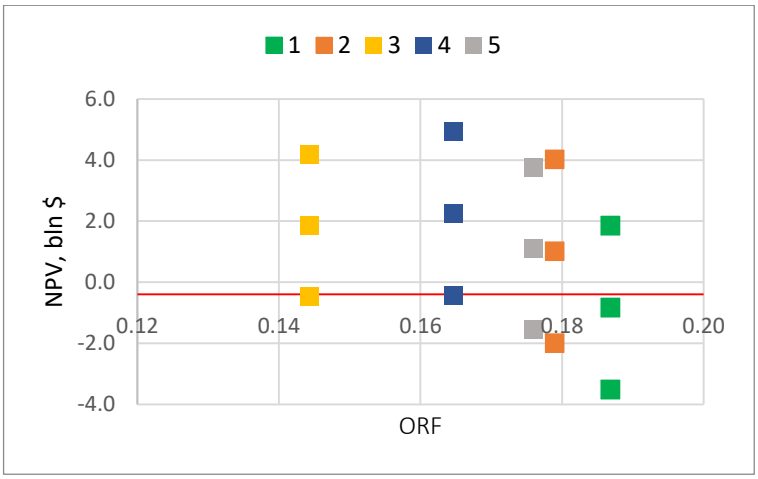

FIgure 4.9 NPV – ORF depending on oil price (P10-case)

Table 4.5 Economic parameters' calculation results (P50)

Parameter / Concept	1 (P50)			2 (P50)			3 (P50)			4 (P50)			5 (P50)		
Number of platforms	2			2			1			1			1		
Number of wells	50			40			20			30			40		
Total headway, km	341.3			244.6			103.7			186.3			283.0		
Cumulative oil production, mln tons	82.4			79.6			60.0			72.4			77.4		
Volume of the inkected fluid, m^3	344.4			339.3			277.6			314.7			317.9		
ORF	0.17			0.16			0.12			0.15			0.16		
Oil price, $/bbl	**30**	**50**	**70**	**30**	**50**	**70**	**30**	**50**	**70**	**30**	**50**	**70**	**30**	**50**	**70**
Revenue, bln $	16.7	27.8	38.9	16.1	26.9	37.6	12.1	20.2	28.3	14.7	24.4	34.2	15.7	26.1	36.6
OPEX, bln $	3.3			3.2			2.4			2.6			2.7		
CAPEX, bln $	7.4			6.3			3.8			4.3			5.3		
Revenue before the taxes, bln $	6.0	17.2	28.3	6.6	17.4	28.1	6.0	14.1	22.2	7.8	17.6	27.4	7.7	18.1	28.6
Taxes, bln $	1.9	5.2	8.5	2.0	5.2	8.5	1.8	4.2	6.7	2.4	5.3	8.2	2.3	5.4	8.6
Net profit, bln $	4.2	12.0	19.8	4.6	12.1	19.7	4.2	9.9	15.5	5.4	12.3	19.1	5.3	12.7	20.0
NPV, bln $	-5.3	-3.9	-2.4	-4.0	-2.4	-0.8	-2.2	-1.0	0.1	-2.4	-1.1	0.3	-3.3	-1.9	-0.5
IRR	0.02	0.05	0.08	0.03	0.07	0.10	0.04	0.09	0.12	0.05	0.09	0.13	0.04	0.08	0.11
PI	0.28	0.48	0.67	0.36	0.62	0.87	0.42	0.73	1.03	0.44	0.75	1.07	0.38	0.64	0.90

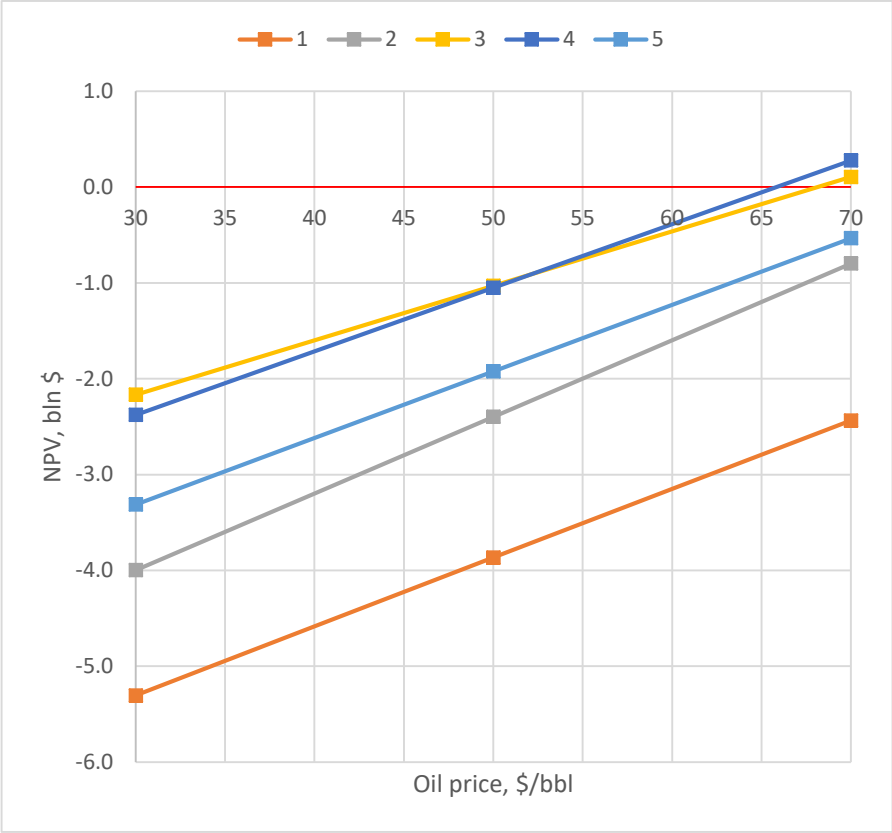

Figure 4.10 Oil price sensitivity study (P50)

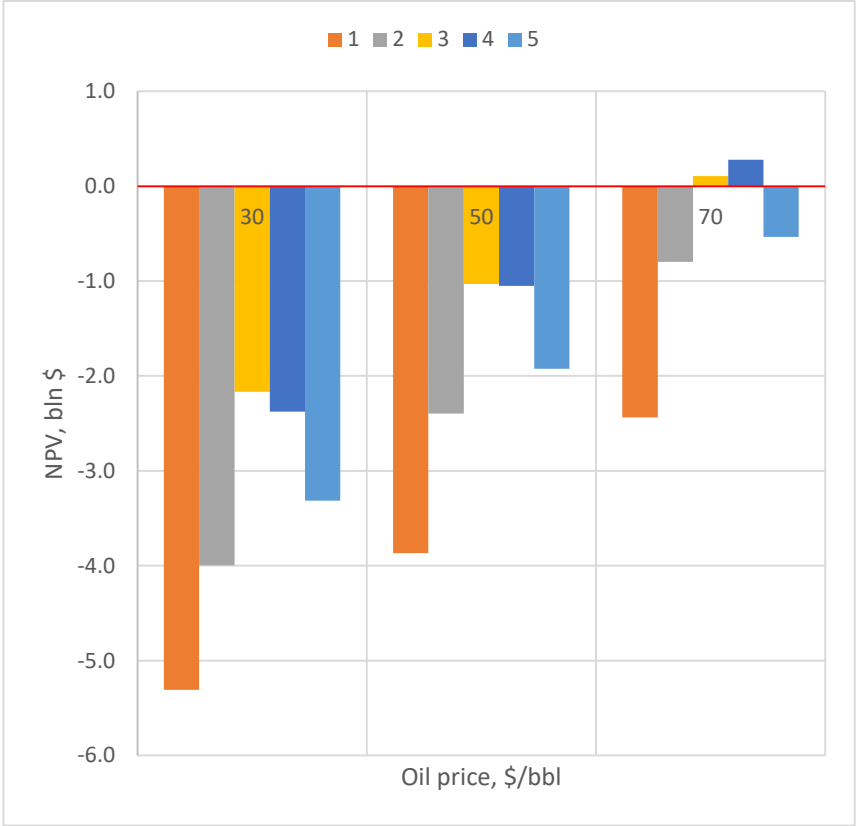

Figure 4.11 Oil price sensitivity study diagram (P50)

Table 4.6 Economic parameters' calculation results (P10)

Parameter / Concept	1 (P10)			2 (P10)			3 (P10)			4 (P10)			5 (P10)		
Number of platforms	2			2			1			1			1		
Number of wells	50			40			20			30			40		
Total headway, km	341.3			244.6			103.7			186.3			283.0		
Cumulative oil production, mln tons	138.2			132.2			105.9			121.4			129.9		
Volume of the inkected fluid, m3	378.2			365.8			339.4			350.0			349.7		
ORF	0.18			0.17			0.14			0.16			0.17		
Oil price, $/bbl	**30**	**50**	**70**	**30**	**50**	**70**	**30**	**50**	**70**	**30**	**50**	**70**	**30**	**50**	**70**
Revenue, bln $	28.0	46.6	65.3	26.8	44.6	62.5	21.4	35.7	50.0	24.8	41.4	57.9	26.6	44.3	62.0
OPEX, bln $	3.9			3.7			2.9			3.1			3.2		
CAPEX, bln $	7.4			6.3			3.8			4.3			5.3		
Revenue before the taxes, bln $	16.7	35.4	54.0	16.7	26.7	52.4	14.8	29.1	43.4	17.4	34.0	50.5	18.0	35.7	53.4
Taxes, bln $	5.0	10.6	16.2	5.1	8.0	15.7	4.4	8.7	13.0	5.2	10.2	15.2	5.4	10.7	16.0
Net profit, bln $	11.7	24.8	37.8	11.7	24.2	36.7	10.3	20.3	30.4	12.2	23.8	35.4	12.6	25.0	37.4
NPV, bln $	-3.5	-0.8	1.9	-2.0	1.0	2.1	-0.5	1.9	4.2	-0.4	2.3	4.9	-1.5	1.1	3.8
IRR	0.06	0.11	0.15	0.08	0.14	0.16	0.10	0.18	0.24	0.11	0.18	0.25	0.08	0.14	0.20
PI	0.52	0.89	1.25	0.68	1.916	1.34	0.88	1.50	2.12	0.90	1.53	2.16	0.71	1.21	1.71

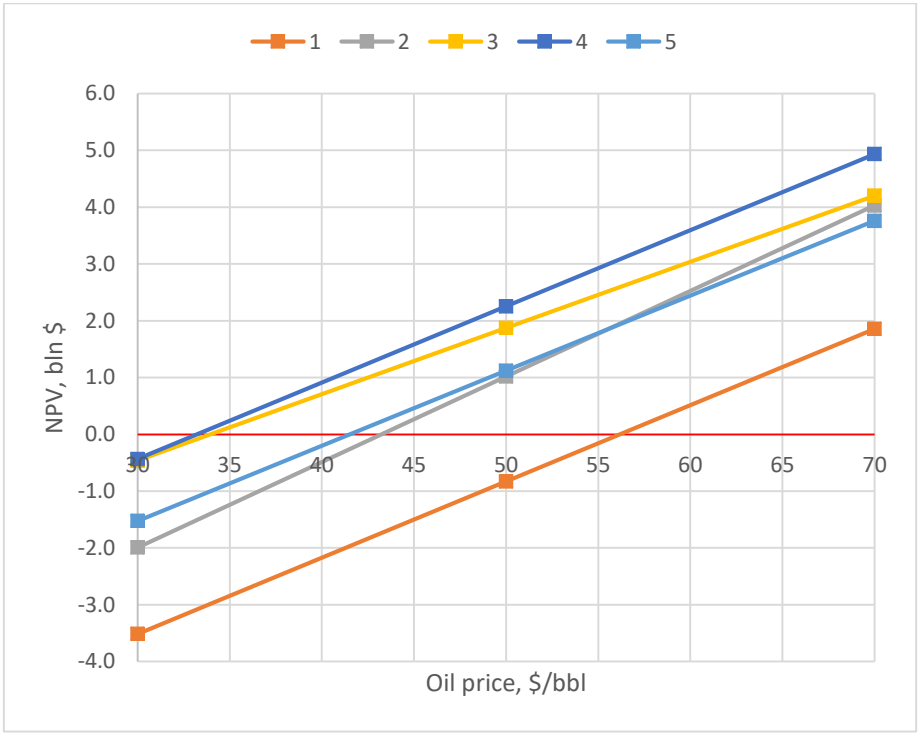

Figure 4.12 Oil price sensitivity study (P50)

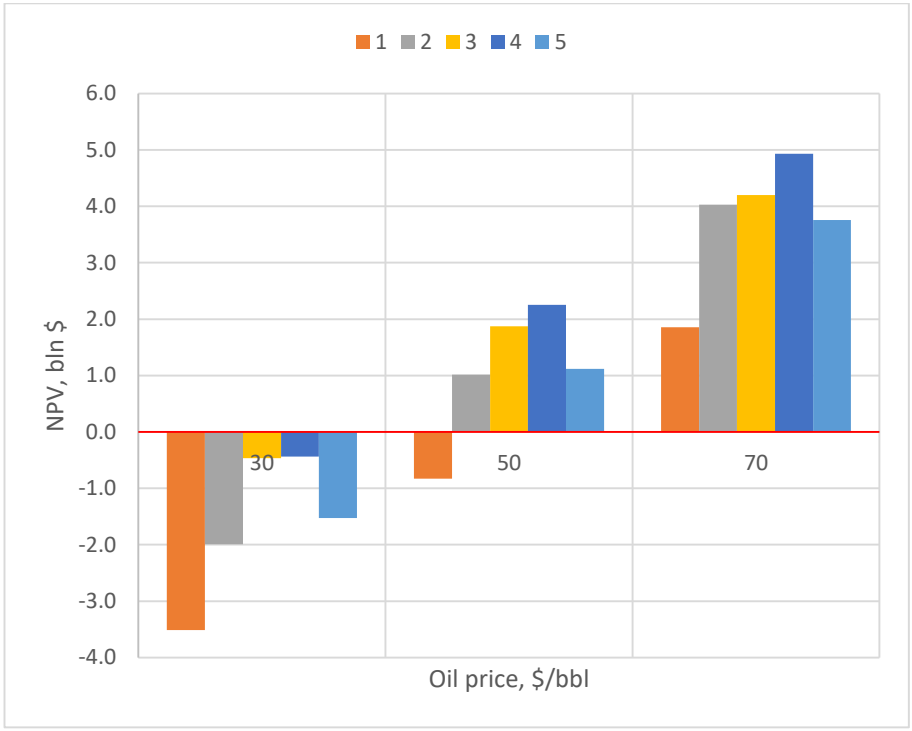

Figure 4.13 Oil price sensitivity study diagram (P50)

Conclusions

In this thesis, the development concept study were carried out. 5 options are considered, and the optimal one is identified. Nevertheless, the development of the field is unprofitable in the case of P50, despite significant oil reserves. High oil viscosity primarily determines the behaviour of the reservoir system, with characteristic low production indicators. At the same time, the vast area of the field requires the need to drill long wells, which significantly increases the capital costs of the project. The unstable economic situation and high taxes also determine the profitability of the project. Thus, it can be concluded that further research on issues related to the development of field should lie primarily in the economic sphere.

References

1. Zolotukhin P.A. Petroleum resources in a modern world // Offshore F. Dev. Lect. 1. 2019.
2. Прохоров А.М. Большой энциклопедический словарь. 2004. 1456 p.
3. Basic information about the Arctic [Electronic resource]. URL: https://www.arcticcentre.org/EN/arcticregion.
4. Gautier D.L. et al. Assessment of undiscovered oil and gas in the arctic // Science (80-.). 2009. Vol. 324, № 5931. P. 1175–1179.
5. Zolotukhin P.A. Challenges associated with the Arctic resources development // Offshore F. Dev. Lect. 6. 2019.
6. Degeer D. et al. SURVEY OF ARCTIC & COLD REGION TECHNOLOGY FOR OFFSHORE FIELD // Offshore Mag. 2014. Vol. 250. P. 984.
7. Никитин Б.А. et al. Освоение нефтегазовых месторождений континентального шельфа Часть 1 Прединвестиционная и инвестиционная стадии. 2018. 335 p.
8. Zolotukhin P.A. Main offshore and arctic development projects // Offshore F. Dev. Lect. 3. 2019.
9. Вяхирев Р.И., Никитин Б.А., Мирзоев Д.А. Обустройство и освоение морских нефтегазовых месторождений. Издательст. 1999. 374 p.
10. ISO 19906. INTERNATIONAL STANDARD Petroleum and natural gas industries. 2011. Vol. 2010.
11. Løset S. et al. Comparison of the physical environment of some Arctic seas // Cold Reg. Sci. Technol. 1999. Vol. 29, № 3. P. 201–214.
12. Li H. et al. Review and outlook on arctic offshore facilities & technologies // OTC Arct. Technol. Conf. 2015. 2015. № July 2008. P. 777–800.
13. Speight J.G. Handbook of Offshore Oil and Gas Operations // Subsea and Deepwater Oil and Gas Science and Technology. 2015. 1–43 p.
14. Условия проектирования месторождения А (Роснефть, 2019). 2019. 15 p.
15. Sukhotin A., Denisenko S., Galaktionov K. Pechora Sea ecosystems: current state and future challenges // Polar Biol. Springer Berlin Heidelberg, 2019. Vol. 42, № 9. P. 1631–1645.
16. Дымов В.И., Зубакин Г.К. Ветер и волны в Печорском море // Проблемы Арктики и Антарктики. 2012. Vol. 4, № 94. P. 23–40.
17. DNV GL. OFFSHORE STANDARD DNV GL AS Winterization for cold climate operations. 2015. № July 2015.
18. Conference P.E., Engineers P. Analysis of Various Designs of the Stationary Platform Substructures for the Pechora Sea Shelf. 2000. Vol. I. P. 737–742.
19. ZOLOTUKHIN A.B., GUDMESTAD O.T. BASICS OF THE OFFSHORE OIL AND GAS FIELD DEVELOPMENT AND CONSTRUCTION. 2000.
20. Abramov V. Atlas of Arctic Icebergs. 1996. 68 p.
21. Løset S. et al. Actions from ice on Arctic offshore and coastal structures. 2006. 272 p.
22. «ЛУКОЙЛ-Транс» О. Варандейский терминал [Electronic resource]. URL: https://trans.lukoil.ru/ru/About/Structure/VarandeyTerminal.
23. Agarcov S., Kozmenko S., Teslya A. Organizing an oil transportation system in

the Arctic // IOP Conf. Ser. Earth Environ. Sci. 2020. Vol. 434, № 1.
24. Plotkin B.K., KHAIKIN M.M. Formation and Development of Theoretical Principles for Mineral Resources Logistics. 2017. Vol. 223. P. 139–146.
25. Газпром. Приразломное месторождение [Electronic resource]. URL: https://www.gazprom.ru/projects/prirazlomnoye/.
26. Bambulyak A., Frantzen B. Oil transport from the Russian part of the Barents Region. Status per January 2011. 2011. № January. P. 101.
27. Posey C.J., Silvester R. Offshore structures // Nature. 1975. Vol. 258, № 5532. 192 p.
28. Мирзоев Д.А. Основы морского нефтегазопромыслового дела. Том 1. Обустройство и эксплуатация морских нефтегазовых месторождений Мирзоев Д.А.
29. Hoang V., Alamsyah O., Roberts J. Darajat Geothermal Field Expansion Performance-A Probabilistic Forecast // Iga.Igg.Cnr.It. 2005. № April. P. 24–29.
30. SPE. Petroleum Reserves and Resources Definitions [Electronic resource]. URL: https://www.spe.org/en/industry/reserves/.
31. Пятибратов П.В. Гидродинамическое моделирование нефтяных месторождений. 2014.
32. Молчанова А.Г., Назарова Л.Н., Нечаева Е.В. Введение в разработку и эксплуатацию месторождений углеводородов.
33. Еремин Н.А. et al. Выбор метода воздействия на нефтяную залежь. 2007.
34. Nazarova L.N. Oil and gas field development with hard-to-recover reserves. 2011.
35. Золотухин А.Б. et al. Оценка Применимости Методов Увеличения Нефтеотдачи // Труды Ргу Нефти И Газа Имени И.М. Губкина. 2016. Vol. 2 (283).
36. Желтов Ю.П. Разработка нефтяных месторождении. 1986.
37. Sheng J.J., Leonhardt B., Gmbh W.H. Status of Polymer-Flooding Technology. 2015. № October 2014.
38. Абиров Р.Ж. et al. ОПЫТНО - ПРОМЫШЛЕННОЕ ВНЕДРЕНИЕ ПОЛИМЕРНОГО ЗАВОДНЕНИЯ НА МЕСТОРОЖДЕНИИ ЮЖНО - ТУРГАЙСКОГО БАССЕЙНА. 2014. P. 15–19.
39. Wang D. et al. Actual Field Data Show that Production Costs of Polymer Flooding can be Lower than Water Flooding // Proc. - SPE Int. Improv. Oil Recover. Conf. Asia Pacific. 2003. P. 15–17.
40. Kang X., Zhang J. Offshore heavy oil polymer flooding test in JZW area // Soc. Pet. Eng. - SPE Heavy Oil Conf. Canada 2013. 2013. Vol. 2, № June. P. 1127–1134.
41. Lu Q. et al. Full field offshore surfactant-polymer flooding in bohai bay China // Soc. Pet. Eng. - SPE Asia Pacific Enhanc. Oil Recover. Conf. EORC 2015. 2015. № August. P. 312–323.
42. Полимерное заводнение в условиях Русского месторождения // ООО “Тюменский нефтяной научный Центр.” 2017.
43. Бородавкин П.П. Морские нефтегазовые сооружения. Учебник для вузов. Часть 1. Конструирование. 2006. 555 p.
44. Veritas D.N. DNV Environmental conditions and environmental loads // Dnv.

2010. № October. P. 9–123.
45. Chakrabarti S.K. Hydrodynamics of offshore structures // CIRED - Open Access Proceedings Journal. 1987. Vol. 2017, № July. 435 p.
46. Gudmestad O.T. Marine Technology and Operations 4. 2014. 71–104 p.
47. Sea Loads on Ships & Offshore Structures_Faltinsen.pdf.
48. Rahman M. Second order wave loads on large monolithic offshore structures // Appl. Math. Model. 1986. Vol. 10, № 6. P. 401–408.

Appendix 1 Table 1

№	Project discription					Production vessel/structure	Export Technology
	Country & Project		Year	Location	Water Depth, m		
1	Russia	Arkutun-Dagi	2014	Sea of Okhotsk, Sakhalin Island	35	Concrete GBS	Pipelines
2		Sakhalin I -Orlan	2008	Sea of Okhotsk, Sakhalin Island	15	Block-type GBS	Pipelines
3		Sakhalin II - MolikPaq (PA-A)	1999	Sea of Okhotsk, Sakhalin Island	30	Steel GBS	Currently pipelines
4		Sakhalin II - MolikPaq (PA-B)	2007	Sea of Okhotsk, Sakhalin Island	30	Multi-column GBS	Pipelines
5		Sakhalin II - LUN-A	2008	Sea of Okhotsk, Sakhalin Island	48	Multi-column GBS	Pipelines
6		Sakhalkin III - Kirinskoye	2014	Sea of Okhotsk, Sakhalin Island	90	Subsea system	Pipelines
7		Prirazlomnoye	2014	Barents Sea (Pechora Sea)	20	Block-type GBS	Offloading - GBS to ice-strengthened shuttle tankers
8		Shtokman	TBD	Barents Sea	340	FPSO & Subsea System	Pipelines
9		Kravtovskoye D-6	2004	Baltic Sea	25-35	Jacket platforms (2)	Pipelines
10	Canada	White Rose	2005	Grand Banks, Newfoundland	122	FPSO & Subsea System	Tandem offloading - FPSO to ice-strengthened shuttle tankers
11		Terra Nova	2002	Grand Banks, Newfoundland	90-100	FPSO & Subsea System	Tandem offloading - FPSO to ice-strengthened shuttle tankers
12		Hebron	2017	Grand Banks, Newfoundland	95	Block-type GBS	Offloading - GBS to ice-strengthened shuttle tankers
13		Hibernia	1997	Grand Banks, Newfoundland	80	Block-type GBS	Offloading - GBS to ice-strengthened shuttle tankers
14		Bjarni/North Bjarni	TBD	Labrador Shelf	140-150	TBD	TBD
15		Drake Point	TBD	Melville Island	55	Subsea System	Pipelines
16		Amauligak	TBD	Beaufort Sea	27-32	TBD	TBD
17		Tarsiut	TBD	Beaufort Sea	21	GBS	TBD
18	USA	Sivulliq	TBD	Beaufort Sea, Alaska	34	Conical-type GBS	Pipelines
19		Kuvlum	TBD	Beaufort Sea, Alaska	34	TBD	Pipelines
20		Liberty	TBD	Beaufort Sea, Alaska	6	Artificial Island (Gravel)	Pipelines
21		Endicott	1987	Beaufort Sea, Alaska	4	Artificial Island (Gravel)	Pipelines
22		Northstar	2001	Beaufort Sea, Alaska	12	Artificial Island (Gravel)	Pipelines
23		Nikaitchuq	2011	Beaufort Sea, Alaska	2	Artificial Island (Gravel)	Pipelines
24		Oooguruk	2008	Beaufort Sea, Alaska	2	Artificial Island (Gravel)	Pipelines
25		Cook Inlet Area	1958-2000	Cook Inlet, Alaska	14-56	Jacket platforms	Pipelines
26	Norway	Goliat	2014	Barents Sea (Norwegian)	360-420	FPSO & Subsea System	Offloading - FPSO to shuttle tankers
27		Johan Castberg	TBD	Barents Sea (Norwegian)	370	FPSO & Subsea System	Offloading - FPSO to shuttle tankers
28		Snøhvit	2007	Barents Sea (Norwegian)	310-340	Subsea System	Pipelines to Melkøya terminal
29	China - Bohai Bay Area Developments		1999	Bohai Bay of South, China Sea	25 (max 85)	Jacket platforms	Pipelines
30	Kazakhstan - Kashagan		2013	North Caspian Sea	3 - 6	Artificial Islands	Pipelines
31	Norway	Asgard B gasfield	1999-2001	Norwegian Sea	240-300	Semi-submersible platform	
32		Asgard A oilfield	1999-2001	Norwegian Sea	240-300	FPSO & Subsea System	
33		Aasta Hansteen Field	2018	Norwegian Sea	1270	SPAR & Subsea System	Pipelines
34		Norne FPSO	TBD	Norwegian Sea	1300	FPSO	Pipelines
35		Balder oilfield	1999	Norwegian Sea	125	FPSO & Subsea System	
36		Heidrun Field	1995	Norwegian Sea	350	Concrete TLP	pipeline for gas/ offloading for oil
37		Ormen Lange	2007	Norwegian Sea	800-1100	Subsea system	

Appendix 2

```
%reset -f
#EOR SCREENING . V.MIKHALKIN, 2020
from numpy import arange, pi, prod, fabs, linspace
from matplotlib import pyplot as plt

# INPUT DATA ==================================================
FIELD = {
                    'Depth': [1353, 1500],         # m
                   'NetPay': [73, 89],             # m
                 'Porosity': [11, 12],             # %
             'Permeability': [47/1e3, 98.7/1e3],   # D
            'OilSaturation': [0.86, 0.88],         #
              'Temperature': [30, 35],             # gradC
             'OilViscosity': [28.7,  61.3] ,       # mPa*s
                 'Pressure': [13.9, 15.4],         # MPa
              # 'Fractures': 0             # no - 0, yes - 1

        }


WEIGHTS = {
                    'Depth': 0.1,
                   'NetPay': 0.1,
                 'Porosity': 0.1,
             'Permeability': 0.2,
            'OilSaturation': 0.1,
              'Temperature': 0.1,
             'OilViscosity': 0.2,
                 'Pressure': 0.1,
          }
# BASE ========================================================

BASE = {
        # Termo ---------------------------------------------------
 'Steam':{ # ПТВ
           'Depth': (0, 0, 0, 1400, 1450, 1500),      # m
     'ClueContent': (0, 0, 0, 5, 7, 10),              # %
          'NetPay': (0, 6, 0, 0, 0, 0),               # m
        'Porosity': (0, 18, 0, 0, 30, 0),             # %
    'Permeability': (0, 0.2, 0, 0, 0, 0),             # D
   'OilSaturation': (0, 0.5, 0, 0, 0, 0),             #
     'Temperature': (0, 0, 0, 0, 50, 0),              # gradC
    'OilViscosity': (0, 50, 0, 0, 0, 0),              # mPa*s
   'WaterSalinity': (0, 0, 0, 0, 20, 0)               # g/l
```

```
                },
'HotWater':  { # ГВ
          'Depth': (0, 0, 0, 1400, 1450, 1500),      # m
     'ClueContent': (0, 0, 0, 5, 7, 10),             # %
          'NetPay': (0, 3, 0, 0, 0, 0),              # m
        'Porosity': (0, 18, 0, 0, 30, 0),            # %
    'Permeability': (0, 0.03, 0, 0, 0, 0),           # D
  'OilSaturation': (0, 0.5, 0, 0, 0, 0),             #
     'Temperature': (0, 0, 0, 0, 50, 0),             # gradC
    'OilViscosity': (0, 5, 0, 0, 0, 0),              # mPa*s
   'WaterSalinity': (0, 0, 0, 0, 20, 0)              # g/l
                },
'SteamWellTreatment { # ПТОС
          'Depth': (0, 0, 0, 1400, 1450, 1500),      # m
     'ClueContent': (0, 0, 0, 5, 7, 10),             # %
          'NetPay': (0, 6, 0, 0, 0, 0),              # m
    'Permeability': (0, 0.2, 0, 0, 0, 0),            # D
  'OilSaturation': (0, 0.5, 0, 0, 0, 0),             #
    'OilViscosity': (0, 30, 0, 0, 0, 0),             # mPa*s
                },
'SAGD ':  {
          'Depth': (0, 0, 0, 1100, 1150, 1200),      # m
     'ClueContent': (0, 0, 0, 5, 7, 10),             # %
          'NetPay': (12, 13, 15, 0, 0, 0),           # m
    'Permeability': (0, 1, 0, 0, 0, 0),              # D
  'OilSaturation': (0, 0.5, 0, 0, 0, 0),             #
    'OilViscosity': (0, 500, 0, 0, 0, 0),            # mPa*s
                },
# GAS ------------------------------------------------------------
'Methane':  {
           'Depth': (0, 1000, 0, 0, 0, 0),           # m
          'NetPay': (0, 0, 0, 0, 15, 0),             # m
     'Permeability': (0, 0.005, 0, 0, 0.1, 0),       # D
    'OilSaturation': (0, 0.3, 0, 0, 0, 0),           #
     'OilViscosity': (0, 0.4, 0, 0, 10, 0),          # mPa*s
         'Pressure': (0, 20, 0, 0, 0, 0),            # MPa
      'Temperature': (0, 0, 0, 0, 100, 0),           # gradC
                  },
'EnrichedGas':   {
          'Depth': (0, 1000, 0, 0, 0, 0),            # m
          'NetPay': (0, 0, 0, 0, 15, 0),             # m
    'Permeability': (0, 0.001, 0, 0, 0.15, 0),       # D
  'OilSaturation': (0, 0.6, 0, 0, 0, 0),             #
    'OilViscosity': (0, 0, 0, 0, 5, 0),              # mPa*s
        'Pressure': (0, 8, 0, 0, 0, 0),              # MPa
     'Temperature': (0, 0, 0, 0, 100, 0),            # gradC
                },
'NGL':  {
          'Depth': (0, 1500, 0, 0, 0, 0),            # m
          'NetPay': (0, 0, 0, 0, 15, 0),             # m
    'Permeability': (0, 0.001, 0, 0, 0.5, 0),        # D
```

```
98.    'OilSaturation': (0, 0.6, 0, 0, 0, 0),            #
99.     'OilViscosity': (0, 0, 0, 0, 10, 0),             # mPa*s
100.             'Pressure': (0, 8, 0, 0, 0, 0),          # MPa
101.          'Temperature': (0, 0, 0, 0, 96, 0),         # gradC
102.                       },
103.       'CO2':   {
104.                'Depth': (0, 600, 0, 0, 0, 0),        # m
105.               'NetPay': (0, 2, 0, 0, 15, 0),         # m
106.         'Permeability': (0, 0.002, 0, 0, 0.2, 0),    # D
107.        'OilSaturation': (0, 0.2, 0, 0, 0, 0),        #
108.         'OilViscosity': (0, 0, 0, 0, 60, 0),         # mPa*s
109.          'Temperature': (0, 10, 0, 0, 120, 0),       # gradC
110.          'ClueContent': (0, 0, 0, 0, 10, 0),        # %
111.             'Porosity': (0, 10, 0, 0, 35, 0),       # %
112.        'WaterSalinity': (0, 0, 0, 0, 350, 0),        # g/l
113.                       },
114.       'N2':   {
115.                  'Depth': (0, 1000, 0, 0, 0, 0),     # m
116.                'NetPay': (0, 4.8, 0, 0, 240, 0),     # m
117.          'Permeability': (0, 0.03, 0, 0, 0, 0),      # D
118.         'OilSaturation': (0, 0.4, 0, 0, 0, 0),       #
119.          'OilViscosity': (0, 1, 0, 0, 10, 0),        # mPa*s
120.              'Pressure': (0, 3, 0, 0, 0, 0),         # MPa
121.           'Temperature': (0, 0, 0, 0, 120, 0),       # gradC
122.           'ClueContent': (0, 0, 0, 0, 10, 0),        # %
123.              'Porosity': (0, 4, 0, 0, 33, 0),        # %
124.         'WaterSalinity': (0, 0, 0, 0, 350, 0)        # g/l
125.                        },
126.       'WAG':   {
127.                  'Depth': (0, 1800, 0, 0, 0, 0),     # m
128.                'NetPay': (0, 2, 0, 0, 19, 0),        # m
129.          'Permeability': (0, 0.02, 0, 0, 0.8, 0),    # D
130.         'OilSaturation': (0, 0.4, 0, 0, 0, 0),       #
131.          'OilViscosity': (0, 1, 0, 0, 10, 0),        # mPa*s
132.              'Pressure': (0, 15, 0, 0, 18, 0),       # MPa
133.           'Temperature': (0, 0, 0, 0, 50, 0),        # gradC
134.           'ClueContent': (0, 0, 0, 5, 7, 10),        # %
135.              'Porosity': (0, 10, 0, 0, 35, 0),       # %
136.                        },
137.       'WAG&FOAM':   {
138.                  'Depth': (0, 1800, 0, 0, 0, 0),     # m
139.                'NetPay': (0, 2, 0, 0, 20, 0),        # m
140.          'Permeability': (0, 0.004, 0, 0, 0.8, 0),   # D
141.         'OilSaturation': (0, 0.4, 0, 0, 0, 0),       #
142.          'OilViscosity': (0, 5, 0, 0, 100, 0),       # mPa*s
143.              'Pressure': (0, 15, 0, 0, 18, 0),       # MPa
144.           'Temperature': (0, 0, 0, 0, 50, 0),        # gradC
145.           'ClueContent': (0, 0, 0, 5, 7, 10),        # %
146.              'Porosity': (0, 10, 0, 0, 35, 0),       # %
147.                        },
148.       # Ph ------------------------------------------------------------------
```

```
149.       'Polymer':  {
150.                 'Depth': (0, 213, 0, 0, 2883, 0),          # m
151.             'ClueContent': (0, 0, 0, 0, 5, 0),             # %
152.                'Porosity': (0, 10.4, 0, 0, 33, 0),         # %
153.            'Permeability': (0, 0.6/1e3, 0, 0, 5500/1e3, 0), # D
154.           'OilSaturation': (0, 0.6, 0, 0, 0, 0),           #
155.             'Temperature': (0, 0, 0, 75, 80, 90),          # gradC
156.            'OilViscosity': (0, 0.3, 0, 0, 130, 0),         # mPa*s
157.           'WaterSalinity': (0, 0, 0, 0, 20, 0)             # g/l
158.                                                 },
159.       'SAA':  {
160.                 'Depth': (0, 20, 0, 0, 4500, 0),           # m
161.             'ClueContent': (0, 0, 0, 0, 5, 0),             # %
162.                'Porosity': (0, 10, 0, 0, 35, 0),           # %
163.            'Permeability': (0, 0.1, 0, 0, 2, 0),           # D
164.           'OilSaturation': (0, 0.7, 0, 0, 0, 0),           #
165.             'Temperature': (0, 0, 0, 0, 50, 0),            # gradC
166.            'OilViscosity': (0, 1, 0, 0, 60, 0),            # mPa*s
167.           'WaterSalinity': (0, 0, 0, 0, 10, 0)             # g/l
168.                           },
169.      }
170.
171.
172.      # FUCTIONS DIDINITION
    ============================================================
173.      def mu(x, SixValues):                          # Membership function defini-
    tion
174.          if SixValues == None: # if there are no criteria in BASE
175.              return 1
176.          # DEFUALT MODE: SixValues=[x,x,x,x,x,x]
177.          xmin1, xm1, xmax1, xmin2, xm2, xmax2 = SixValues
178.          # SPECIAL MODES: SixValues=[0,x,0,0,x,0], SixValues=[x,x,x,0,0,0], ...
179.          #... SixValues=[0,0,0,x,x,x], SixValues=[0,x,0,x,x,x],
    SixValues=[x,x,x,0,x,0]
180.          block = 1
181.          if sum([xmin1, xmax1, xmin2, xmax2]) == 0 or xmin1+xmax1 == 0 \
182.          or xmin2+xmax2 == 0:
183.              r = .3
184.              xmin1 = xm1 - r*fabs(xm2 - xm1)
185.              xmax1 = xm1 + r*fabs(xm2 - xm1)
186.              xmin2 = xm2 - r*fabs(xm2 - xm1)
187.              xmax2 = xm2 + r*fabs(xm2 - xm1)
188.              if xm1 == 0: #for SixValues=[0,0,0,x,x,x]
189.                  xmin1 = 0
190.                  xmax1 = 0
191.              if xm2 == 0: #for SixValues=[x,x,x,0,0,0]
192.                  xmin2 = 0
193.                  xmax2 = 0
194.          if xmin2 == 0:
195.              xmin2 = 2000
196.              block = 0
```

```
197.
198.          #FUNCTION
199.          mu=[]
200.          if not(isinstance(x, list)): x = [x,x]
201.          if x[0] == x[1]: x = [x[0]]
202.          else: x = arange(x[0], x[1], .01)
203.          for i in range(len(x)):
204.              if x[i] < 0:
205.                  mu.append(0)
206.              elif x[i] <= xmin1:
207.                  mu.append(0)
208.              elif x[i] > xmin1 and x[i] < xmax1:
209.                  y = ((xmax1-xm1)/(xm1-xmin1)*(x[i]-xmin1)/(xmax1-x[i]))**(-2)
210.                  mu.append((1+y)**(-1))
211.              elif x[i] >= xmax1 and x[i] <= xmin2:
212.                  mu.append(1)
213.              elif x[i] > xmin2 and x[i] < xmax2:
214.                  y = ((xmax2-xm2)/(xm2-xmin2)*(x[i]-xmin2)/(xmax2-x[i]))**(2)
215.                  mu.append((1+y)**(-1))
216.              elif x[i] >= xmax2:
217.                  mu.append(0**block)
218.          #print(mu[0], mu[1])
219.          return sum(mu)/len(mu)
220.
221.      def c(values, weights, method):
222.          from numpy import prod
223.          if round(sum(weights),4) != 1:
224.              print('WARNING! WEIGHTS sum = ', sum(weights))
225.          t = []
226.          for i in range(len(weights)):
227.              t.append(values[i]*weights[i])
228.          if method == 1:
229.              return sum(t)
230.          if method == 2:
231.              return prod(t)**(1/len(t))
232.          if method == 3:
233.              return min(values)
234.
235.      # CALCULATIONS
     ======================================================================
236.      MATRIX = {}
237.      RESULTS = {}
238.      for BASEkey in BASE:
239.          TempDict = {}
240.          for FIELDkey in FIELD:
241.              TempDict[FIELDkey] = mu(FIELD[FIELDkey], BASE[BA-
     SEkey].get(FIELDkey))
242.          RESULTS[BASEkey]=c(list(TempDict.values()), list(WEIGHTS.values()), 3)
243.          MATRIX[BASEkey] = TempDict
244.          del TempDict
245.
```

```
246.      #TABLE DRAWING
    ========================================================================
247.      line ='{:22}'.format('Parameter/Method')                              # Head
248.      for MATRIXkey in MATRIX:
249.              line = line + '{:11.7}'.format(MATRIXkey)
250.      print(line, '\n')
251.      del line
252.      for j in FIELD:                                                       # Body
253.          line = '{:22}'.format(j)
254.          for i in MATRIX:
255.              line = line + '{:^3.2f}{:7}'.format(MATRIX[i][j], ' ')
256.          print(line)
257.          line = ''
258.      del line
259.      line ='\n{:22}'.format('Evaluation:')
260.      for RESULTSkey in RESULTS:
261.          line = line + '{:^3.2f}{:7}'.format(RESULTS[RESULTSkey], '  ')
262.      print(line, '\n')
263.
264.      # PLOT DRAWING
    ========================================================================
265.      method = 'Polymer'
266.      f, axs = plt.subplots(2,4,figsize=(15,10))
267.      # Membership function drawing
268.      i=1
269.      for parameter in BASE[method]:
270.          x1 = BASE[method][parameter][1]
271.          x2 = BASE[method][parameter][-2]
272.          if x1 == 0:
273.              x1 = x2 - 0.5*x2
274.          if x2 == 0:
275.              x2 = x1 + 0.5*x1
276.          xx = fabs(x2-x1)
277.          xx = linspace(x1-.7*xx, x2+.7*xx, 200)
278.          yy = [mu(i, BASE[method].get(parameter)) for i in xx]
279.          plt.subplot(2, 5, i)
280.          plt.plot(xx, yy, '-')
281.          plt.xlabel(parameter)
282.      # Property range/point drawing
283.          if FIELD.get(parameter) != None:
284.              if isinstance(FIELD[parameter], list):
285.                  xx = arange(FIELD[parameter][0], FIELD[parameter][1], .01)
286.                  j=0
287.                  while (mu(xx[j], BASE[method][parameter]) \
288.                         <= 0.98*MATRIX[method][parameter] \
289.                  or mu(xx[j], BASE[method][parameter]) >= \
290.                         1.02*MATRIX[method][parameter]) and xx[j]<xx[-1]:
291.                      j+=1
292.                  plt.plot([FIELD[parameter][0],FIELD[parameter][1]] ,[0,0],
    color="r")
```

```
293.                 plt.scatter(xx[j],mu(xx[j], BASE[method][parameter]),
    color="r")
294.
295.             else:
296.                 plt.scatter(FIELD[parameter],mu(FIELD[parameter], \
297.                                                 BASE[method][parameter]),
    color="r")
298.         plt.grid()
299.         i+=1
300.
```

Appendix 3

sdfvsdvsvsdv

```
%reset -f
#WAVELOAD ON A LARGE STRUCTURE . V.MIKHALKIN, 2020
import sys
from numpy import arange, pi
from matplotlib import pyplot as plt
print('This script calculates wave loads on large bodies (cylinder or square).\n')

# FUNCTIONS for CALCULATIONS
def DispersionRelationSolution(k, T, d, N, e): #Newton iterations for the DispersionRelation
    from math import tanh, cosh, fabs, pi
    t = 9.81/(2*pi/T)**2 # g/w^2
    for i in range(N):
        f = t*k*tanh(d*k)-1
        dfdk = t * (d*k/(cosh(d*k)**2) + tanh(d*k))
        knew = k - f / dfdk # knew = k - f(x)/f'(x)
        if fabs(knew - k) < e:
            print('ok: k = ', k, ' from ', i+1, ' iterations')
            break
        k = knew
    return k

def CmFunction(L, D):
    from scipy.special import jvp, yvp
    pi=3.1415
    k = 2*pi/L
    A = jvp(1, k*D/2, n=1)**2+yvp(1, k*D/2, n=1)**2
    return 4 /(pi*(k*D/2)**2*A**0.5)

def Force(x, t, H, k, w, rho, d, Cm, A, S):
    from math import sin, cos, sinh, cosh
    g = 9.81
    ksi0 = H/2
    ksi = ksi0*sin(w*t-k*x)
    #Mass
    R = S*rho*Cm
    N = ksi0*k*g*cos(w*t-k*x)/cosh(k*d)
    FM = R*N/k*sinh(k*(ksi+d))
    return FM

def wave(t, x, H, w, k):
    from math import sin
    ksi0 = H/2
    return ksi0*sin(w*t-k*x)

def ac(x, t, k, w, d):
```

```
46.     from math import sin, cos, sinh, cosh
47.     g = 9.81
48.     ksi0 = H/2
49.     ksi = ksi0*sin(w*t-k*x)
50.     return ksi0*k*g*cos(w*t-k*x)/cosh(k*d)*cosh(k*(ksi+d))
51.
52. def IsThisASquareBody(type, D):
53.     if type == 'no':
54.         return D
55.     elif type == 'yes':
56.         D = 2*D/pi**0.5
57.         return D
58.
59. #INITIA DATA
60. # The calculations are made for 2 type of bodies
61. D = 70                          # Characteristic dimension. Side length for squre
62. D = IsThisASquareBody('no', D)# yes / no
63. rho = 1025                     # Water density
64. d = 20+4.7                     # Water depth
65. H = 12.7                       # Hmax
66. T = 11.3                       # Peak wave period
67.
68. #CALCULATIONS
69. A = D          # Reference area per unit length. Cylinder.
70. S = pi*D**2/4  # Square of a body's cross-section. Cylinder.
71. w = 2*pi/T     # Angular frequency calculation
72. k = DispersionRelationSolution(1, T, d, 10, 0.00001) # k-number calculation
73. L = 2*pi/k # Wave length calculation
74.
75. # Determination of water depth category. Not used in calculation
76. if d/L < 1/20:
77.     print('This is shallow water.')
78. elif d/L < 1/2:
79.     print('This is intermidiate water.')
80. else:
81.     print('This is deep water.')
82.
83. # Morison equation for large bodies
84. if D/L < 0.2:
85.     print('D/L=', round(D/L, 2), ' < 0.2 -- OK - The body is considered as a small
    body - no reflection.')
86.     sys.exit("STOP - the body is considered as a small body - no reflection.")
87. elif H/L >= 0.14:
88.     print('H/L =', round(H/L, 2), '> 0.14 -- STOP - breaking wave')
89.     sys.exit("STOP - breaking wave")
90. else:
91.     print('D/L=', round(D/L, 2), ' > 0.2 -- OK - The body is considered as a large
    body - reflection presents.')
92.     print('H/L =', round(H/L, 2), '< 0.14 -- OK - Non-breaking waves condition.')
93.     print('A/D < 0.2 -- OK. The body is supposed to be fixed, A=0.\n')
94.
```

```
Cm = CmFunction(L, D) # Cm calculation
t = arange(0,2*T,0.01) # Time period observed, and the timestep

F  = [ Force(0, i, H, k, w, rho, d, Cm, A, S) for i in t] # Total force calculation for each time-step
M = [ i*2/3*d for i in F] # Moment calculation for each time-step
      print('RESULTS:')
      print('Maximum force: ', round(max(F), 2)/1e6, ' MH')
      print('Maximum moment: ', round(max(M), 2)/1e6, ' MHm')

      #PLOTS
      import matplotlib.pyplot as plt
      fig=plt.figure(figsize=(18, 7))
      ax1=fig.add_subplot(121, label="F")
      ax2=fig.add_subplot(121, label="ksi", frame_on=False)
      #ax3=fig.add_subplot(111, label="a", frame_on=False)
      # The first axes -- FORCE
      F = [i * 1e-6 for i in F]
      ax1.plot(t, F, color="k")
      ax1.set_xlabel("Время, s", color="k",  fontsize=13)
      ax1.set_ylabel("Сила волновой нагрузки, MH", color="k",  fontsize=13)
      ax1.tick_params(axis='x', colors="k")
      ax1.tick_params(axis='y', colors="k")
      to = 2*pi/w + .9
      F0to = Force(0, to, H, k, w, rho, d, Cm, A, S)
      #print('\nF(0, ',to ,') = ', round(F0to/1e6, 2), ' MN  -- red point')
      #ax1.scatter(to, F0to/1e6, color="r")
      # The second axes -- WAVE PROFILE
      ksi = [wave(i, 0, H, w, k) for i in t] # Wave profile calculation for each time-step
      ax2.plot(t, ksi, color="C0")
      ax2.yaxis.tick_right()
      ax2.set_xlabel('', color="k")
      ax2.set_ylabel('ξ, m', color="C0")
      ax2.yaxis.set_label_position('right')
      ax2.tick_params(axis='x', colors="k")
      ax2.tick_params(axis='y', colors="C0")
      ax2.set_ylim([-2*H,2*H])
      #ax2.scatter(to, wave(to, 0, H, w, k), color="r")
      a = [ac(0, i, k, w, d) for i in t]
      #ax3.plot(t, a, color="r")
      #ax3.yaxis.tick_right()
      #ax3.set_xlabel('', color="k")
      #ax3.set_ylabel('a, m/s/s', color="r")
      ##ax3.yaxis.set_label_position('right')
      #ax3.tick_params(axis='x', colors="k")
      #ax3.tick_params(axis='y', colors="r")
      #ax3.set_ylim([2*min(a),2*max(a)])
      plt.grid()

      # Cm(D/L)
```

```
144.      x = arange(.01,1,0.01)
145.      Lx = [D / i for i in x]
146.      Cmy = [CmFunction(i, D) for i in Lx]
147.      ax=fig.add_subplot(122, label="F")
148.      ax.plot(x, Cmy, color="k")
149.      ax.set_xlabel("D/L", color="k",  fontsize=13)
150.      ax.set_ylabel("Cm", color="k",  fontsize=13)
151.      ax.tick_params(axis='x', colors="k")
152.      ax.tick_params(axis='y', colors="k")
153.      ax.scatter(D/L, Cm, color="r")
154.      plt.grid()
155.      plt.show()
156.
```

Appendix 4

```
%reset -f
#ICELOAD (LevelIce, DriftIce) ON A LARGE STRUCTURE . V.MIKHALKIN, 2020
from numpy import exp, tan, pi, arange
from matplotlib import pyplot as plt
width = arange(65,105,5)
F = []
for j in width:
    h = 3 #3 the thickness of the ice sheet, expressed in metres;
    w = j # the projected width of the structure, expressed in metres;
    h1 = 1 # a reference thickness of 1 m;

    CR = 2.8*1e6 # the ice strength coefficient, expressed in pascals. For Arctic FY and MY ice (e.g. Beaufort) equals to 2.8*1.6 Pa
    m = -0.16 # an empirical coefficient equal to -0.16;
    if h < 1: n = -.5+h/5 # an empirical coefficient, equal to -0.50 + h/5 for h < 1.0 m,
    else: n = -.3          # and to -0.30 for h ≥ 1.0 m;
    fAR = exp(-w/3/h)*(1+5*h/w)**.5 # empirical term
    pG = CR*((h/h1)**n*(w/h)**m+fAR) # the global average ice pressure, expressed in megapascals;
    F.append(pG*h*w) #

F = [i * 1e-6 for i in F]
fig =plt.figure(figsize=(7, 7))
ax1=fig.add_subplot(111, label="F")
ax1.set_xlabel("Ширина кессона, м", color="k", fontsize=13)
ax1.set_ylabel("Максимальная сила воздействия \n припая (толщина - 1.6 м), МН", color="k", fontsize=13)
ax1.plot(width, F, color="k", label = 'sin(x)')
plt.grid()
plt.show()
```

Appendix 5

```
%reset -f
from numpy import tan, pi, linspace, arange, exp
from matplotlib import pyplot as plt

depth = arange(14,22,1)
fact_width = 100
fact_depth = 18
Width = [100, 70]
clr = ['k', 'r']
fig =plt.figure(figsize=(14, 7))
ax1=fig.add_subplot(121, label="F")
ax2=fig.add_subplot(122, label="M")
l=0
for j in Width:
    FR = []
    MR = []
    for i in depth:
        d = (4.7+i)
        w = j # the width of the structure
        hc = 3.6 # consolidated layer thickness
        h = hc # the thickness of the ice sheet, expressed in metres;
        h1 = 1
        CR = 2.8*1e6 # the ice strength coefficient, expressed in pascals. For Arctic FY and MY ice (e.g. Beaufort) equals to 2.8*1.6 Pa
        m = -0.16 # an empirical coefficient equal to -0.16;
        if h < 1: n = -.5+h/5 # an empirical coefficient, equal to -0.50 + h/5 for h < 1.0 m,
        else: n = -.3          # and to -0.30 for h ≥ 1.0 m;
        fAR = exp(-w/3/h)*(1+5*h/w)**.5 # empirical term
        pG = CR*((h/h1)**n*(w/h)**m+fAR) # the global average ice pressure, expressed in megapascals;
        Fc = pG*h*w #

        hk = d - hc # vertical distance between the base of the consolidated layer and the base of the keel
        g = 9.81
        e = 0.3 # the keel porosity;
        rhow = 1025 # the water density;
        rhoi = 900 # the ice density;
        c = 10*1e3 # kPa the apparent keel cohesion (an average value over the keel volume should be used);
        PHI = 30 # the angle of internal friction
        gammae = (1-e)*(rhow-rhoi)*g # the effective buoyancy, in units consistent with c.
        muPHI = tan((45+PHI/2)*pi/180) # the passive pressure coefficient;
        Fk = muPHI*hk*w*(hk*muPHI*gammae/2+2*c)*(1+hk/6/w) # the keel action component.
        FR.append(Fc+Fk) # horizontal action caused by a FY ridge;
        MR.append(Fc*d+Fk*d/2)
```

```
        if i == fact_depth and j == fact_width:
            factF = FR[-1]
            factM = MR[-1]
    # The first axes -- FORCE
    FR = [i * 1e-6 for i in FR]
    MR = [i * 1e-6 for i in MR]
    ax1.plot(depth, FR, color=clr[l], label = str(Width[l])+' м')
    ax2.plot(depth, MR, color=clr[l], label = str(Width[l])+ ' м')
    l=+1

ax1.grid()
ax1.legend()
ax1.set_xlabel("Глубина установки, м", color="k", fontsize=13)
ax1.set_ylabel("Сила, МН", color="k", fontsize=13)

ax2.grid()
ax2.legend()
ax2.set_xlabel("Глубина установки, м", color="k", fontsize=13)
ax2.set_ylabel("Момент, МНм", color="k", fontsize=13)

#ax1.scatter(fact_depth,factF/1e6, color="r")
#ax2.scatter(fact_depth,factM/1e6, color="r")
#print(factF/1e6)
#print(factM/1e6)
plt.show()
```